3rd Baltic Biophysics Conference

Abstract Book

2022 October 6-7th

Center for Physical Sciences and Technology

Saulėtekio av. 3,

Vilnius

Lithuania

Content

Foreword

Dear Baltic Biophysics Conference Participants,

It is a great pleasure and honor to welcome all guests and outstanding researchers from all over the world to the 3rd Baltic Biophysics conference taking place in Vilnius, Lithuania.

The aim of the conference is to gather researchers in the field of biophysics from the Baltic States and the entire Baltic Sea region to share their newest knowledge, to introduce innovative discoveries among professionals and young minds, promote awareness about biophysical sciences, and strengthen international collaboration. I believe that multidisciplinary thinking is an important aspect of success in the accumulation of grants, the development of new ideas and visions, and scientific progress. I am firmly convinced that we will succeed together in taking advantage of the international environment and the experience of last years to strengthen further the synergy created by the innovation of Baltic Biophysics conferences.

This year there will be 2 Keynote Lectures, 7 Invited Lectures, 17 Oral Presentations, 1 Poster Session, and the Meeting of Lithuanian Biophysical Society Members. Our sincere thanks go to all those who made these lectures and presentations possible for the success of the conference.

I am grateful to all Sponsors for their positive response and encouragement in a way of providing funding.

This meeting is jointly organized by the National Cancer Institute, Vilnius University, Vytautas Magnus University, VilniusTech University, Center for Physical Sciences and Technology, Kaunas University of Technology, and Lithuanian University of Health Sciences.

In conclusion, I would like to extend a warm welcome to you all once again and wish you success in your work during the BBC-2022 conference.

Kind regards,

Conference Chairman

Prof. Ričardas Rotomskis

The Team

Conference chairman:

Prof. Ričardas Rotomskis, National Cancer Institute

Scientific organizing committee:

Prof. Ričardas Rotomskis, National Cancer Institute

Prof. Saulius Šatkauskas, Vytautas Magnus University

Prof. Vytenis Arvydas Skeberdis, Lithuanian University of Health Sciences, Institute of Cardiology,

Prof. Aidas Alaburda, Vilnius University, Life Sciences Center,

Prof. Saulius Bagdonas, Vilnius University, Faculty of Physics

Prof. Vitalijus Karabanovas, VilniusTech University,

Prof. Leonas Valkūnas, Center for Physical Sciences and Technology,

Prof. Tomas Tamulevičius, Kaunas University of Technology.

Local organizing committee:

Dr. Arūnas Stirkė, Center for Physical Sciences and Technology,

Dr. Paulius Ruzgys, Vytautas Magnus University,

Dr. Indrė Lapeikaitė, Vilnius University, Life Sciences Center,

Dr. Agnė Kalnaitytė, Vilnius University, Faculty of Physics

Dr. Povilas Šimonis, Center for Physical Sciences and Technology,

Greta Jarockytė, National Cancer Institute,

Joana Smirnovienė Vilnius University, Life Sciences Center,

Vilmantas Pupkis, Vilnius University, Life Sciences Center,

Evelina Voronovič, VilniusTech University,

Rokas Mickus, Lithuanian University of Health Sciences,

Neringa Barauskaitė, Vytautas Magnus University.

Program

Day 1 – October 6th (Thursday) 2022			
Time	Presenter	Institution	Title of the Lecture
8.30-9.00 Hall	Registration of the participants		
A101	***Opening Ceremony*** Head of Conference Organizing Committee – Greta Jarockytė		
9.00-9.05	Mayor of Vilnius **Remigijus Šimašius**	Vilnius municipality City council, **Lithuania**	Welcome address
9.05-9.10	Chairman of Lithuanian Biophysical Society **Prof. Saulius Šatkauskas**	Vytautas Magnus University, **Lithuania**	Welcome address
9.10-9.15	Head of Conference Scientific Committee **Prof. Ričardas Rotomskis**	Vilnius University & National Cancer Institute, **Lithuania**	Conference agenda
A101	***Session 1 – Electric Fields Effects on the Biological Systems*** Chairmen – Prof. Saulius Šatkauskas and Prof. Vytenis Arvydas Skeberdis		
9.15-10.00	**Prof. Rodolphe Fischmeister** *Keynote*	Paris-Saclay University, **France**	Cyclic AMP Signaling in the Normal and Failing Heart: Compartmentation and Therapeutic Implications
10.00-10.20	**Prof. Vytenis Arvydas Skeberdis** *O01*	Lithuanian University of Health Sciences, **Lithuania**	Phosphorylation of Cx43 by Ca^{2+}/Calmodulin Kinase II Increases the Sensitivity of Cx43 Gap Junction Channels to Chemical Gating
10.20-10.40	**PhD student Viktorija Reinikovaitė** *O02*	Center for Physical Sciences and Technology, **Lithuania**	Conducting Polymers Improve Yeast's Electrical Properties for Better Microbial Fuel Cell Development
10.40-11.10 Hall	***Coffee Break***		
11.10-11.30	**Prof. Saulius Šatkauskas** *O03*	Vytautas Magnus University, **Lithuania**	Electroporation: a Versatile Tool for Cell and Tissue Manipulation and Therapy
11.30-11.50	**Prof. Gintautas Saulis** *O04*	Vytautas Magnus University, **Lithuania**	Platform for Modeling and Analysis of Cell Electroporation and Associated Phenomena
11.50-12.10	**PhD student Veronika Malyško-Ptašinskė** *O05*	Vilnius Gediminas Technical University, **Lithuania**	Sub-microsecond Electrochemotherapy with High Pulse Repetition Frequency
12.10-12.30	**PhD student Greta Gančytė** *O06*	Center for Physical Sciences and Technology, **Lithuania**	Enhancement and Reversion of Irreversible Electroporation via Osmotic Shock Treatment

12.30-13.30	***Lunch Break***		
13.30-15.00 Hall	***Poster Session & Coffee Break***		
A101	***Session 2 – Nanobiophysics and Nanotechnology*** Chairmen – Prof. Vitalijus Karabanovas and Prof. Tomas Tamulevičius		
15.00-15.30	**Prof. Juris Prikulis** *Invited*	University of Latvia, **Latvia**	Nanoporous Anodic Alumina Based Hybrid Multilayers for Colorimetric and Interferometric Optical Sensing
15.30-16.00	**Dr. Vladimir Sivakov** *Invited*	Leibniz Institute of Photonic Technology, **Germany**	Nanostructured Silicon – a Platform for Biophotonics
16.00-16.30	**Dr. Artiom Skripka** *Invited*	Lawrence Berkeley National Laboratory, **USA** Universidad Autónoma de Madrid, **Spain**	New Architectures of Photon Avalanching Nanoparticles for Superresolution Imaging
16.30-16.50	**Prof. Yuri Dekhtyar** *O07*	Riga Technical University, **Latvia**	Electric Charge of Nanoparticle Surface Towards its Engineered Interaction with Cell
16.50-17.10	**Dr. Domantas Peckus** *O08*	Kaunas University of Technology, **Lithuania**	The Size, Shape and Crystal Structure of Metal Nanoparticles Influence on their Ultrafast Plasmonic Properties
17.10-17.30	**Dr. Živilė Jurgelėnė** *O09*	National Cancer Institute & Nature Research Centre, **Lithuania**	The Bioaccumulation of Nanoparticles During Fish Development: Towards a Deeper Understanding of Potential Nanotoxicity
18.00-22.00	***Social Event***		

Day 2 – October 7th (Friday) 2022			
Time	Presenter	Institution	Title of the Lecture
A101	***Session 3 – Photosynthesis and Molecular Spectroscopy*** Chairman – Prof. Leonas Valkūnas		
9.00-9.45	**Prof. Herbert van Amerongen** *Keynote*	Wageningen University, **Netherlands**	Regulating Light Harvesting in Oxygenic Photosynthesis
9.55-10.15	**Prof. Arvi Freiberg** *Invited*	University of Tartu & Estonian Academy of Sciences, **Estonia**	Towards the Understanding of Pressure-Induced Phase Transitions in Proteins
10.15-10.45	**Prof. Donatas Zigmantas** *Invited*	Lund University, **Sweden**	Mapping Energy Transfer in Photosynthetic Bacteria *in vivo*
10.45-11.15 Hall	***Coffee Break***		

11.15-11.35	**Dr. Andrius Gelžinis** *O10*	Vilnius University & Lithuania Center for Physical Sciences and Technology, **Lithuania**	Molecular Structure and Electronic Excitation Dynamics in FCP Complex
11.35-11.55	**Dr. Jevgenij Chmeliov** *O11*	Center for Physical Sciences and Technology & Vilnius University, **Lithuania**	Inter-Molecular Charge Transfer States in the Light-Harvesting Complexes
11.55-12.15	**Prof. Asko Uri** *O12*	University of Tartu, **Estonia**	Protein Kinase-Sensitive Tandem Photoluminescent Probes Possessing Förster-Type Resonant Energy Transfer from a Donor Phosphor to a Fluorophore
12.15-12.35	**PhD student Michał K. Białobrzewski** *O13*	Polish Academy of Sciences, **Poland**	Hydrodynamics and Intermolecular Interactions Between Proteins Involved in Gene Expression by Fluorescence Correlation Spectroscopy (FCS)
12.35-12.55	**Dr. Joana Smirnovienė** *O14*	Vilnius University, **Lithuania**	Switching the Enzyme-Inhibitor Recognition Profile via Chimeric Carbonic Anhydrases
12.55-14.00	***Lunch Break***		
A101	***Session 4 – Advanced Microscopy in Life-Sciences*** Chairman – Prof. Saulius Bagdonas		
14.00-14.30	**Prof. Bruno Robert** *Invited*	CEA Paris-Saclay University, **France**	Photosynthetic Structures and their Regulations: Microscopy
14.30-15.00	**Dr. Gražvydas Lukinavičius** *Invited*	Max Planck Institute for Multidisciplinary Sciences, **Germany**	Labeling Biomolecules in Living Cells – are there General Rules for Probe Design?
15.00-15.20	**PhD student Aurimas Kopūstas** *O15*	Vilnius University & Center for Physical Sciences and Technology, **Lithuania**	Fluorescence Microscopy-Based Studies of Individual Protein-DNA Interactions *in vitro vs. in vivo*: Challenges, Solutions and Outcomes
15.20-15.40	**PhD student Emilija V. Plorina** *O16*	University of Latvia & LTD Longenesis, **Latvia**	Multispectral Imaging of Neurofibromatosis Type 1 Skin Lesions
15.40-16.00	**PhD student Mykolas Mačiulis** *O17*	Vilnius University, **Lithuania**	Eosin and Hematoxylin Harmonophores for Histopathology Investigations with Nonlinear Microscopy
16.00-16.30	***Closing Ceremony & Coffee Break***		
16.30-18.00	***Meeting of Lithuanian Biophysical Society Members***		

Poster Presentations		
Poster	Presenter	Title
P01	Dobilas Kirvelis	Bio-Physics as Bio-Engineering: techno-recursive life-basics functional organization and STEAM for creative education
P02	Vilius Marma	Psychophysical study of the area of influence of distractors on the geometric illusion of extent
P03	Raminta Bartulienė	Artificial intelligence application in synaesthesia research
P04	Vytautas Baranauskas	Rabbit model of meibomian gland disfunction
P05	Vadims Parfejevs	Co-culture of human pancreatic organoids with cells of the peripheral nervous system
P06	Irma Martišienė	Effect of 2-acetylfuran on smooth muscles in rat prostate and aorta
P07	Rimantas Treinys	Electrophysiological and antihypertensive action of *Elsholtzia ciliata* essential oil in large animal model
P08	Vilma Zigmantaitė	Evaluation of the *Elsholtzia ciliata* essential oil effect on heart rate variability and blood composition in a large animal model
P09	Anita Elizabeth Clarke	What can $\delta^{13}C$ Reveal About Plant Fitness? A Primary Investigation of a Lycophyte, *Spinulum annotinum*
P10	Gintarė Dalmantaitė	Valuable Compounds Extraction From Microalgae Using Cold Plasma and Pulsed Electric Fields
P11	Dominyka Gabulaitė	Comparison between titanium and stainless-steel electrodes on electroporation and gene transfer efficiency
P12	Ahmed Taha	Emulsifying Properties of PEF-treated BSA/Soluble Starch Conjugates
P13	Aras Rafanavičius	Investigation of oligonucleotide, propidium iodide and plasmid DNA electrotransfer efficiency into cells
P14	Ugnė Borinskytė	Bleomycin Electrotransfer or Irreversible Electroporation between different Cell Lines: An Investigation of the Bystander Effect
P15	Eivina Radzevičiūtė	Electrotransfection of Cancer and Primary Murine Dendritic Cells
P16	Rita Saulė	Influence of Oxygen Concentration on the Effectiveness of Electrochemotherapy *in vitro*: Modeling and Experiments
P17	Augustinas Želvys	Tumor Elimination *In Vivo* Using Combined Calcium Electroporation
P18	Rūta Palepšienė	$CaCl_2$ influence on the electrotransfection potency of pDNA and cell viability
P19	Baltramiejus Jakštys	DAMPs Obtained from Irreversibly Electroporated Cells Prevent Cell Death After Electroporation
P20	Kamilė Jonynaitė	Pulsed electric field (PEF) treatment of marine microalgae
P21	Neringa Barauskaitė	The Influence of Bystander Effect to the Viability of Directly Unaffected Cells After Electroporation Based Treatments
P22	Simona Gelažunaitė	The differences between viability evaluation by using colony formation and metabolic activity methods of *Streptococcus Thermophilus* after application of pulsed electric field
P23	Paulius Ruzgys	Cell size change after electroporation and its influence to triggered electrotransfer
P24	Anastasiia Shelest	Functional activity of L-type Ca^{2+} channels in bone marrow-derived human mesenchymal stem cells during chondrogenic differentiation and in chondrocytes
P25	Inga Andriulė	Modulation of TRPM6 and TRPM7 channel expression by experimental conditions (medium ionic composition, acidosis, and TRP channel inhibitors)
P26	Rokas Bertašius	Towards purification of recombinant TMEM106B
P27	Rokas Mickus	Terpenes are Potent Cx43 Gap Junction Inhibitors
P28	Gytis Baranauskas	An efficient rAAV vector for protein expression in cortical parvalbumin expressing interneurons
P29	Vytautas Raškevičius	Integral actin facilitates connexin-43 hemichannel docking between daughter cells
P30	Diana Macaitytė	Towards Nanomolar Detection of Neurotransmitters: Application of Functionalized Horseradish Peroxidases in Organic Solvents
P31	Kamilė Čerepenkaitė	Biochemical characterization of SARS-CoV-2 3-chymotrypsin like protease
P32	Tautvydas Kojis	Catalytic activity and small molecule binding of cytosolic murine carbonic anhydrases
P33	Kamilė Mikalauskaitė	Exploring the Effect of Amyloid-Specific Molecules on Protein Aggregation

P34	Marius Gedgaudas	Tool for assisting high-throughput screening of protein-ligand interactions
P35	Lukas Krasauskas	Prion Protein Amyloid Aggregates Associate with Tau Protein Monomers in Conformationspecific Manner
P36	Martynas Bagdonas	Discovery of novel SARS-CoV-2 papain-like protease inhibitors by thermal shift assay
P37	Alytis Gruodis	Influence of Fe(II) on Lipid Orientation in the Lipid Bilayer: Quantum Chemical Simulations
P38	Modestas Mažerimas	Bacterial membrane mimicking model and its interaction with antimicrobial peptides
P39	Arun Prabha Shivabalan	Effect of pH on tethered Bilayer Lipid Membranes
P40	Simonas Norvaišis	Development of a directed protein evolution method based on droplet microfluidics and DNA microparticles
P41	Neringa Bakutė	Fabrication of microfluidic chip for electroporation of cells
P42	Martynas Gavutis	Scanning Probe Based Rapid Prototyping of Single Cell Chips
P43	Gvidas Klyvis	Superlattice Fabrication Employing Multi Exposure Laser Interference Lithography
P44	Elžbieta Ragauskaitė	Towards Supramolecular Neurotransmitters Sensor based on a Dibenzo-18-crown-6 Polymer
P45	Aida Kamarauskienė	Chirality-Induced Spin Selectivity through an Electrografted Polyaniline
P46	Marijus Plečkaitis	Principles of self-assembly and structure of sulfonatophenyl porphine aggregates resembling giant "sea urchin"
P47	Kornelija Buivydaitė	^{99m}Tc-BSA-Au bioconjugates – potential *in vivo* imaging agents for diagnostics
P48	Alėja Marija Daugėlaitė	Mesenchymal Stem Cells and Rare Earth Nanoparticles – a Potent Combination for Photodynamic Therapy of Cancer
P49	Aušra Sasnauskienė	Molecular and cellular aspects of intracellular delivery of bacteriophage-derived nanoparticles
P50	Emilija Januškaitė	Photostability of Cd and Cu based quantum dots in different biological media
P51	Mindaugas Kazlauskas	Effect of quantum dots on green algae *Scenedesmus quadricauda* in various media
P52	Emilė Pečiukaitytė	Accumulation of Quantum Dots and Chlorin e6 Complex in Distinct Phenotypes of Human Colon Cancer Cells
P53	Agnė Bučaitė	Toxicity of Polystyrene Nanoparticles on Salmonid Fish
P54	Augustas Morkvėnas	Does morphology matter? Toxicity and magnetic properties of $GdPO_4:Eu^{3+}$ nanoparticles
P55	Renata Butrimienė	Influence of graphene oxide on the accumulation of metals in *Salmo trutta* at early life stages
P56	Džiugas Jurgutis	Measuring Microviscosity of Lipid Droplets in Human Breast Cancer Cells via Fluorescence Lifetime Imaging
P57	Rimantė Bandzevičiūtė	Application of Fiber-based FT-IR ATR Spectroscopy for Tissue Diagnostics During Oncological Surgery
P58	Gerda Anužienė	Identification of Pathogenic Bacteria and Fungi by means of ATR-IR spectroscopy
P59	Ilya Balmages	Use of a laser speckle system in the determination of antibacterial susceptibility by the disc diffusion method
P60	Justinas Baleišis	Picosecond-domain Nd: YAG laser in vivo study on tattoo removal and microlesion healing dynamics
P61	Goda Mažeikaitė	Spectrophotometric measurements of natural photosensitizers: sodium and copper chlorophyllins
P62	Rasa Miliukaitė	Photoadaptation of Unicellular Algae Cells: Spectroscopic Studies
P63	Aušrinė Navickaitė	Investigation of Autofluorescence of Characean *Nitellopsis obtusa* Cells
P64	Agnė Kalnaitytė	Phototoxicity of CdSe/ZnS-COOH quantum dots with microalgae cells: spectroscopic and microscopic studies
P65	Alexey Lihachev	Dynamic laser speckle imaging for estimation of microbial growth activity
P66	Andrej Dementjev	Recognition of thymine microcrystals by CARS and SHG microscopy
P67	Simona Šalčiūnaitė	Custom-built magnetic tweezers microscope for single-molecule force measurements
P68	Mohammad Nour Alsamsam	The miEye: Bench-top super-resolution microscope with cost-effective equipment
P69	Miglė Šarpilo	Mechanism of CRISPR-Cas3 helicase using magnetic tweezers
P70	Martynas Maciulevičius	The inactivation of Bacteria using Ultrasonic Techniques

Oral Presentations

Cyclic AMP signaling in the normal and failing heart: Compartmentation and therapeutic implications

Rodolphe Fischmeister[1]

[1]Université Paris-Saclay, INSERM UMR-S 1180, Orsay, France
rodolphe.fischmeister@inserm.fr

Cyclic nucleotide phosphodiesterases (PDEs) modulate the neuro-hormonal regulation of cardiac function by degrading cAMP and cGMP. In cardiomyocytes, multiple PDE isozymes with different enzymatic properties and subcellular localization regulate local pools of cyclic nucleotides and specific functions. In this talk, I will describe cAMP signalling in cardiomyocytes, its control by PDE2 and PDE4 as well as their modifications in pathological cardiac hypertrophy and heart failure (HF). I will also present evidence pointing to the concept of PDE activation that could have future therapeutic potential in HF.

Keynote Presentation

Regulating light harvesting in oxygenic photosynthesis

Herbert van Amerongen[1,2]

[1]Laboratory of Biophysics, Wageningen University, Stippeneng 4, Wageningen, The Netherlands.
[2]MicroSpectroscopy Research Facility, Wageningen University, Stippeneng 4, Wageningen, The Netherlands.
herbert.vanamerongen@wur.nl

Photosynthetic organisms are crucial for life on Earth as they provide food and oxygen and are at the basis of most energy resources. They have a large variety of light-harvesting strategies that allow them to live nearly everywhere where sunlight can penetrate. They have adapted their pigmentation to the spectral composition of light in their habitat, they acclimate to slowly varying light intensities and they rapidly respond to fast changes in light quality and quantity. These regulatory processes are particularly important for oxygen-producing organisms because an overdose of light in combination with oxygen can be lethal [1]. The study of light harvesting and its regulation is not only a fascinating research field in itself, it will hopefully also provide the knowledge that is required for optimizing light harvesting in algae and plants to improve light-driven production processes.

Cryo-electron microscopy has recently started to allow the determination of near-atomic resolution structures of so-called supercomplexes of photosystems I and II, which can be even larger than 1 MDa. These structures lie at the basis of the light-harvesting reactions in photosynthesis. Together with the insights obtained from numerous spectroscopic studies these structures help to understand the primary processes in oxygenic photosynthesis [2] and this will be illustrated with several examples.

Now that we have so much structural and spectroscopic information about purified and isolated (super-)complexes it is important to study the (ultra)fast light reactions *in vivo* to see the photosystems at work in their natural environment, where additional elements are present and regulation can be studied. For this *in vivo* research, spectroscopy methods can be combined with microscopy to obtain molecular, structural and functional information of those dynamic systems. Several examples will be given of recently studied regulatory processes of light harvesting *in vivo* and how they can differ at the molecular and cellular level in different organisms. Finally, new directions for future biophysical research for the study of photosynthesis will be discussed.

[1] R. Croce, H. van Amerongen, *Nature Chem. Biol.* **10**, 492-501 (2014).
[2] R. Croce, H. van Amerongen H *Science* 369: eaay2058 (2020)

Keynote Presentation

PAAO Based Hybrid Multilayers for Colorimetric and Interferometric Optical Sensing

Juris Prikulis, Uldis Malinovskis, Raimonds Poplausks, Aleksandrs Dutovs, Donats Erts

University of Latvia, Institute of Chemical Physics, Raiņa bulvāris 19, Riga, Latvia
juris.prikulis@lu.lv

Porous anodic aluminum oxide (PAAO) is a fascinating material, that can be grown into highly regular self-organized nanostructured layers using a variety of protocols [1]. The layer morphology (distance between pores, pore diameter, ranging from tenths to hundreds of nanometers) is generally determined by the choice of electrolyte and the anodization voltage, whereas layer thickness can be controlled by anodization time. PAAO synthesis is a very accessible method and can produce low-cost templates for the deposition of different other materials, creating new hybrid systems that can express multiple physical phenomena and simultaneously provide several useful functions for sensing. For instance, after deposition of a thin gold film on anodized aluminum surface one obtains a nanostructured Aluminum-PAAO-Gold (metal-insulator-metal, MIM) system which supports localized and propagating surface plasmon modes as well as Fabry–Pérot like resonances [2]. An alternative MIM structure was produced using capillary force assisted colloidal nanoparticle assembly on PAAO pore openings [3]. Another example of hybrid systems is a high-density array of photoluminescent ZnO nanorods that was synthesized in PAAO pores using atomic layer deposition (ALD) technique [4].

The obtained structures have a large exposed surface area, which can interact with the surrounding medium and is essential for high speed and high sensitivity devices. The presence of the analyte can conveniently be detected as a shift of resonance wavelength or change of the peak intensity using various optical configurations, such as extinction, reflection, photoluminescence (PL) or dark-field setups. However, a careful tuning of substrate geometry is required to benefit from the interplay of the different physical processes that can coexist in the hybrid multilayers. In particular, we demonstrate that PAAO layer thickness tuning can be used to maximize the signal intensity or refractometric sensitivity.

The PAAO layers were synthesized using two stage anodization protocol in 0.3M oxalic acid electrolyte at 40V potential difference. The process was modified to produce PAAO with a variable thickness on the same sample. During the second anodization both electrodes were simultaneously pulled out of the electrolyte solution [2]. Wedge-shaped PAAO layers on Aluminum surface with a thickness gradient ~100 nm/mm were obtained by the selection of the withdrawal speed ~5 mm/min. Thereafter the active sensor layer (ZnO for photoluminescence or Au nanostructures for plasmonic sensing) was deposited on the variable thickness PAAO template. The optical sensor setup was built on a standard fluorescence microscope with a Hg lamp light source and an imaging device (interferometric sensing) or fiber coupled to a spectrometer (colorimetric sensing). For MIM type substrates an S-polarized light source at a 60° incidence angle was used.

Several visible photoluminescence components, which correspond to different types of ZnO defects were identified upon illumination with UV light. By variation of PAAO layer thickness the intensity of individual components could be enhanced or suppressed. The intensity variation of any individual PL component correlated well with anti-reflective properties of ZnO NR–PAAO composite film at the peak wavelength of the particular PL component. This provides a route for selective enhancement or suppression of color components of hybrid fluorescent emitters by tuning only geometric parameters, with potential use in imaging and other optical devices. As an application example we tested the composite film for sensing of human proteins, specifically, vascular endothelial growth factor (VEGF). The intensity of the yellow and green PL components reduced in response to increased VEGF concentrations, whereas blue component remained invariant.

The two MIM type substrates showed similar behavior, namely, that the elastically scattered light upon angled illumination was maximized at specific PAAO thickness and wavelength combinations. In the case of Au film with nanoholes on PAAO, a distinct scattering maximum at $\lambda = 600$ nm vacuum wavelength occurred at 370 nm PAAO thicknesses. For the Au nanoparticle arrays similar effect was observed at $\lambda \approx 550$ nm and ≈ 350 nm PAAO thickness, but only for 60 nm, and 80 nm diameter and not 40 nm diameter particles. This gives a clear advantage for maximizing the signal to background ratio with the PAAO thickness in a narrow range between 300 nm and 375 nm. The best sensitivity expressed as the peak wavelength shift per refractive index unit (RIU) was found for 60 nm Au nanoparticles on 500 nm thick PAAO exceeding 200 nm/RIU.

For the interferometric detection the patterns in the recorded images were matched against refractive index changes. Similar to colorimetric setups, the sensitivity was improved at specific PAAO thickness.

In conclusion, variable thickness PAAO substrates have enabled performance optimization in several different multilayer architectures in various optical sensor configurations. Furthermore, the characterization and parameter tuning can be done using optical-only methods instead of analysis using electron microscopy. This makes the synthesis method easily reproducible and suitable for scalable production.

Funding: Latvian Council of Science fundamental and applied research project LZP-2020/1-0200.

[1] G. D. Sulka, "*Highly Ordered Anodic Porous Alumina Formation by Self-Organized Anodizing.*" In Nanostructured Materials in Electrochemistry, 1–116. Wiley-VCH Verlag GmbH & Co. KGaA, 2008.
[2] R. Poplausks, D. Jevdokimovs, U. Malinovskis, D. Erts, J. Prikulis. *ACS Omega* **3**, 5783–88 (2018).
[3] U. Malinovskis, R. Poplausks, D. Erts, K. Ramser, S. Tamulevičius, A. Tamulevičienė, Y. Gu, J. Prikulis. *Nanomaterials* **9**, 531. (2019)
[4] U. Malinovskis, A. Dutovs, R. Poplausks, D. Jevdokimovs, O. Graniel, M. Bechelany, I. Muiznieks, D. Erts, J. Prikulis. *Coatings* **11**, 756 (2021)

Invited Presentation

Nanostructured silicon - a platform for biophotonics

Vladimir Sivakov[1]

[1]Leibniz Institute of Photonic Technology, Dept. Functional Interfaces, Albert-Einstein Str. 9, 07745 Jena, Germany
vladimir.sivakov@leibniz-ipht

The future of modern society is tied to the availability of sustainable energy resources and effective diseases diagnostics and therapy. Over the last years, top-down and bottom-up silicon nanostructures have been favored in my group at Leibniz IPHT [1-3] as a promising highly effective optoelectronic and (bio)photonic material due to a number of unique physical-chemical properties. In frame of presented paper I am going to speak about three concepts related to the biosensing and theranostics applications based on silicon technology.

The targeted scientific breakthrough of the first task is related to the controlled and self-organized process of localized nanostructures in porous silica matrix on silicon surface where dielectric pores are selectively filled by plasmonically active metals [4-6]. The results presented in this part are highly useful for the design of plasmonic-active surfaces for surface enhanced Raman spectroscopy-based detection of ultra-low concentration of different chemical or biological analytes, where the size of the localized nanostructures is comparable with the spot area of the focused laser beam.

From another side, Surface Enhanced Raman Spectroscopy (SERS) in the deep UV range (< 300 nm) has not yet been systematically explored and applied, but it could be very promising for the structural analysis of proteins and DNAs. For that reason, it is necessary to find cost-efficient and effective alternatives, which could also be used for SERS in broad spectral range, between UV and IR range (250 nm and 800 nm). One of the candidates is a metallic tin (Sn) and metal/metal oxide core-shell structures. In this part I will present a novel effect [7] that corresponds to the disproportionation of thermodynamically stable tetragonal tin dioxide (SnO_2) phase along the silicon nanowire length to lower tin states such as tin monoxide (SnO) and metal tin (β-Sn) on nanostructured silicon surfaces, compared with pure SnO_2 phase on planar surface.

In the last part of my presentation I will discuss nanoparticles of mesoporous silicon (PSi NPs) which have undeniable advantages when used as nanocontainers (NCs) for the drug delivery, due to their unique properties, such as high biocompatibility, biodegradability in non-toxic silicic acid, high loading efficiency for the delivery of both hydrophilic and hydrophobic drugs, adjustable sizes of meso-pores for the delivery of molecules of different sizes, the possibility of chemical functionalization for targeted delivery [8-10].

[1] T. Ming, B. Dietzek-Ivanšić, X. Lu, X. Zuo, V. Sivakov. *ACS Applied Energy Materials* **5**(6), 7466–7472 (2022).
[2] T. Ming, S. Turishchev, A. Schleusener et al. *Small* **17** (8), 2007650 (2021).
[3] S.Y. Turishchev, E.V. Parinova, A.K. Pisliaruk et al. *Sci Rep* **9**, 8066 (2019).
[4] L. A. Osminkina, O. Žukovskaja, S. N. Agafilushkina et al., *Appl. Surf. Sci.* **507**, 144989 (2020).
[5] O. Žukovskaja, S. Agafilushkina, V. Sivakov et al. *Talanta* **202**, 171-177 (2019).
[6] D. V. Yakimchuk, V. D Bundyukova, J. Ustarroz, H. Terryn et al. *Sensors* **20**(16), 4397 (2020).
[7] P. Liu, A. Schleusener, G. Zieger et al, unpublished (2022).
[8] M. Gongalsky, G. Gvindzhiliia, K. Tamarov et al. *ACS Omega* **4**(6), 10662-10669 (2019).
[9] P. V. Maximchik, K. Tamarov, E. V. Sheval et al. *ACS Biomaterials Science &Engineering* **5** (11), 6063-6071 (2019).
[10] E. Tolstik, M. B. Gongalsky, J. Dierks et al. *Frontiers in Pharmacology* **13**, 962763 (2022).

Invited Presentation

New Architectures of Photon Avalanching Nanoparticles for Sub-Diffraction Imaging

Artiom Skripka[1,2], Minji Lee[1], Bruce E. Cohen[1], P. James Schuck[3], Daniel Jaque[2] and Emory M. Chan[1]

[1]The Molecular Foundry, Lawrence Berkeley National Laboratory, Berkeley, California 94720, United States
[2]Nanomaterials for Bioimaging Group, Departamento de Física de Materiales, Facultad de Ciencias, Universidad Autónoma de Madrid, Madrid, 28049, Spain
[3]Department of Mechanical Engineering, Columbia University, New York, New York 10027, United States
artiom.skripka@uam.es

Lanthanide-doped photon avalanching nanoparticles (ANPs) represent a unique and highly-nonlinear class of upconverting nanoparticles (UCNPs), which under lower-energy near-infrared (NIR) excitation emit higher-energy visible light. In ANPs a small increase in the laser excitation power (e.g. by 1%) can lead to a dramatic enhancement of the emission intensity (e.g. 100%). This is due to the exponential scaling of emission intensity with excitation power density ($I \sim P^s$) by a factor, *s*, which represents the nonlinearity of an upconversion process.

The nonlinearity factor, *s*, can reach values of 30 and higher for photon avalanching process vs. 2-5 for the conventional upconversion emission. Although avalanche-like processes in UCNPs have been observed early on,[1] true ANPs, operating at room temperature conditions, were discovered only recently.[2] Due to the highly nonlinear excitation-emission characteristic of these ANPs, they were showcased as optical probes capable of breaking the diffraction limit of conventional laser scanning microscopes, allowing us to resolve structures below 100 nm.

Further development of ANPs is expected to open more possibilities in biomedical applications of sub-diffraction imaging, ultra-sensitive analyte detection, and precision drug delivery. Current research efforts are directed in developing ANPs of varied compositions and architectures – fine-tuned for these specific tasks. Particular improvements are being sought in creating libraries of ANPs for multiplexing applications, in reducing excitation power threshold to initiate photon avalanching processes, and in improving imaging speeds in laser scanning microscopy. These features can be obtained by creating heterostructured core/shell ANPs in which the photon avalanching properties of ions can be adopted by other ions within rationally engineered energy transfer networks. Here, we explore questions associated with developing such ANPs and present a library of heterostructured ANPs that could be fit for undertaking challenges beyond the reach of conventional UCNPs.

[1] E. S. Levy, C. A. Tajon, T. S. Bischof, J. Iafrati, A. Fernandez-Bravo, D. J. Garfield, M. Chamanzar, M. M. Maharbiz, V. S. Sohal, P. J. Schuck, B. E. Cohen, E. M. Chan, Energy-Looping Nanoparticles: Harnessing Excited-State Absorption for Deep-Tissue Imaging. *ACS Nano* **2016**, *10* (9), 8423–8433.

[2] C. Lee, E. Z. Xu, Y. Liu, A. Teitelboim, K. Yao, A. Fernandez-Bravo, A. M. Kotulska, S. H. Nam, Y. D. Suh, A. Bednarkiewicz, B. E. Cohen, E. M. Chan, P. J. Schuck, Giant Nonlinear Optical Responses from Photon-Avalanching Nanoparticles. *Nature* **2021**, *589* (7841), 230–235.

Invited Presentation

Towards the Understanding of Pressure-Induced Protein Phase Transitions

Arvi Freiberg[1,2], Kõu Timpmann[1], Liina Kangur[1]

[1]Institute of Physics, University of Tartu, W. Ostwaldi 1, 50411 Tartu, Estonia
[2]Estonian Academy of Sciences, Kohtu 6, 10130 Tallinn, Estonia
arvi.freiberg@ut.ee

Much of the thermodynamic parameter values that support life are set by the properties of proteins. While the denaturing effects of pressure and temperature on proteins are well documented, their detailed structural nature is rarely revealed. Here, we investigate a cooperative destabilization by hydrostatic high-pressure compression of the sixteen Ca^{2+} binding sites in the cyclic LH1 light-harvesting membrane chromoprotein complexes from calcium-containing sulfur purple bacteria. The native (Ca-saturated) and denatured (Ca-depleted) phases of the complexes are at ambient temperature clearly distinguishable from each other by much-shifted bacteriochlorophyll a exciton absorption bands, serving as innate optical probes in this study. The pressure-induced effects were found irreversible, exposing strong hysteresis in steady-state spectral properties as well as non-exponential and path-dependent pressure-jump relaxation kinetics with half-life constants shortening from tens of hours to minutes across a couple of kilobar pressure range towards compression. Our observations uniquely show a cooperative failure of the LH1 Ca-binding pockets at high pressures (P> ~4 kbar) upon compression and a cooperative reconstruction of the released into the buffer solvent Ca^{2+} ions back into the protein upon decompression at low pressures (P< ~2 kbar).

Invited Presentation

Mapping energy transfer in photosynthetic bacteria in vivo

Donatas Zigmantas[1], Romain Rouxel[1] Julian Lüttig[1,2] and Michael R. Jones[3]

[1]Chemical Physics, Lund University, Lund, Sweden
[2]Institut für Physikalische und Theoretische Chemie, University of Würzburg, Würzburg, Germany
[3]School of Biochemistry, University of Bristol, Bristol, UK

donatas.zigmantas@chemphys.lu.se

The remarkable efficiency of solar energy collection in photosynthetic bacteria is assured by optimized arrangement of chromophores in light-harvesting complexes and by robust connectivity between complexes comprising the photosynthetic unit. While significant progress has been made during recent decades in understanding the energy transfer dynamics within the isolated complexes, information about their functional connectivity in intact cells is still sparse or at least incomplete. A serious challenge for optical studies of energy transfer in intact photosynthetic systems is posed by the great complexity of photosynthetic units, often comprised of hundreds of chromophores. This leads to highly congested spectra, especially at physiological temperature, where absorption lines are very broad. Another obstacle for optical studies is strong light scattering, characteristic for suspensions of photosynthetic cells.

To map and characterize light-harvesting processes in intact photosynthetic cells we use scatter-resistant two-dimensional electronic spectroscopy (2DES) [1]. This non-linear spectroscopy method provides correlation maps between excitation and detection frequencies, which help to elevate spectral congestion problem [2,3]. Here we present physiological temperature measurements of intact cells of the purple bacterium Rhodobacter sphaeroides. Importantly, these measurements were done with relative low intensity laser pulses to avoid complicating annihilation dynamics within individual light-harvesting complexes. We were able to fully map energy transfer processes from light-harvesting complexes LH2 and LH1 down to reaction centers, with ensuing charge separation. As a distinct signature of the last step we observe strong transient electrochromic shift signal of one of the reaction center absorption bands. We then apply global fitting procedure to characterize dynamics of all energy transfer channels in photosynthetic machinery of purple bacteria cells.

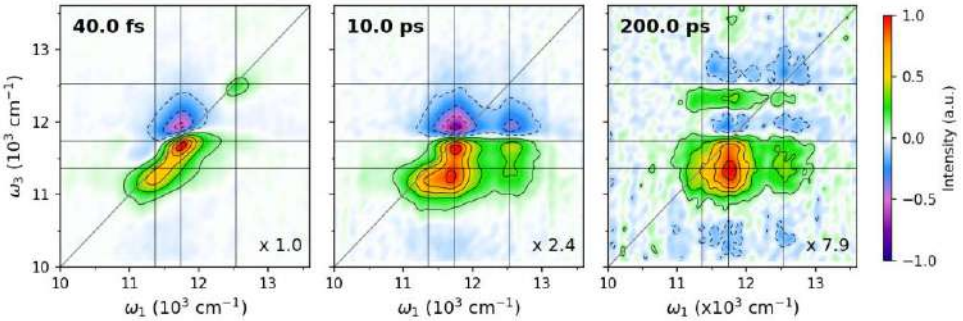

Fig. 1. 2D spectra of Rhodobacter sphaeroides cells at room temperature with at indicated population times, indicating energy transfer and charge separation processes

[1] R. Augulis and D. Zigmantas, *Opt. Express* **19**, 13126 (2011).
[2] J. Dostál, J. Pšenčík, J. and D. Zigmantas, *Nature Chem.* **8**, 705–710 (2016).
[3] P. D. Dahlberg et al., *Nat. Commun*. **8**, 988 (2017).

Invited Presentation

Photosynthetic Structures and their Regulations: Microscopy

Bruno Robert[1], Simona Streckaite[1,2], Cristian Ilioaia[1], Andrew Gall[1]

[1]Institute of Integrative Biology of the Cell, CEA Saclay 91191 Gif sur Yvette, France
[2]Center for Physical Sciences and Technology, Savanorių 231, LT-02300 Vilnius, Lithuania
Bruno.robert@cea.fr

In optical microscopy, the maximum resolution which may be obtained by a microscope is limited by the so-called diffraction barrier, first described by physicist Ernest Abbe in 1874. This limit is close to λ/2, λ being the wavelength used to produce the image. The beginning of this century has seen the development of optical super-resolution fluorescence microscopic methods, which yields pictures to resolutions of a few tens of nanometers. This breakthrough, which has already transformed the field of cellular biology, relies on different approaches, which are generally demanding either in terms of optics or sample preparation, and which all different experimental limitations. We have developed a simple and cheap way of performing super-resolution fluorescence microscopy, based on classical confocal microscopy, but using a detector small as compared to the image of a point fluorophore. In such conditions, confocal microscopy is pushed to its very theoretical limits, and a gain in resolution of 1.4 in every direction can be predicted. Experimentally, a set-up has been constructed, and the measured resolution using a 488 nm wavelength is 180 and 330 nm in the lateral and axial directions, respectively, without any post-processing of the recorded. Such method allows an excellent reconstruction of 3-D volumes of subcellular structures.

We have applied such approach to inner membrane of chloroplasts of different organisms, which dwells the ensemble of proteins involved in the primary steps of photosynthesis. In this case, chlorophyll fluorescence is recorded, and thus gives direct access to the organisation of the photosynthesis apparatus and its remodelling upon light changes. This methodology was also applied on cyanobacteria, to get insight on the spatial organisation of the different photosystems in the photosynthetic membrane of these organisms and suggest a complex partition of these membranes between domains ensuring different functions.

Labeling biomolecules in living cells – are there general rules for probe design?

Gražvydas Lukinavičius[1]

[1]Chromatin Labeling and Imaging research group, Department of NanoBiophotonics, Max Planck Institute for Multidisciplinary Sciences, Am Fassberg 11, 37077 Göttingen, Germany
grazvydas.lukinavicius@mpinat.mpg.de

A large toolbox of fluorescent dyes and proteins enables highlighting cellular structures of interest for following their dynamics in living cells or deciphering fine structural details in the fixed samples. Small fluorescent probes come in particularly handy as they are very easy to use and, most importantly, do not require genetic modification of the cell. These probes are constructed by linking a desired fluorophore to a targeting moiety – a well characterized high affinity drug or inhibitor binding to a particular protein, structure or organelle. Theoretically, this modular design can provide almost endless colour palette of the probes. In practice, finding an optimal fluorophore, ligand and linker combination can make all the difference between useless and top-performing probes. The probes are influenced by multiple factors in the real-world conditions: aggregation, metabolism, off-target interactions, efflux and binding to extracellular structures or proteins (Fig. 1). This is exemplified by examining several series of the probes targeting DNA and cytoskeletal proteins. The optimized probes yield images of outstanding quality in stimulated emission depletion (STED) and single molecule localization (SML) nanoscopy of living and fixed cells.

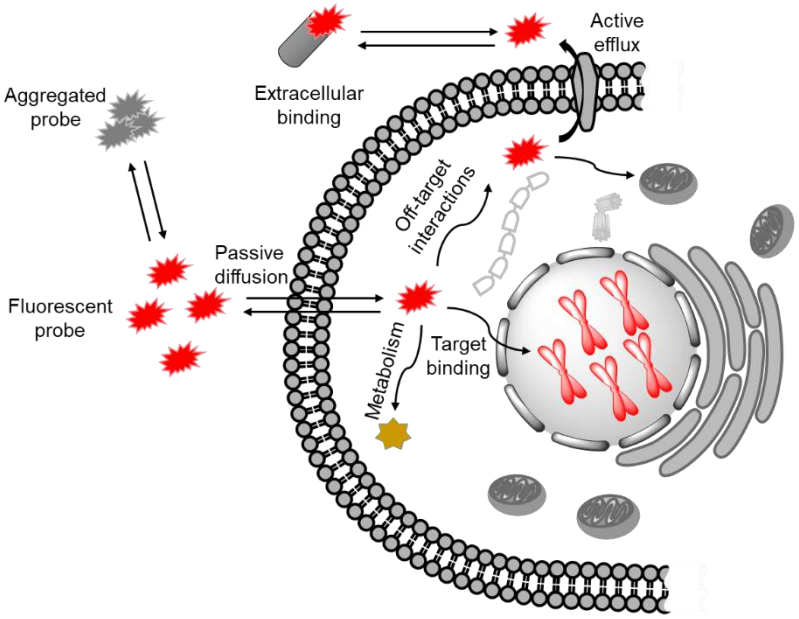

Fig. 1. The possible interactions which are influencing behaviour of the cell membrane permeable fluorescent probes.

Invited Presentation

Phosphorylation of Cx43 by Ca^{2+}/calmodulin kinase II increases the sensitivity of Cx43 gap junction channels to chemical gating

Vytenis Arvydas Skeberdis, Rokas Mickus, Vytautas Raškevičius

Lithuanian University of Health Sciences, Institute of Cardiology, Laboratory of Cell Culture,
Sukilėlių pr. 15, Kaunas, Lithuania
arvydas.skeberdis@lsmuni.lt

Connexin (Cx)-based gap junction (GJ) channels provide a direct pathway for electrical and metabolic signaling between adjacent cells. GJ channels are formed of two apposing hemichannels and each hemichannel is composed of six Cx subunits. Each Cx protein possesses four alpha helical transmembrane domains, intracellular N- and C-termini, two extracellular loops, and a cytoplasmic loop. Cx43 is responsible for GJ intercellular communication in the majority of tissues. Recently we have identified several new GJ inhibitors derived from nutmeg essential oil [1]. In the current study, we aimed at pharmacological characterization of the effect of one of these inhibitors, monoterpene α-pinene, on Cx43 and Cx43EGFP GJs in HeLa cells using dual whole-cell patch-clamp techniques (Fig. 1a). Unexpectedly, we found that at concentrations close to IC_{50} (27 μM) α-pinene exerted extremely unequal effects ranging from „no effect“ to „full block“ of Cx43 and Cx43EGFP GJ conductance.

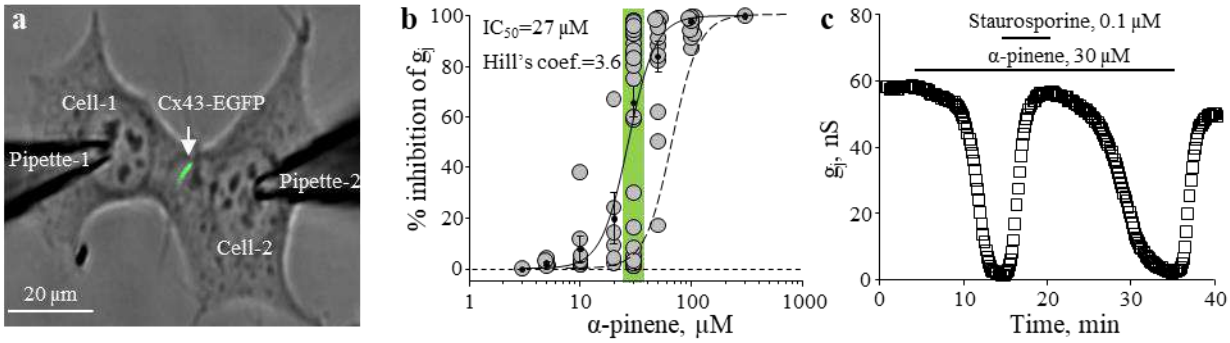

Fig. 1. Modulation of α-pinene effect on Cx43 GJ conductance by staurosporine. (a) By stepping the voltage in the Cell-1 (ΔV_1), junctional current was measured as the change in current in the Cell-2 (ΔI_2) and GJ conductance (g_j) was obtained from the ratio $-\Delta I_2/\Delta V_1$. (b) Dose-dependence of α-pinene effect on g_j (dashed curve corresponds the dose-dependence shift in the presence of 0.1 μM staurosporine). (c) The inhibitory effect of α-pinene on Cx43-EGFP and Cx43 GJs can be completely abolished by non-selective kinase inhibitor staurosporine.

Since the activity of several protein kinases varies along the cell cycle, we guessed that in randomly chosen cell pairs the potency of α-pinene could differ depending on Cx43 phosphorylation levels. In the rat and mouse, Cx43 contains 34 phosphorylatable amino acids in its C-terminus. Indeed, a non-selective inhibitor of protein kinases staurosporine (0.1 μM) completely reversed the effect of α-pinene (30 μM). This effect of staurosporine could be further overcome by higher doses of α-pinene; however, a maximal staurosporine-induced shift of dose-response curve for α-pinene was limited to ~2.5 fold suggesting that phosphorylation could act as an allosteric effector of positive cooperativity. To examine whether α-pinene potency depends on phosphorylation of Cx43 C-terminus, we used Cx43 truncated at amino acid 258 with few remaining phosphorylatable amino acids. Cx43K258Kstop-msfGFP GJ channels remained sensitive to α-pinene but its effect became completely insensitive to staurosporine. More specifically, we demonstrate that the effect of staurosporine could be reproduced by inhibitors of Ca^{2+}/calmodulin-dependent kinase II pathway. Compounds, the potency of which depends on their receptor phosphorylation might be of particular interest in developing targeted therapies for diseases accompanied by high kinase activity, such as cardiac arrhythmias, epilepsy, stroke and cancer.

[1] R.Mickus, G.Jančiukė, V.Raškevičius et al. *Biomed. Pharmacother.* **135**, 111229 (2021).

Conducting polymers improve yeast's electrical properties for better microbial fuel cell development

Viktorija Reinikovaite[1], Eivydas Andriukonis[1,2], Arūnas Ramanavičius[1,2], Aušra Baradokė[1]

[1] Laboratory of Nanotechnology, State Research Institute Center for Physical Sciences and Technology, Sauletekio ave 3, LT-10257 Vilnius, Lithuania;
[2] Department of Physical Chemistry, Faculty of Chemistry and Geosciences, Vilnius University, Naugarduko st. 24, LT-03225, Vilnius, Lithuania;
viktorija.reinikovaite@ftmc.lt

Energy production, storage, and consumption are global issues that are gaining prominence in modern academic disciplines. The potential of coupling waste water cleaning with bioelectricity generation makes yeast an attractive organism for microbial fuel cell development. However, yeast is commonly known to be poor exoelectrogens, therefore improvement strategies are necessary.

In this study, we investigated two electrically conducting polymers (polydopamine (PDA) and polypyrrole (Ppy)) for yeast cell modification to improve charge transfer across the yeast cell membrane/wall. This could potentially help to advance the design of yeast-based microbial fuel cells. The modification utilizing Ppy was based on our previous reports [1]. However, concerns about reduced cell viability over 24-hour modification [2] led us to test shorter modification times. Various modification times with PDA were also examined. The modification with PDA was attempted to control by varying the basicity of the incubation buffer from pH 5.0 to 7.5 [3]. Chemically formed PDA was optically evaluated by utilizing UV/VIS spectrophotometry and FTIR spectroscopy. For subsequent analysis, we constructed a controlled flow-through system with a free-flowing yeast cell to imitate a part of a simplified commercial microbial fuel cell system. The modified cells with both conducting polymers were evaluated electrochemically by subjecting cells to three electrode flow-through system using chronoamperometry; while the generated power density was determined in a two-electrode microbial biofuel cell using potentiometry.

Yeast cell modifications with both conducting polymers increased charge transfer efficiency from cells towards electrodes. Yeast cells, which undergo rather short, a 2-hour long, incubation in polymerization bulk solutions, generated higher electrical current compared to long modification times, and PDA-modified cells generated 5 – 6 times more power density.

Acknowledgments: Dr. Ausra Baradoke is grateful to the European Social Fund (No. 09.3.3-LMT-K-712-23-0159) under a grant agreement with the Research Council of Lithuania (LMTLT)

[1] Andriukonis, E.; Stirke, A.; Garbaras, A.; Mikoliunaite, L.; Ramanaviciene, A.; Remeikis, V.; Thornton, B.; Ramanavicius, A. Yeast-Assisted Synthesis of Polypyrrole: Quantification and Influence on the Mechanical Properties of the Cell Wall. *Colloids Surf. B Biointerfaces* **2018**, *164*, 224–231.
[2] Andriukonis, E.; Ramanaviciene, A.; Ramanavicius, A. Synthesis of Polypyrrole Induced by [Fe(CN)6]3− and Redox Cycling of [Fe(CN)6]4−/[Fe(CN)6]3−. *Polymers* **2018**, *10* (7), 749.
[3] Yang, S. H.; Kang, S. M.; Lee, K.-B.; Chung, T. D.; Lee, H.; Choi, I. S. Mussel-Inspired Encapsulation and Functionalization of Individual Yeast Cells. *J. Am. Chem. Soc.* **2011**, *133* (9), 2795–2797.

Electroporation: a versatile tool for cell and tissue manipulation and therapy

Paulius Ruzgys, Neringa Barauskaitė, Rūta Palepšienė, Baltramiejus Jakštys, Dovilė Uždavinytė, Salvijus Vykertas, Martynas Maciulevičius, Saulius Šatkauskas

Vytautas Magnus University, Faculty of Natural Sciences, Vileikos st. 8, Kaunas, Lithuania
saulius.satkauskas@vdu.lt

Cell exposure to electric field pulses can lead to reversible (EP) or irreversible electroporation (IRE) of prokaryotic and eukaryotic cells. Reversible EP allows bidirectional facilitated transport of bioactive compounds through plasma membrane. This phenomenon has gained wide applications in biotechnology labs as a versatile tool to introduce into cells genetic material as well as other bioactive compounds. On the other hand, IRE provides possibility for nonthermal cell degradation, that has been applied in food industry for extraction of bioactive compounds, food pasteurization and biomass drying. Tool versality and easiness of application allowed translation of electroporation into various clinical trials: irreversible tissue ablation (for cancer and atrial fibrillation patients), antitumor electrochemotherapy, gene electrotransfer and vaccination.

We have recently demonstrated that cells exposed to IRE release various substances, like ATP, proteins, and RNA that potentially may have an immunoregulating effect in vivo. We also showed cells treated with cytotoxic compounds release death associated molecular patterns, that have negative impact on neighbouring cells, what is called bystander effect. We translated these in vitro studies into preclinical studies aiming to find out whether these treatments may have antitumor effect not only on directly treated tumours, but also on secondary, directly non-treated tumours (abscopal effect). Experiments were performed on BALB/c mice bearing two 4T1 tumours on both back flanks. To enhance possible abscopal effect some mice were additionally treated with IL2-coding plasmid electrotransfer into the mice hind limb muscles. The obtained results and possible future directions are discussed.

Platform for Modeling and Analysis of Cell Electroporation and Associated Phenomena

Gintautas Saulis, Rita Saulė

Department of Biology, 58 K. Donelaičio str., Kaunas, Lithuania
gintautas.saulis@vdu.lt

Despite large number of theoretical papers on cell electroporation available, two main obstacles prevent a wide use of existing theoretical models for analysing before experiments, understanding the mechanisms of cell electroporation and related phenomena, and optimizing the technology: 1) the models created are not freely available and/or difficult to use, since only the idea of the model and the equations used are usually published, while the model itself is not available; thus, a reconstruction of the model from scratch is required, 2) the reductionist approach of research is still used, i.e., only single processes occuring in the cell (pore creation, molecular transfer, volume changes) or media (pH changes, release of metal ions) are studied.

The aim of this work was to address these issues. By using *CellDesigner* [1], a platform for modeling and analysis of the processes, occurring during high-voltage pulse not only in the cell but also in the medium, and their consequences has been created. It consists of a core cell electroporation model describing the creation, growth, reduction, and disappearance of pores as well as cell death. Separate models describing various processes can be linked to it.

Transitions between different states of the cell, which show the processes of pore formation, disappearance, enlargement, reduction, and cell death, are described by differential equations. The probabilities that the cell is in electroporated, electropermeabilized, and dead states are described by algebraic equations. This is the modification of the model of cell electroporation, which was used to describe only the processes of pore creation and disappearance [2].

The kinetic scheme of the model along with the equations for the case when just 1 pore can be present in the cell is shown in Fig. 1. In such a case, the model consists of just 4 cell states and 6 transitions between them. As a result, the kinetics is described by the set of 4 differential and 3 algebraic equations. In the case when up to 5 pores can be present in the cell, the number of the states and transitions between them (and corresponding differential equations) increases to 24 and 80, respectively. To describe the case with the largest number of pores in the cell equal to 30, which consists of approximately 500 states, it is necessary to solve the set of about 4200 differential equations.

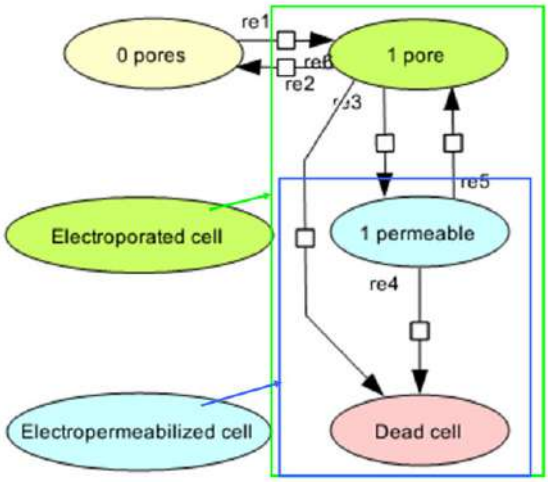

$$\frac{dP_0(t)}{dt} = -k_{f0}P_0(t) + k_r P_1(t)$$

$$\frac{dP_1(t)}{dt} = k_{f0}P_0(t) - \left(k_r + k_{perm} + k_{irr1}\right)P_1(t) + k_{-perm}P_{1p}(t)$$

$$\frac{dP_{p1}(t)}{dt} = k_{perm}P_1(t) - \left(k_{-perm} + k_{irr}\right)P_{p1}(t)$$

$$\frac{dP_{dead}(t)}{dt} = k_{irr1}P_1(t) + k_{irr}P_{p1}(t)$$

$$F_r(t) = P_0(t)$$

$$F_p(t) = P_1(t) + P_{p1}(t) + P_{dead}(t)$$

$$F_{perm}(t) = P_{p1}(t) + P_{dead}(t)$$

Fig. 1. Kinetic scheme of cell electroporation describing the creation, growth, reduction, and disappearance of pores, as well as cell death. The case when only one pore can be present in the cell is shown.

The model has been drawn following Systems Biology Graphical Notation (SBGN) format [3] and stored using the Systems Biology Markup Language (SBML) [4]. This allows to link various models of the processes occurring in the cell (molecular transfer, cell volume changes, cell death, etc.), the medium (equlibration of O_2, electrochemical reactions, etc.), and the whole system (e.g., Petri dish in the incubator) to this core model, provided they are stored using SBML. Upon completion, this models will be submitted to database Biomodels.net, where it will become freely available. Thanks for the user-friendly systems biology software, anyone will be able conveniently to modify the model, simulate, and view the dynamics of the cell electroporation.

[1] A. Funahashi, N. Tanimura, M. Morohashi, and H. Kitano, *Biosilico*, **1**, 159-162 (2003).
[2] G. Saulis, *Food Eng. Rev.*, **2**, 52–73 (2010).
[3] N. Le Novère, M. Hucka, H. Mi et al., *Nat. Biotechnol*. **27**, 735-741 (2009).
[4] M. Hucka, H. Bolouri, A. Finney, et al., *Bioinformatics* **19**, 524-531 (2003).

Sub-microsecond Electrochemotherapy with High Pulse Repetition Frequency

Veronika Malyško-Ptašinskė[1], Eivina Radzevičiūtė[2], Irutė Girkontaitė[2], Jurij Novickij[1], Julita Kulbacka[3], Nina Rembiałkowska[3], and Vitalij Novickij[1]

[1]Institute of High Magnetic Fields and Department of Electrical Engineering, Vilnius Gediminas Technical University, Vilnius, Lithuania
[2]State Research Institute Centre for Innovative Medicine, Department of Immunology, Vilnius, Lithuania
[3]Department of Molecular and Cellular Biology, Faculty of Pharmacy, Wroclaw Medical University, Wroclaw, Poland
veronika.malysko-ptasinske@vilniustech.lt

Electroporation is a phenomenon, which occurs when cell membrane becomes permeable due to short high intense electric pulses, which is used in many fields of application, including electrochemotherapy [1], [2]. Electrochemotherapy is usually performed with microsecond range electrical pulses according to ESOPE (100 µs x 8 pulses) procedures [3]. However, shorter high repetition frequency pulses may result in efficiency-wise ESOPE-equivalent treatment minimizing muscle contractions [4] and thermal damage [5], therefore, sub-microsecond electrochemotherapy is under the scope. Hence, depending on pulsing parameters (pulse duration, strength, repetition, frequency) different approaches on cells response, including viability, are obtained.

This study is covering sub-microsecond electrochemotherapy with bleomycin and doxorubicin on murine Lewis lung carcinoma (LLC1) cell line. Nanosecond electroporation procedures were applied as follows: pulse amplitude (6–10 kV/cm), duration (100–500 ns), and pulse repetition frequency (10 kHz, 100 kHz, and 1 MHz) with bursts of 10 pulses were used. Electric pulses were delivered using 0–3 kV, 100 ns–1 ms square wave high voltage and high up to 1 MHz frequency pulse generator [6] and commercially available 1 mm gap electroporation cuvette. For detection of cell permeabilization, Yo-Pro-1 and flow cytometry were employed. Cell viability was evaluated 24-, 48-, and 72-hours after electroporation. Additionally, for adequate comparison ESOPE protocol was used, and optimal concentrations of bleomycin and doxorubicin were selected.

Obtained results show that LLC1 cells permeabilization rate using nano-second pulses can be manipulated by changing pulsing parameters, i.e. pulse amplitude, repetition frequency and duration. For instance, 10 kV/cm x 200 ns x 10 pulses delivered at 10 kHz frequency, resulted in half of the cells being permeabilized, at the same time for 300 ns pulses, the same level of permeabilization is reached already with 7 kV/cm electric field. When 10 kHz pulses were used, permeabilization higher than 75% was achievable with greater amplitude (8–10 kV/cm) pulses and pulse durations (300–500 ns). Similar response was noticed with 100 kHz pulses. The significant improvement was observed with 1 MHz repetition frequency, where high permeabilization rates could be reached with shorter pulses (200 ns) pulses and 6–8 kV/cm range PEF amplitudes. Additionally, high cell death rates for both drugs were observed with MHz protocols, therefore, were assumed to be most effective. The identical pulses delivered at a lower frequency resulted in a significantly lower cell viability inhibition rate. The efficiency of sub-microsecond electrochemotherapy was saturated already when pulses longer than 200 ns were applied for all PEF amplitudes (6–10 kV/cm).

Our study confirmed that high-frequency sub-microsecond electrochemotherapy with bleomycin or doxorubicin could be an effective alternative for already established ESOPE procedures.

Acknowledgment: The research was funded by the Research Council of Lithuania within the DAINA 2 framework grant No.: S-LL-21-4 (PI: V. Novickij) and supported by National Science Centre (Poland) within a framework of DAINA 2 (2020/38/L/NZ7/00342; PI: J. Kulbacka).

[1] Kotnik, T., Rems, L., Tarek, M. and Miklavčič, D., 2019. Membrane electroporation and electropermeabilization: mechanisms and models. Annual review of biophysics, 48, pp.63-91.
[2] Miklavčič, D., Serša, G., Brecelj, E., Gehl, J., Soden, D., Bianchi, G., Ruggieri, P., Rossi, C.R., Campana, L.G. and Jarm, T., 2012. Electrochemotherapy: technological advancements for efficient electroporation-based treatment of internal tumors. Medical & biological engineering & computing, 50(12), pp.1213-1225.
[3] Marty, M., Sersa, G., Garbay, J.R., Gehl, J., Collins, C.G., Snoj, M., Billard, V., Geertsen, P.F., Larkin, J.O., Miklavcic, D. and Pavlovic, I., 2006. Electrochemotherapy–An easy, highly effective and safe treatment of cutaneous and subcutaneous metastases: Results of ESOPE (European Standard Operating Procedures of Electrochemotherapy) study. European Journal of Cancer Supplements, 4(11), pp.3-13.
[4] Arena, C.B., Sano, M.B., Rossmeisl, J.H., Caldwell, J.L., Garcia, P.A., Rylander, M.N. and Davalos, R.V., 2011. High-frequency irreversible electroporation (H-FIRE) for non-thermal ablation without muscle contraction. Biomedical engineering online, 10(1), pp.1-21.
[5] Mi, Y., Rui, S., Li, C., Yao, C., Xu, J., Bian, C. and Tang, X., 2017. Multi-parametric study of temperature and thermal damage of tumor exposed to high-frequency nanosecond-pulsed electric fields based on finite element simulation. Medical & biological engineering & computing, 55(7), pp.1109-1122.
[6] V. Novickij et al., High-frequency submicrosecond electroporator. Biotechnol. Biotechnol. Equip., vol. 30, no. 3, pp. 607–613, May 2016.

Enhancement and Reversion of Irreversible Electroporation via Osmotic Shock Treatment

Greta Gančytė[1], Povilas Šimonis[1], Arūnas Stirkė[1,2]

[1] Laboratory of Bioelectrics, Center for Physical Sciences and Technology, Lithuania
[2]Micro and Nanodevices Laboratory, Institute of Solid State Physics, University of Latvia, Kengaraga str. 8, LV-1063, Riga, Latvia
greta.gancyte@gmail.com

Saccharomyces cerevisiae yeast employs the HOG pathway to recover after dangerous shape modifications and intracellular water disbalance caused by environmental osmotic pressure changes. Pulsed electric field (PEF) treatment is known to cause plasma membrane permeabilization, an effect known as electroporation. Yet, there is no information on whether the HOG biochemical pathway has a role in yeast response to PEF treatment.

It was investigated if post-PEF osmotic pressure change of the media affects yeast cells' viability, size and if the HOG pathway is involved in recovery. Experiments were performed with wild type (WT) Y00000 yeast and a mutant strain derived from WT, Y02724, with no active *HOG1* gene. Yeast suspension was exposed to a single electric field pulse with a duration of 150 µs and electric field strength of up to 10 kV/cm. Electroporation buffer was used as a reference point to represent isoosmotic conditions. Swift osmotic pressure change is defined as osmotic shock. After PEF treatment, cells were transferred to hyperosmotic, isoosmotic or hypoosmotic solution. Viability was assesed by counting colony forming units. Cell size was evaluated by measuring the turbidity of the solution. Protein and DNA efflux was observed by measuring light absorbtion of the media at 260 and 280 nm wavelengths.

We showed that post-pulsed electric field treatment by a sudden change of osmolarity of the media has a significant impact on the yeasts' viability (Fig. 1), cell size and leakage of intracellular components into the media when compared to isoosmotic conditions. We show that electroporation efficiency depends not only on electric field strength, duration and the number of impulses applied, but also on whether post-PEF treatment was applied. While it is known that electric fields of 8-10 kV/cm cause irreversible damage to the membrane, after incubation in hyperosmotic conditions after PEF, viability increased by ~30% and the radius of the cell was reduced by ~2 µm. After weaker field strengths of 2 and 4 kV/cm PEF and hyperosmotic shock treatment, the viability of WT yeasts was restored to 100 %, for Δ*hog* this result was achieved only after 2 kV/cm treatment. Hipoosmotic shock caused the opposite effect: after exposure to pulse of 4 kV/cm viability decreased by 12 % (WT) and 39 % (Δ*hog*); after exposure to 6 kV/cm pulse, by 16 % and 25 %. The size of the cells almost doubled, after 10 kV/cm treatment. Protein and DNA leakage evaluation revealed that amount of intracellular compounds in the media decreased after hyperosmotic shock and increased after hipoosmotic shock, supporting the hypothesis that mechanical cell shape alteration influences cells' reaction to PEF. Cell membrane recovery rate was also shown to be impacted. Hyperosmotic shock application post-PEF decreased membrane recovery time while hipoosmotic shock lenghthened it. Furthermore, Δ*hog* strain was more sensitive to treatments suggesting that HOG pathway is of relevance to recovery.

To summarise, yeast membrane recovery after exposure to PEF can be altered by subsequent change in osmolarity of media. HOG pathway involvement was linked to recovery after electroporation.

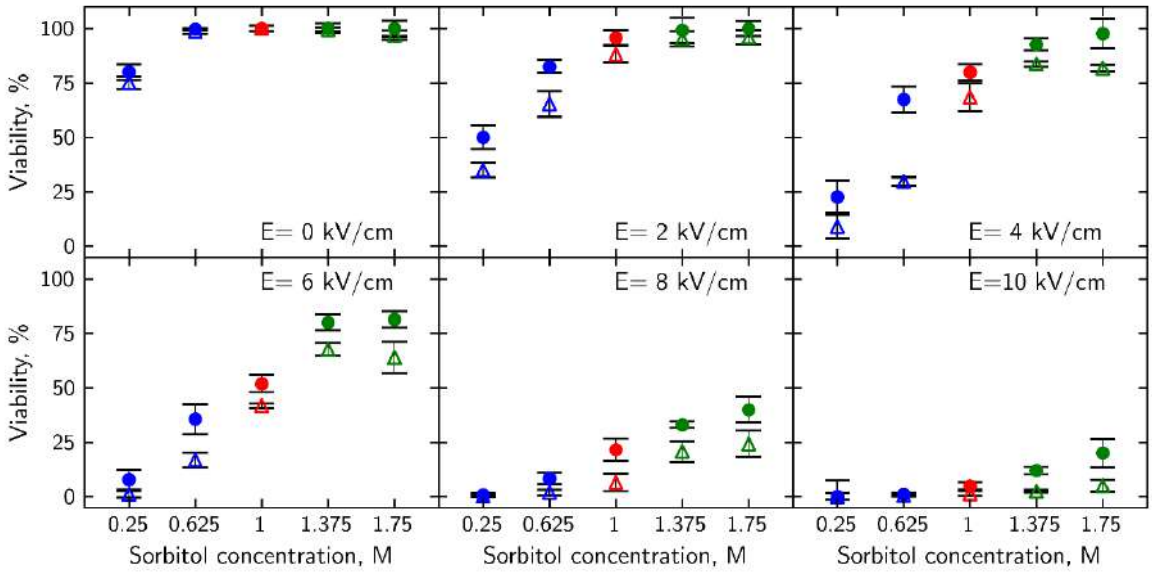

Fig. 1. Osmotic shock effects on the viability of PEF treated yeast cells. WT cells are depicted as filled circles, *Δhog* as hollow triangles. Hyperosmotic shock (0.25 M and 0.625 M sorbitol) depicted in blue, isoosmotic (1 M sorbitol) in red and hypoosmotic (1.375 M and 1.75 M sorbitol) in green.

Electric charge of nanoparticle surface towards its engineered interaction with cell

Yuri Dekhtyar, Dagnis Abols, Lada Bumbure

Riga Technical University, Institute of Biomedical Engineering and Nanotechnologies, Kipsalas str, 6B, Riga, LV1048, Latvia

Attachment of a bio-object (cell/biomolecule) to a surface of the nanoparticle/nanolayer, etc.(nano-object) follows adhesion mechanisms. The latter is significantly controlled with coulomb forces delivering a long-distance interaction.

To engineer the coulomb forces, the surface of the nano-object may be deposited with the electric charge. Approaches (hydrogenation, radiation, doping, surface morphology) to reach these are motivated.

Special attention is given to the diamond nanoparticles processed with ultraviolet radiation.

To identify the surface electric charge deposited with radiation, the electron work function increment of the irradiated substance against the native one was measured. For this, near-threshold photoelectron emission was employed. Fig. 1 demonstrates that the electron work function increases when radiation exposure rises. This means that the surface charge moves to a negative value because of radiation.

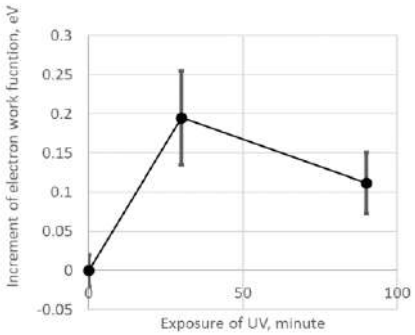

Fig. 1. The electron work function increment of the diamond nanoparticles in dependence on their ultraviolet exposure.

Yeast cell were used as the model to be attached to the particles. Cell-particle complex provision was identified due to cell-particle water solution optical absorbance in time relaxation. The latter characterised segregation the cell-particle complexes. The optical absorbance diagrams were approximated with exponential functions within the time interval of full relaxation. Exponential functions at several time intervals (t) were used, each function having a specific relaxation time constant (τ). Fig. 2 presents τ in dependence on radiation exposure.

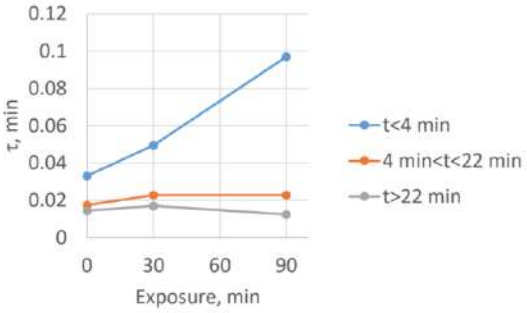

The relaxation time constant at t< 4 minutes increases with the growth of exposure. This evidence that radiation deposited positive electric charge of the diamond surface nanoparticles induces cell-particle complexes.

The results indicate that irradiated particles demonstrated around two times higher ability to develop cell-particle complex against non-radiated particles.

Acknowledgment: The research was supported with the Horizon ERA-Net project ES RTD/2021/4 “Bioactive cardiovascular stent for antiatherosclerosis treatment and reduced restenosis” (CARANAT)

The size, shape and crystal structure of metal nanoparticles influence on their ultrafast plasmonic properties

Domantas Peckus[1], Nadzeya Khinevich[1], Asta Tamulevičiene[1,2], Joel Henzie[3], Karine Mougin[4,5], Arnaud Spangenberg[4,5], Tomas Tamulevičius[1,2], Sigitas Tamulevičius[1,2]

[1]Institute of Materials Science of Kaunas University of Technology, K. Baršausko st. 59, LT-51423, Kaunas, Lithuania

[2]Department of Physics, Kaunas University of Technology, Studentų st. 50, LT-51368, Kaunas, Lithuania

[3]International Center for Materials Nanoarchitectonics (WPI-MANA), National Institute for Materials Science (NIMS), Tsukuba, 305-0044, Japan

[4]Institut de Science des Matériaux de Mulhouse IS2M UMR 7361, 15 rue Jean Starcky, F 68100 Mulhouse, France

[5]Université de Strasbourg, 4 Rue Blaise Pascal, CS 90032, F-67081 Strasbourg, France
domantas.peckus@ktu.lt

Recently, plasmonic metal nanoparticles due to their unique localized surface plasmon resonance (LSPR) properties have demonstrated great promise in various electro-optical applications like biosensors, solar cells, lasers, photocatalysis, nonlinear optics, medicine, etc. [1]. The practical use of these nanoparticles depends on the metal, their shape, size, homogeneity and crystal structure. At the moment, gold and silver nanoparticles show the best promising results for practical applications, because of their stability and well-developed synthesis procedures. The advanced synthesis methods of gold nanoparticles allow preparing high-quality nanoparticles of various shapes, such as spheres, nanorods, bipyramids, and decahedra, etc. [1, 2], while silver nanoparticles can be formed in the shapes of nanocubes, spheres, or triangles [1].

In our research, we demonstrated the method of transient absorption spectroscopy (TAS) as a perspective tool for the analysis of the plasmonic and optomechanical properties of various crystal structures and the size/shape of gold or silver nanoparticles. In addition to the TAS measurements, we have used steady-state UV-vis absorption, scanning electron microscope, transmission electron microscopy (TEM), and X-ray diffraction method. We have analyzed gold nanoparticles of different shapes, such as nanorods, decahedra, and spheres (Fig. 1) prepared by methods of wet chemical synthesis, and they have demonstrated different steady-state absorption spectra due to LSPR properties [2]. We also analyzed different crystalline structures of various sizes silver nanoparticles influence on plasmon ultrafast relaxation dynamics.

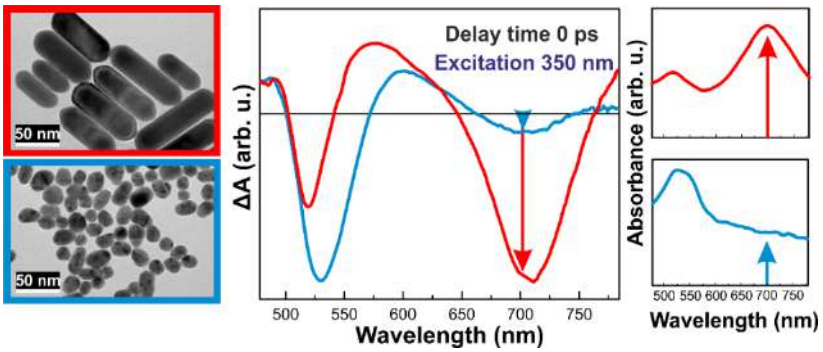

Fig. 1. Summary of gold nanoparticle shape-influenced differences in TAS spectra that are hindered in steady-state UV-VIS spectra

The TAS was found to be an efficient technique for the detection of small amounts of gold nanorods in the sample where Au nanospheres dominate. While optomechanical oscillation can give information about the size, and homogeneity of sizes of metal NPs.

TAS is able to detect differences in the crystallinity of the different size silver NPs. That could be useful for the structural analysis of plasmonic metal nanoparticles in the future.

Our research has shown that TAS can be an effective tool for crystal structure evaluation, shape/size analysis, and control of gold and silver nanoparticles.

Acknowledgements. This research was performed within a project LaSensA under the M-ERA.NET scheme and was funded by the Research Council of Lithuania (LMTLT), agreement No. S-M-ERA.NET-21-2, National Science Centre (Poland) agreement No. UMO-2020/02/Y/ST5/00086, Saxon State Ministry for Science, Culture and Tourism (Germany) and co-financed with tax funds based on the budget passed by the Saxon state parliament.

[1] G.V. Hartland, *Chem. Rev.* **111**, 3858-3887 (2011).
[2] D. Peckus et al, *Opt. Express* **30,** 27730 (2022).

The bioaccumulation of nanoparticles during fish development: towards a deeper understanding of potential nanotoxicity

Živilė Jurgelėnė[1,2], Augustas Morkvėnas[1,4], Nijolė Kazlauskienė[2], Danguolė Montvydienė[3], Ričardas Rotomskis[1,3], Vitalijus Karabanovas[1,3,4]

[1]Biomedical Physics Laboratory, National Cancer Institute, Baublio 3b, LT-08406, Vilnius, Lithuania
[2]Nature Research Centre, Akademijos st.-2, LT-08412 Vilnius, Lithuania
[3]Biophotonics Group of Laser Research Centre, Vilnius University, Saulėtekio Ave. 9, LT-10222 Vilnius, Lithuania
[4]Department of Chemistry and Bioengineering, Vilnius Gediminas Technical University, Sauletekio Ave. 11, LT-10223 Vilnius, Lithuania
zivile.jurgelene@nvi.lt

Nanoparticles (NP) are extensively examined in biomedicine but the understanding of the mechanism underlying the uptake of them by biological systems is still poor [1]. The studies of NP biodistribution in tissues and their possibilities to cross biological barriers, especially at early stages of fish development (embryos, early-stage and late self-feeding alevins) are also still limited [2]. To contribute to answering these questions, we investigated different uptake routes in Salmonidae embryos and alevins, and how they affect quantum dots (QDs) uptake into external tissues and within whole organisms. This is addressed by exposing three different life stages of the Salmonidae using confocal fluorescence microscopy in order to cover the following exposure routes: via chorion; dermal exposure; dietary and dermal exposures. To advance the understanding of the mechanism underlying NPs penetration abilities, we compared 3D reconstruction images of test organisms and 2D images of the histological samples showing a similar QDs fluorescence in the tissues. In our experimental study, we showed that NPs uptake in embryos is restricted by chorion, whereas NPs resulted in adsorption to the gills and eyes in early-stage alevins (Fig. 1). Our study results showed that NPs were predominantly adsorbed onto the intestinal tract of late self-feeding alevins. Results of the performed toxicity tests showed that survival of NPs-exposed test-organism remained statistically unchanged, i.e. no statistically significant changes in test organism's mortality rates were recorded. However, the recorded changes in the heart rate of test organism point to the developmental toxicity induced by NPs aggregates. This study has, for the first time, expressed concern about the probable uptake of QDs in fish and provide more in-depth information of the biodistribution of NPs in aquatic organisms.

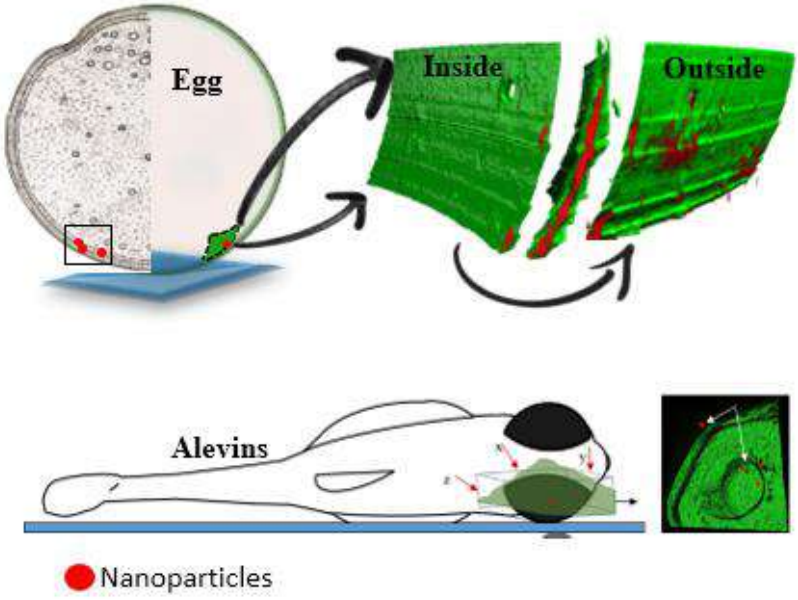

Fig. 1. 3D reconstruction scheme of live fish embryos and alevins

[1] M. van Pomeren, W.J.G.M. Peijnenburg, R.C. Vlieg, S.J.T. et al., *Nanotoxicology*. **13**, 558-571 (2019)
[2] D. K. Khajuria, V. B. Kumar, D. Karasik et al., *ACS Appl. Mater. Interfaces*, **9**, 18557−18565 (2017)

Molecular structure and electronic excitation dynamics in FCP complex

Andrius Gelzinis[1,2], Austėja Mikalčiūtė[1,2], Mindaugas Mačernis[1], Ramūnas Augulis[2], Claudia Büchel[3], Bruno Robert[4], Jevgenij Chmeliov[1,2], Leonas Valkunas[1,2]

[1]Institute of Chemical Physics, Faculty of Physics, Vilnius University, Vilnius, Lithuania
[2]Department of Molecular Compound Physics, Center for Physical Sciences, Vilnius, Lithuania
[3]Institute of Molecular Biosciences, Goethe University Frankfurt, Frankfurt, Germany
[4]Université Paris-Saclay, CEA, CNRS, Institute for Integrative Biology of the Cell (I2BC), Gif-sur-Yvette, France
andrius.gelzinis@ff.vu.lt

Diatoms are a major group of marine algae, responsible for a significant part of the global primary production on planet Earth. Their adaptation to aqueous environment is ensured by their major light-harvesting complex (LHC) – the fucoxanthin-chlorophyll protein (FCP) complex, which exhibits different pigment composition than LHCs of plants and absorbs strongly in the blue–green spectral region due to the presence of chlorophyll (Chl) *c* and fucoxanthin. Only in 2019 the 3D structures of several FCP complexes were obtained. The structure of an FCP dimer for the pennate diatom *Phaeodactylum tricornutum* was resolved by crystallography [1] while the structure of the PSII-FCP supercomplex from the centric diatom *Chaetoceros gracilis* was obtained by electron microscopy [2,3]. We evaluated how these available FCP structures may account for previously obtained 2D spectroscopy results on FCP from another centric diatom *Cyclotella meneghiniana* and found that the published FCP structures are somewhat at odds with a few observations obtained from ultrafast spectroscopy. We constructed a trimer-based FCP model for *Cyclotella meneghiniana* (see Fig. 1), that is consistent with experimental data [4].

Furthermore, we used the crystallographic information on the FCP complex from *Phaeodactylum tricornutum* diatom together with quantum chemistry-based calculations to evaluate the Chl transition dipole moments, atomic transition partial charges from electrostatic potential, and the couplings between Chls in this complex [5]. The obtained structure-based excitonic couplings should form the foundation for further modelling of stationary and time-resolved spectroscopic data. In addition, we also calculated the inter-pigment Förster energy transfer rates and identified two quickly equilibrating chlorophyll clusters.

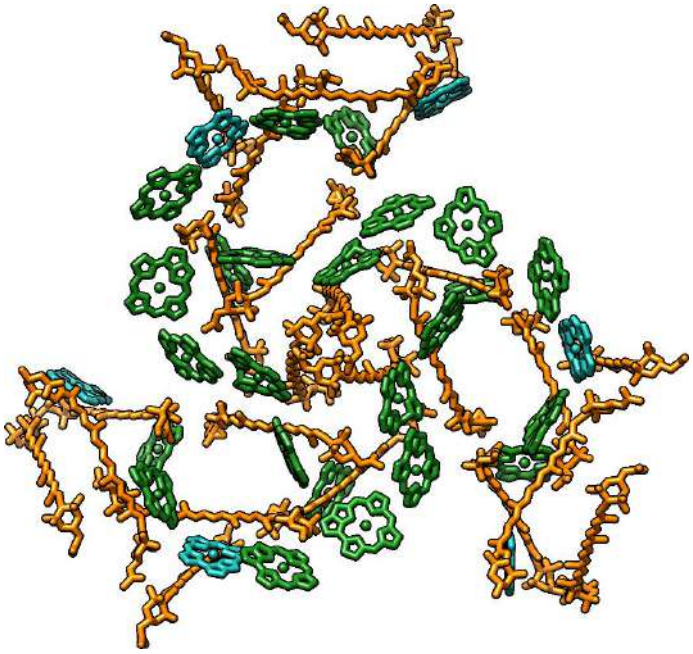

Fig. 1. Proposed trimer-based FCP structure for *Cyclotella meneghiniana*. Chlorophyll *a* are colored in green, chlorophyll *c* in light blue and fucoxanthin in orange. For clarity, Chls are only shown as porphyrins.

Acknowledgement: This project has received funding from European Regional Development Fund under grant agreement No 01.2.2-LMT-K-718-03-0048 with the Research Council of Lithuania (LMTLT).

[1] W. Wang et al., *Science* **363**, 6427 (2019).
[2] Pi et al., *Science* **365**, 6452 (2019).
[3] Nagao et al., *Nat. Plants.* **5**, 890 (2019).
[4] Gelzinis et al., *Phys.Chem.Chem.Phys.* **23**, 806 (2021).
[5] Mikalčiūtė et al., *J. Chem. Phys.* **156**, 234101 (2022).

Inter-Molecular Charge Transfer States in the Light-Harvesting Complexes

Jevgenij Chmeliov[1,2], Kazimieras Tamoliūnas[1,2], Andrius Gelžinis[1,2], Juozas Šulskus[2], Leonas Valkūnas[1,2]

[1]Center for Physical Sciences and Technology, Department of Molecular Compound Physics, Sauletekio Ave. 3, Vilnius, Lithuania
[2]Vilnius university, Faculty of Physics, Institute of Chemical Physics, Sauletekio Ave. 9, Vilnius, Lithuania
jevgenij.chmeliov@ff.vu.lt

Photosynthetic light-harvesting complexes are an example of such molecular systems that have been thoroughly investigated during the last few decades. Determination of their crystal structure [1] provided possibility to make more precise structure-based calculations and further reveal subtle structure–function relation. Particularly, the thorough analysis of the temperature-dependent time-resolved fluorescence spectra of the aggregates of major light-harvesting complexes from plants (LHCII, see Fig. 1a), binding about the half of all the terrestrial chlorophyll (Chl) pigments, indicated the co-existence of at least 3 distinct conformational states of the LHCII complexes [2]: the dominating light-harvesting state, the quenching state responsible for excitation energy dissipation, and the red-emitting state exhibiting red-shifted fluorescence that becomes more pronounced at low temperatures. Based on simulations of the excitation energy transfer in the LHCII aggregate at various temperatures, we associated the physical origin of these states with the underlying molecular mechanisms, the later red-emitting state having been attributed to the formation of chlorophyll–chlorophyll intermolecular charge transfer (CT) state.

To further investigate which particular Chls participate in the formation of this CT state, we performed quantum chemistry-based calculations on various Chl dimers from the LHCII complex. We also evaluated the influence of the close environment, namely the possible protonation of the nearby amino acids of the surrounding protein scaffold on the energetics of the Chl–Chl CT state. Particularly, we revealed that protonation of the Gln131 amino acid reduces the energy of the inter-molecular CT state of the Chl *a*604–*b*606 dimer, located at the luminal side of LHCII, by almost 0.9 eV. As a result, the energy of the CT state becomes smaller than the energy of the 1st excitonic state, which makes this Chl dimer a good candidate to be responsible for experimentally observed red-shifted fluorescence state of the LHCII complexes.

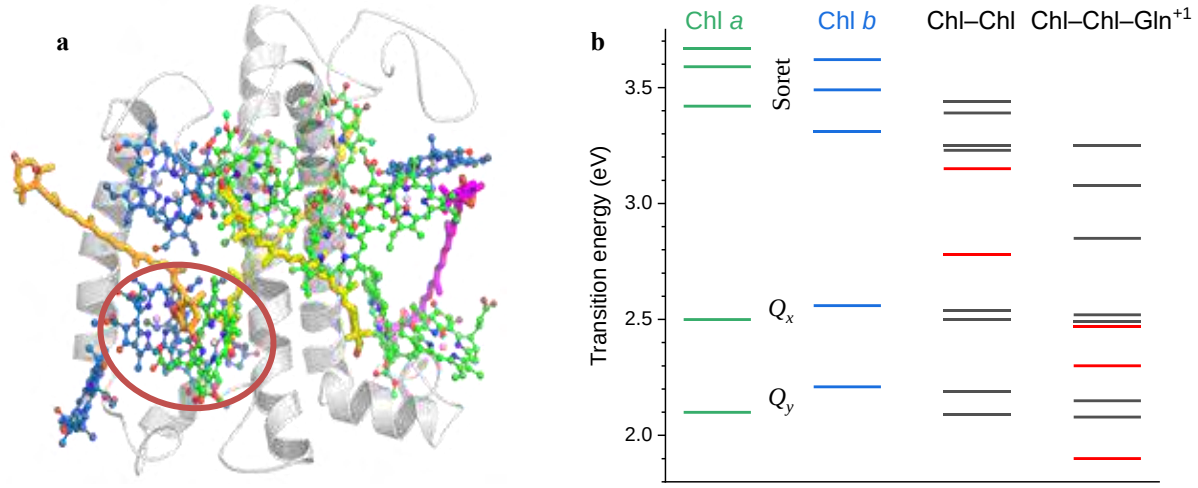

Fig. 1. a) Crystal structure of the LHCII monomer [1]. Chlorophylls *a* and *b* are indicated with green and blue, respectively, the molecular dimer Chl *a*604–*b*606 located at the luminal side of the membrane is highlighted by a circle. (b) Calculated energy spectrum of the Chl *a* and Chl *b* pigments, the Chl *a*604–*b*606 molecular dimer, and the charged Chl*a*604–Chl*b*606–Gln131^{+1} trimer with the protonated amino acid. Red bars indicate inter-chlorophyll charge transfer states.

Acknowledgement: The research was supported by the Research Council of Lithuania (LMT grant no. S-MIP-22-75)

[1] Z. F. Liu, H. C. Yan, K. B. Wang, et al., *Nature* **428**, 287–292 (2004).
[2] J. Chmeliov, A. Gelzinis, E. Songaila, R. Augulis, C. D. P. Duffy, A. V. Ruban, and L. Valkunas, *Nature Plants* **2**, 16045 (2016).

Protein kinase-sensitive tandem photoluminescent probes possessing Förster-type resonant energy transfer from a donor phosphor to a fluorophore

Asko Uri, Erki Enkvist

University of Tartu, Institute of Chemistry, 14A Ravila St., 50416 Tartu, Estonia
asko.uri@ut.ee

Protein kinases have been the most important target proteins for the cancer drug development in this century, resulting in more than 70 FDA-approved medicines in clinic. New chemical and photoluminescent probes are needed to support further developments in this field.

We have constructed [1] purely organic tandem ARC-Lum(Fluo) probes for protein kinases of the AGC group that upon excitation with a flash UV-light (350 nm) reveal strong long-lifetime (τ= 30 -250 µs) signal in orange or red spectral region if bound to the enzyme (Figure). The latter molecule hinders molecular motions and shields the phosphor's excited triplet state from the effect of dissolved molecular oxygen and other quenchers. Free probes in buffer solution possess no such property.

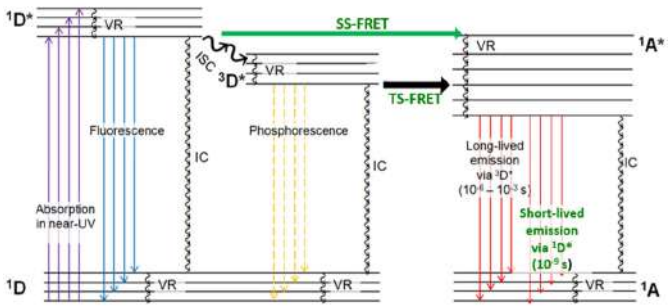

Figure. The Jablonski diagram of energy transfer mechanisms of ARC-Lum(Fluo) probes.

The phosphor-sensitized fluorescence occurs as the result of efficient radiationless energy transfer from the excited dim phosphor to the nearly positioned fluorescent dye by Förster-type resonant energy transfer (TS-FRET) mechanism, leading to huge amplification of luminescence intensity of the distinct phosphor. ARC-Lum(Fluo) probes are powerful tools for biomedical studies.

TS-FRET mechanism was theoretically proposed by Theodor Förster in 1959 [2]. The phenomenon was first experimentally demonstrated for intermolecular energy transfer from a donor phosphor to an acceptor chromophore at 93 K by Ermolaev and Sveshnikova in 1962 [3]. Unfortunately, organic materials utilizing TS-FRET mechanism and possessing unique luminescent properties have not found wider practical use before.

1. E. Enkvist et al, ACS Chem. Biol. (2011) 6, 1052.
2. T. Förster, Discuss. Faraday Soc. (1959) **27**, 7.
3. V. L. Ermolaev, E. B. Sveshnikova, Izv. Acad. Sci. USSR, ser. phys. (1962) **26**, 29.

Hydrodynamics and Intermolecular Interactions Between Proteins Involved in Gene Expression by Fluorescence Correlation Spectroscopy (FCS)

M. K. Białobrzewski[1], A. M. Michaś[1], M. K. Cieplak-Rotowska[2], M. Duszka[1], A. Niedźwiecka[1]

[1]Polish Academy of Sciences, Institute of Physics, Laboratory of Biological Physics, Al. Lotnikow 32/46, 02-668, Warsaw, Poland

[2]Polish Academy of Sciences, The International Institute of Molecular Mechanisms and Machines, Laboratory of RNA Biology, B. Smetany 2, 00-783, Warsaw, Poland
bialy@ifpan.edu.pl

Gene silencing is a process at the post-transcriptional level that interferes with gene expression through a variety of molecular mechanisms. microRNAs are responsible for a recognition of an imperfect complementary sequence at the 3' UTR of the targeted mRNA. This silencing pathway triggers a recruitment of a multiprotein machinery that leads to deadenylation and translational repression. Elucidating the intermolecular mechanism of the interactions between recruited proteins has significant implications for our understanding of miRNA-mediated silencing.
The key molecular hub that is responsible for binding the CNOT1 subunit of the 3' deadenylase complex CCR4-NOT [1] is the glycine and tryptophan rich protein of 182 kDa (GW182) [2]. The C-terminal domain of the GW182 protein is almost completely intrinsically disordered [3]. This domain is involved in the regulation of the intermolecular interactions between GW182 protein and the deadenylase complex CCR4-NOT. Although the crucial GW182 protein sequence motif responsible for interaction with the deadenylase complex has been characterized [5], a role of the RNA Recognition Motif (RRM) remains elusive.

In our work, we present Fluorescence Correlation Spectroscopy (FCS) studies of the hydrodynamic properties of a large set of globular proteins and intrinsically disordered proteins in the context of protein dynasome [6]. We discuss binding affinities and intermolecular interactions of the crucial components of the GW182 Silencing Domain and CNOT1 subunit of the deadenylase complex CCR4-NOT. Our results provide biophysical insights into how local structural feature might contribute to the regulation of the interactions between CNOT1(800-999) fragment and the GW182 protein Silencing Domain.

[1] M. Chekulaeva et al., *Nat. Struct. Mol. Biol.* **18**, 1218-1226 (2011).
[2] J. Braun et al., *Mol. Cell.* **44**, 120-133 (2011).
[3] M. K. Cieplak-Rotowska et al., *J. Am. Soc. Mass Spec.*, **29**, 158-173 (2018).
[4] M. R. Fabian et al., *Nat. Struct. Mol. Biol.* **18**, 1211-1217 (2011).
[5] A. Eulalio et al., *Nucleic Acids Research* vol. **37**, 9 (2009).
[6] U. Hensen et al., *PLoS One*, **7**, e33931 (2012).

Switching the Enzyme-Inhibitor Recognition Profile via Chimeric Carbonic Anhydrases

Joana Smirnovienė[1], Justina Kazokaitė-Adomaitienė[1], Alexey Smirnov[1], Visvaldas Kairys[1], Aurelija Mickevičiūtė[1], Vilma Michailovienė[1], Elena Manakova[1], Lina Baranauskienė[1], Daumantas Matulis[1]

[1]Institute of Biotechnology, Life Sciences Center, Vilnius University, Vilnius, Lithuania
joana.smirnoviene@gmc.vu.lt

The family of human carbonic anhydrases (CA) contains 12 catalytically active isoforms that play a role in various diseases, including cancer, glaucoma, epilepsy, and altitude sickness. Unfortunately, CA inhibitors used as drugs lack selectivity for the target isozyme and cause serious side effects.

To understand the mechanism of inhibitor recognition and selectivity profiles, we have generated chimeric CA that resemble CA Va, CA VI, or CA XII [1, 2]. The off-target isoform - CA II was used as a core, and 5-7 amino acids in the active site were mutated to those specific for CA Va, CA VI, or CA XII. The binding affinities of a series of sulphonamide inhibitors binding to the off-target, chimeric, and target isoforms were determined using isothermal titration calorimetry, enzymatic activity inhibition, and fluorescent thermal shift assays. In addition, X-ray crystallography and computational modeling were used to compare the binding modes of selected inhibitors in the active sites of native and engineered CA isoforms.

The detailed thermodynamic and structural analysis revealed that chimeric CAs recognized and bound inhibitors with similar binding affinities and binding modes as target isoforms (CA Va, CA VI, and CA XII), but not as the off-target isoform CA II. The chimeric CAs were confirmed as valuable models for the design of isozyme-selective inhibitors.

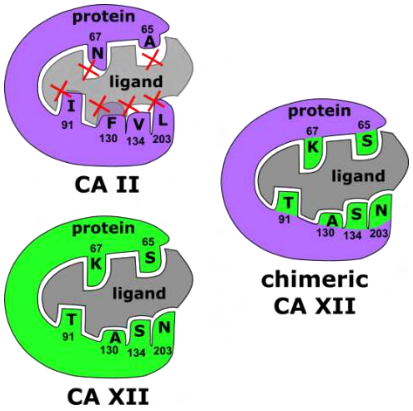

Fig. 1. General scheme for engineering chimeric CA XII [2].

[1] J. Kazokaitė *et al.*, *Sci. Rep.* 9(1):12710 (2019).
[2] J. Smirnovienė *et al.*, *ChemistryOpen* 10(5):567–580 (2021).

Fluorescence microscopy-based studies of individual protein-DNA interactions *in vitro* vs. *in vivo*: challenges, solutions and outcomes

Aurimas Kopūstas[1,2], Mohammad Nour Alsamsam[1,2], Meda Jurevičiūtė[1], Justė Paksaitė[1], Marijonas Tutkus[1,2]

[1]Institute of Biotechnology, Life Sciences Center, Vilnius University, Saulėtekio Ave. 7, 10257 Vilnius, Lithuania
[2]Department of Molecular Compound Physics, Center for Physical Sciences and Technology, Savanorių Ave. 231, 02300 Vilnius, Lithuania
aurimas.kopustas@gmc.vu.lt

Recently, we have developed a high-throughput Soft DNA Curtains platform designed for single-molecule (SM) fluorescence microscopy-based studies of protein-DNA interaction dynamics in real time [1]. This next-generation flow-stretch assay can be used to accurately assess the binding specificity and kinetics of various DNA-binding proteins *in vitro*. Nevertheless, it is most likely that the values of these characteristics are completely different in living cells because of the complex and dynamic environment, where such factors as DNA condensation and other protein molecular crowding majorly affect the interactions between a protein of interest and the DNA. With the current technological breakthroughs and methodological advances in the field, SM fluorescence imaging and super-resolution microscopy became invaluable tools for such studies, since in comparison with more traditional widely used techniques as X-ray crystallography or cryogenic electron microscopy, they not only offer the experimental capabilities *in vivo* but can also provide rather a dynamic than static picture of the aforementioned biomolecular processes. Our newly built cost-effective microscopy system – miEye platform – is capable of performing diverse SM localization microscopy measurements with <5 nm/min stability of the sample on all axes and <30 nm lateral resolution and can be readily applied for probing individual protein-DNA interaction dynamics in living cells.

However, before proceeding further down to the experimental stage, in most cases a few fundamental questions arise. Which method – dSTORM, sptPALM or any other – suits better? What kind of fluorophore – organic dye or fluorescent protein – and which one of them in particularly to choose? How the sample should be prepared and what are the optimal imaging conditions and parameters? How to be sure that one is tracking the correct (e.g., protein of interest) and the same individual molecule during a prolonged period of time?

To answer these and other similar questions, we employed a well-characterized and convenient model system – kinesin translocation along the microtubules which has a defined directionality and often takes place only in the manner of linear trajectories. By tracking the movement of this motor protein under different circumstances (diverse fluorescent protein tags, various imaging techniques and conditions, experiments performed *in vitro* and *in vivo*, etc.) with our miEye microscope, we gained a plentiful of valuable knowledge regarding the preferable imaging approach and parameters, most appropriate sample preparation, optimal experimental conditions, use of various photoactivable fluorescent proteins and processing and analysis of the collected data. Majorly benefiting from such experiments, in the near future we are aiming to perform SM tracking of numerous proteins derived from different bacteria antiviral systems, like CRISPR-Cas, prokaryotic Argonaute and other systems, in living cells and thus uncover the unique target search mechanisms that these proteins most likely employ in a natural biological environment.

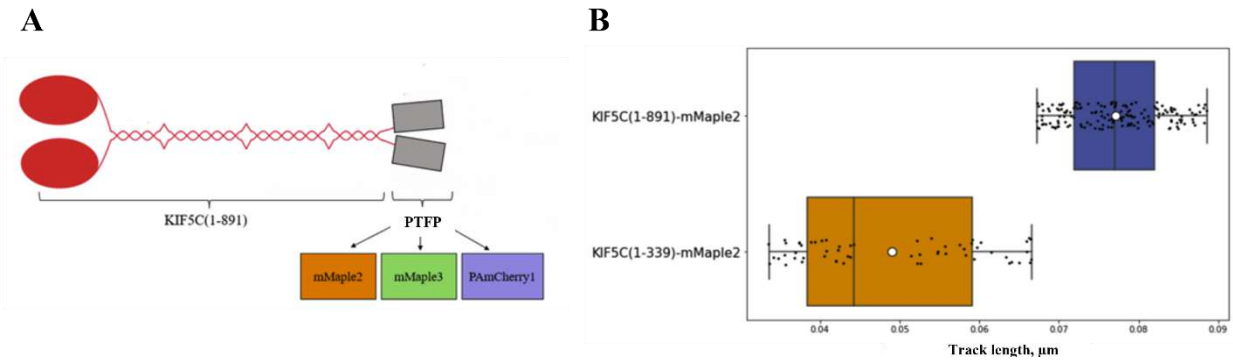

Fig. 1. Single-particle tracking of kinesin-1 movement along the microtubules. A) Fusion of kinesin heavy chain (KHC) dimer, which has its tail domain removed (KIF5C(1-891)), with various phototransformable fluorescent proteins (PTFPs) – mMaple2, mMaple3 and PAmCherry1. B) Experimentally *in vivo* obtained track lengths of two different kinesin-1 variants labelled with PTFP mMaple2 – the one mentioned before (KIF5C(1-891)) and KIF5C(1-339), which is a truncated monomeric version of kinesin that cannot move processively.

[1] A. Kopūstas, et al., *Langmuir* **37**, 3428–3437 (2021).

Multispectral imaging of neurofibromatosis type 1 skin lesions

Emilija V. Plorina[1,2], Kristina Saulus[1], Ainars Rudzitis[3], Tatjana Linova[4], Dmitrijs Bliznuks[5], Alexey Lihachev[1], Ilze Lihacova[1]
[1] University of Latvia, Institute of Atomic Physics and Spectroscopy, Jelgavas 3, Riga, Latvia, LV-1004;
[2]LTD Longenesis, Dzirnavu 41A-5, Riga, Latvia, LV-1010;
[3] Pauls Stradiņš Clinical University Hospital, Pilsonu 13, Riga, Latvia, LV-1002;
[4] Health Center 4, Dermatologu Clinic, Skanstes 50, Riga, Latvia, LV-1013;
[5]Riga Technical University, Faculty of Computer Science and Information Technology, Kipsalas 6A, Riga, Latvia, LV-1048;
plorina@edu.lu.lv

Von Recklinghausen's neurofibromatosis also known as neurofibromatosis type 1 (NF1) is an autosomal dominant genetic condition caused by mutations in the NF1 gene with a prevalence of 1 in 3,500 people. It results in multiple, a few to thousands of tumour growths along nerves, which may turn malignant. In addition, a variety of other tumours may develop. The two main cutaneous lesions are café-au-lait spots and dermal neurofibromas. Café-au-lait spots are round or oval coffee-coloured macules, which get their colour from increased melanin pigment content. They often appear in the first year of life. Dermal neurofibromas are small nodules that appear during childhood and increase in number over lifetime. Other characteristic findings are plexiform, neurofibromas, axillary or inguinal freckles (Crowe's sign) and increased base pigmentation [1, 2]. While there is no treatment for NF1, if a proper diagnosis is obtained the symptoms can be managed and the patient can be monitored in case more serious manifestations are developed. However, the rarity and variability of the disease means that many patients remain without diagnosis for many years or even generations [3].

A multispectral imaging device that uses four sets of narrow-band LEDs - 526nm, 663nm and 964nm for diffuse reflectance imaging and 405nm LEDs filtered through a 515nm long-pass filter for autofluorescence imaging - has been previously tested on pigmented lesions with high accuracy [3]. Therefore, it could be used for imaging of café-au-lait lesions, freckles and increased skin base pigmentation. The imaging parameters then could be compared with other pigmented lesions such as benign nevus or pigmented keratosis. If a patient does not have many neurofibromas, they can be misdiagnosed as dermal melanocytic nevi, dermatofibromas, lipomas and other cutaneous lesions [5]. The imaging parameters of neurofibromas could be compared to other similar looking lesions.

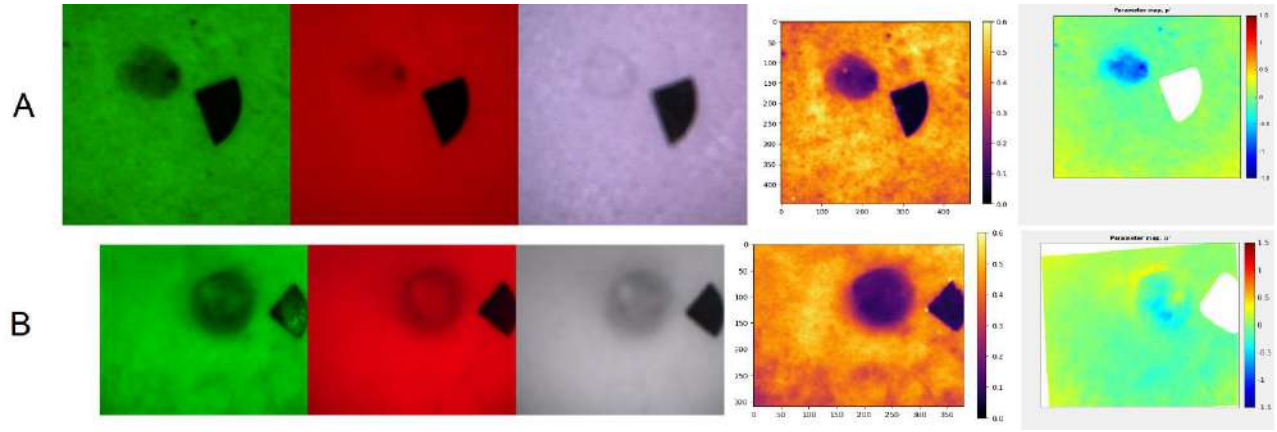

Fig. 1. Multispectral images of nevus (A) and neurofibroma (B) from left to right: under 526nm, 663nm, 964nm illumination, autofluorescence intensity in G channel, parameter p'

Acknowledgement

This work has been supported by the European Regional Development Fund project "Rare skin diseases efficient identification and multi-modal diagnostic system" (agreement No.1.1.1.1/20/A/072).

[1] Boyd, K. P., Korf, B. R., & Theos, A., 2009, J Am Acad Dermatol, 61(1), 1–16. https://doi.org/10.1016/j.jaad.2008.12.051.
[2] Gawkrodger, D., Ardern-Jones, M.R., *Dermatology, 7th Edition*,Elsevier, 2021.
[3] Tolentino ES, Souza Pinto GN, Maciel L, Soares CT, Lara VS, Moreschi ARC. Exuberant manifestation of neurofibromatosis type 1 affecting 3 generations: delayed diagnosis and the importance of the multidisciplinary approach. Oral Surg Oral Med Oral Pathol Oral Radiol. 2019 Sep;128(3):e108-e112. doi: 10.1016/j.oooo.2019.03.003. Epub 2019 Mar 15. PMID: 31101459.
[4] K. Boločko et al., 2019, Proc Spie, 110741O, doi: 10.1117/12.2527173.
[5] Messersmith L, Krauland K. Neurofibroma. [Updated 2022 May 15]. In: StatPearls [Internet]. Treasure Island (FL): StatPearls Publishing; 2022 Jan-. Available from: https://www.ncbi.nlm.nih.gov/books/NBK539707/

Eosin and Hematoxylin Harmonophores for Histopathology Investigations with Nonlinear Microscopy

Mykolas Mačiulis[1], Viktoras Mažeika[1], Viltė Gabrielė Samsonė[2], Lukas Kontenis[3], Vitalijus Karabanovas[4,5], Edvardas Žurauskas[6], Virginijus Barzda[7,8]

[1]Laser Research Centre, Faculty of Physics, Vilnius University, Saulėtekio Ave. 10, LT–10223, Vilnius, Lithuania
[2]Faculty of Medicine, Vilnius University, M. K. Čiurlionio g. 21, LT-03101, Vilnius, Lithuania
[3]Light Conversion, 2B Keramikų st., LT–10233, Vilnius, Lithuania
[4]Biomedical Physics Laboratory, National Cancer Institute, P. Baublio st. 3b, LT–08406, Vilnius, Lithuania
[5]Department of Chemistry and Bioengineering, Vilnius Gediminas Technical University, Saulėtekio Ave. 11, LT–10223, Vilnius, Lithuania
[6]Department of Pathology, Forensic Medicine and Pharmacology, Faculty of Medicine, Vilnius University, M.K. Čiurlionio st. 21/27, LT–03101, Vilnius, Lithuania
[7]Department of Physics, University of Toronto, 60 St. Georges st., Toronto, ON M5S 1A7, Canada
[8]Department of Chemical and Physical Sciences, University of Toronto Mississauga, 3359 Mississauga Rd. N., Mississauga L5L 1C6, ON, Canada
mykolas.maciulis@ff.vu.lt

Multimodal nonlinear laser–scanning microscopy is a powerful technique for noninvasive biological imaging [1]. Several nonlinear signals can be generated simultaneously at the focus of a microscope objective, including multiphoton excitation fluorescence, second–harmonic generation (SHG) and third–harmonic generation (THG). Collagen, the main constituent of extracellular matrix in the biological tissue can be visualized with SHG microscopy, which can be used for cancer diagnostics [2]. Changes in the collagen structure are observed in hematoxylin–and–eosin–stained (H&E–stained) histology sections, which contrast cell nuclei from the cytoplasm and extracellular structures and are considered as the gold standard for histological investigations [3]. Although collagen fibers are visualized with SHG microscopy, in this work THG is used for collagen visualization and characterization. The potential for cancer diagnostics using THG from H&E–stained samples is also investigated. Fig.1(**a**) visualizes collagen fibrils in SHG, while THG (Fig.1(**b**)) shows endotendineum which wraps individual fascicles. Collagen fibrils are also faintly visible in the THG image. In addition cell nuclei of tendocytes are highlighted in THG. The combined image (Fig.1(**c**)) shows the colocalization between collagen fibrils, endotendineum and tendocytes. Multimodal nonlinear microscopy imaging can be incorporated into the tissue histology investigations without additional modifications of the H&E–stained histopathology samples. Multimodal imaging can be applied for investigation of structural changes in connective tissue due to various diseases and also is beneficial in observing extracellular matrix and cell nuclei in cancer diagnostics.

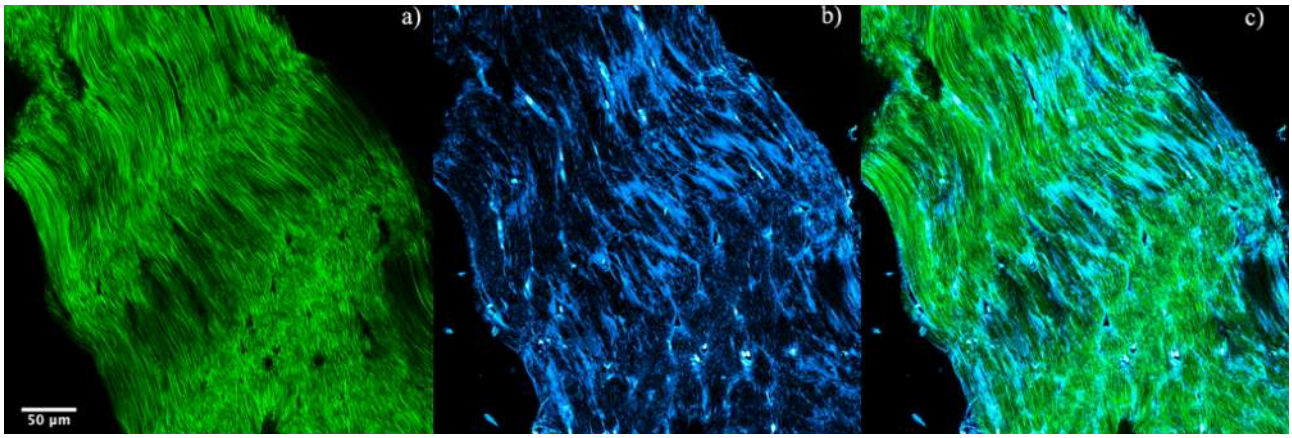

Fig. 1. Multicontrast nonlinear optical microscopy images of rat tail tendon histology section stained with hematoxylin and eosin (H&E staining). **a**) SHG image of collagen tissue, **b**) THG image from the same sample area and **c**) combined image of both.

[1] R. Carriles, D. N. Schafer, K. E. Sheetz, J. J. Field, R. Cisek, V. Barzda, and J. Squier, "Imaging techniques for harmonic and multi-photon absorption fluorescence microscopy," Rev. Sci. Instrum. 80, 081101 (2009).
[2] A. Golaraei, L. Kontenis, R. Cisek, D. Tokarz, S. J. Done, B. C. Wilson, and V. Barzda, "Changes of collagen ultrastructure in breast cancer tissue determined by second-harmonic generation double Stokes-Mueller polarimetric microscopy," Biomed. Opt. Express 7(10), 4054–4068 (2016).
[3] J. A. Kiernan, Histological and Histochemical Methods, 3rd ed., Butterworth Heinemann, Woburn, MA (1999).

Poster Presentations

Bio-Physics as Bio-Engineering: techno-recursive life-basics functional organization and STEAM for creative education

Dobilas Kirvelis

Lietuvos Mokslininkų Sąjunga, Club *LAISVIEJI*, J.Basanavičiaus 6, Vilnius, Lithuania
dobilas@kirvelis.lt

Today Bio-Physics turns into transhumanistic – multimodal technological interpretation of life. The Living organisms and Bio-systems are considered as the Organized Bio-Physical Systems from the point of view of the Bio-engineering. This report is continuation of ideas of the report "*Biophysics is becoming Bioengineering*" of the EBSA 2018 Conference in Kaunas [1]. CL-CD (*Closed-Loop Coding-Decoding*) or A-by-S (*Analysis by Synthesis*) concept shows, that these are working on the RECURSyves organized systems principles, operating as the mathematicians-informatics thinking – on the principles of the Computers [2].

The first steps of this approach have been initiated in Vilnius 60 years ago, 1962, when VU Rector, President of the Lithuanian Cybernetics Council, mathematician prof. Jonas Kubilius, guided by the strategic - bio-cyber-systemic approach, that the future of science life is not Physics, not Chemistry, but Bio-sciences, based on the systematic foundation of natural sciences, and, in disobeying Moscow, creates the Department of Biophysics and Biochemistry at the VU GMF. As a result of this, today we have a powerful VU Life Sciences Center, whose scientific research provisions are dominated by studies, regrettable, not of organized bio-systemic activities - scientific positions of information management, but biochemical components life activities.

CL-CD is presented as the concept of the essential functional organization of Life is directly connected with the more general concept of organized systems - systems capable of fighting entropy, that CL-CD is a fundamental concept of Cybernetics as well. In essence, it is close to Jakob von Uexküll's concept of the functional cycle *Umwelt* (1926), on the basics principle of the functioning of life and senses is explained. This diagram of *Umwel*'s functional organization is very reminiscent automatic regulation-control scheme of technical cybernetics. Drawing attention to is the fact that living systems are essentially cybernetic. Although humanitarians (Kull Kalevi) see in it more the principled semiotics of signals-signs [3]. Therefore, on its basis, the humanities create and develop the basic science of life - Biosemiotics. Humanitarika uses Ch. Sanders Peirce's theory [4]. In general, from the point of view of Cybernetics, signal science is understood as part of Information Theory. These approaches the essence of living systems is seen not so much in the material - from which the living organism is made, but in the functional organization and signaling of its parts. From that point of view, the importance of the traditional atomic-molecular-Biochemical organization of Biophysics is pushed to the background cybernetic - CL-CD engineering approach - Bioengineering is put forward.

But in the 21st in the decades, especially today - 2022 - sharp ecological ones emerge - becomes obvious: - Europe and the World, acutely feel the devastating effect of traditional energy-material, based on inanimate nature's physico-chemical fire technologies, using fossil fuels, on the future Earth and Humanity. It is not only the accelerating climate change. But it also raises a strategic scientific-technological problem. Won't the FIRE technologies discovered and widely implemented by *Home-Erectum* ~ 1 billion years ago be a global MISTAKE of Humanity's techno-evolution ? The natural Living Nature that exists next to Man, the Bio-technologies used in it, do not use fire at all. Life technologies fit at a temperature of several tens (20-45 C^0) and fulfil all the requirements necessary for the existence and development of a living "machine" - as an organized system - as an organism. The Man must merge into the Earth Ecological System with the technologies of the Living Nature.

Today emerges humanitarian innovation - Transhumanist Bio-STEAM education for the formation of a Creative Society as multimodal Techno-scientific cultural progress, as an essential key to solving Post-humanity's problems. An achievable vision of the world through the prism of STEAM sciences is connected to the creation of a new perfect society. Special ambition to multimodal Bio-Systemic technological education. Techno-scientific cultural progress is seen not only as a positive phenomenon, but as an essential key to solving humanity's problems. An achievable vision of the world through the prism of STEAM sciences is connected with the empowerment of mankind to rule and with the creation of a new, more perfect society. Special ambition lies in Bio-Systemic education, emphasizing its importance in the technological continuity of life [5].

[1] *http://dobilas.kirvelis.lt/mokslas/36-biophysics-is-becoming-bioengineering,* 2018.
[2] *http://dobilas.kirvelis.lt/files/KIRVELIS-ANTICIPATION-Bremen2.pdf ,* 2016.
[3] Kull, Kalevi; Velmezova, Ekaterina. Jesper Hoffmeyer: Biosemiotics is a discovery. Biosemiotics **12**(3): 373–379, 2019.
[4] Marchello Barbieri. *From Biosemiotics to Code Biology*, Biological Theory **9**(2), 2014.
[5] L. Duoblienė. *Pohumanistinis Ugdymas: Dekoduoti*, VUL, 2018.

Psychophysical study of the area of influence of distractors on the geometric illusion of extent

Vilius Marma[1], Aleksandr Bulatov[1,2], Natalia Bulatova[2], Laimutis Kučinskas[2]

[1]Laboratory of Visual Neurophysiology, Institute of Biological Systems and Genetics Research, Lithuanian University of Health Sciences, Eivenių St. 4, Kaunas, Lithuania
[2] Institute of Biological Systems and Genetics Research, Lithuanian University of Health Sciences, Eivenių St. 4, Kaunas, Lithuania
Vilius.Marma@lsmu.lt

Aim:

The aim of the study was to further develop a quantitative model of the filled-space illusion and test it to account for the effects caused by stimuli containing distracting line-segments of along or perpendicular to the main stimulus axis.

Methods:

Illusion was studied as a function of the distance between the distracting lines and the lateral terminator of the reference spatial interval of the three-dot stimulus. Data obtained in three different series were fitted with relevant functions of the model.

Results:

It was shown that the model satisfactorily describes all changes in the illusion magnitude for various stimulus. For distractors shifted along the stimulus axis, the magnitude of the illusion increases to a certain maximum value with the increase of distractors displacement and smoothly decreases to zero thereafter. For distractors shifted orthogonally to the stimulus axis, the illusion magnitude monotonically decreases with the increase of distractors displacement. In the case of the distractor rotation, the greatest illusion magnitude refers to orientations of the distracting line segment along the stimulus axis and decreases to the minimum value for the orthogonal orientation.

Conclusions:

A good correspondence between the experimental and theoretical results supports the suggestion that the two-dimensional profile of the AWS can be described as the absolute value function of the first derivative of a Gaussian along the radial direction in the visual field and the Gaussian function along the tangential direction.

Artificial intelligence application in synaesthesia research

Raminta Bartulienė[1], Rūta Davidavičienė[1], Gustavas Davidavičius[1], Aušra Saudargienė[1,2], Šarūnas Ašmantas[1], Saulius Šatkauskas[1]

[1]Vytautas Magnus University, Faculty of Natural Sciences, Vileikos g. 8, Kaunas, Lithuania
[2] Lithuanian University of Health Sciences, Neuroscience Institute, Eivenių g. 4, Kaunas, Lithuania
raminta.bartuliene@vdu.lt

Synaesthesia is an unusual neurological condition in which a cognitive process or stimulation in one sensory modality triggers another type of sensory sensation. One of the most common forms of synaesthesia is colored hearing – when sounds elicit an automatic involuntary sensation of color. To test the authenticity of the case, when studying synaesthesia, a test of genuineness (TOG) is usually applied. A positive TOG result confirms the temporal stability of synesthetic experiences.

This study analyses a reported case of color hearing synaesthesia of a girl (SB) with a visual deficiency. She can only see colorless silhouettes and reports people develop a person-specific color after communicating with them. The case was confirmed to be genuine with a 75% TOG result. This study hypothesized that SB synesthetic sensations are evoked by different parameters of people's voices. To confirm this hypothesis, we extracted 68 voice features from study participants' voice recordings and used them to train a multilayer perceptron (MLP). The MLP classified previously unseen recordings with 94% accuracy.

To find the most relevant features a random forest classifier was applied. It was determined, that by reducing the number of features to 21 of the most relevant ones, the MLP classification increased to 97%. This study used a novel approach to investigate a case of synaesthesia. The approach confirmed the different color synesthetic experiences to be linked to certain voice features.

Rabbit model of meibomian gland disfunction

Vytautas Baranauskas[1], Saulius Galgauskas[2] Simona Steponkiene[3], Vitalijus Karabanovas[3,4], Ricardas Rotomskis[3]

[1]Vilnius University Institute of Biochemistry, Life Science Centre, Sauletekio av 7, Vilnius, LT 10257, Lithuania
[2]Vilnius University Faculty of Medicine, M. K. Čiurlionio str. 21, Vilnius, LT 03101, Lithuania
[3]Biomedical Physics Laboratory of National Cancer Institute, Baublio 3B, LT-08406, Vilnius, Lithuania
[4]Department of chemistry and Bioengineering, Vilnius Gediminas Technical University, Sauletekio av. 11, LT-10223, Vilnius, Lithuania
Vytautas.baranauskas@gmc.stud.vu.lt

The meibomian glands are vertically arranged sebaceous glands that are located in the upper and lower tarsal plates (Miyake et al., 2017). These glands synthesize and secrete meibomian, which is a secretion comprising of phospholipids, cholesterol, wax esters, and cholesterol esters. Meibomian forms a layer on the eye called the tear film, that functions in preventing the eyes from drying thus playing a protective role against various diseases. One of the principal causes for dry eye disease (DED) is damage to the tear film and other contributors are hyperosmolarity, ocular surface inflammation and damage, and neurosensory abnormalities have been observed to cause dry eye disease as well (Ganesalingam et al., 2019; Yu et al., 2021).

Air pollution, dryness, allergy, smoke, and UV light affect tear osmolarity and can consequently cause tear film damage (Heidari et al., 2019). Transmembrane and secretory mucins might additionality promote dried eye disease by increasing friction between tear fluid in epithelial cells of the eye causing tear film instability. Eyelid notching also causes poor film formation which can equally cause dried eye disease (Aragona et al., 2021). Meibomian plays an important role in tear film stability and the protection of the ocular surface against microbial agents and meibomian gland dysfunction (MGD) as a result of functional abnormalities, such as hyperosmolarity, tear evaporation, and ocular surface staining, might occur if the glands synthesise insufficient meibomian containing the proper quality and quantity of lipids (Baudouin et al., 2016; Miyake et al., 2017; Yamaguchi, 2018). The most common cause of dried eye disease is caused by MGD. Environmental stress, stem cell renewal, and ageing can also cause MGD (Baudouin et al., 2016; Miyake et al., 2017). Corneal damage can occur as a result of corneal injury associated with inflammation and hypersensitivity of the corneal nerves, and this can result as well from apoptosis, goblet cell loss, and reduced secretions (Fakih et al., 2019). Treatment for dried eye disease can be performed using lactoferrin and mimetic lactobionic acids due to their moisture retaining capacity (Ganesalingam et al., 2019; Rusciano et al., 2018). Damaged epithelial cells and environmental stress might trigger inflammatory mediators, such as chemokines and cytokines, on the cornea surface, causing tear film instability, which causes irritation, and the vicious cycle of dried eye disease might continue (Ganesalingam et al., 2019).

DED is also associated with the inflammation of the lacrimal and meibomian glands, the cornea, aqueous tears, and conjunctiva and an increase in hormones, such as androgens and oestrogen might also be correlated to the onset of DED (Matossian et al., 2019; Yamaguchi, 2018). It has been hypothesized that adaptive immunological reactions can appear due to prolonged exposure to external stimuli, and the patient may experience chronic diseases in the eye if the immune system cannot prevent DED pathogenesis due to tear film loss (Aragona et al., 2021; Matossian et al., 2019). DED affects ocular function, corneal structure integrity, and overall eye health. Thermal pulsation therapy, intraductal probing, intense pulsed light, antibiotics, non-steroid essential fatty acid, and hormonal therapy are suitable for the treatment of MGD (Arita et al., 2021; Sabeti et al., 2020; Villani et al., 2020).

Liposomes have been investigated for ophthalmic drug delivery since 1981. It offers advantages as a carrier system: it can encapsulate both the hydrophilic and hydrophobic drug molecules, possess biodegradable and biocompatible compounds, and can enhance the permeation of poorly absorbed drug molecules by binding to the corneal surface. Thus improves residence time of active compounds. In addition, liposomes can improve pharmacokinetic profile, enhance therapeutic effect, and reduce toxicity associated with higher dose [1].

In this study we created a unique rabbit model for meibomian gland disfunction. This model mimics the symptoms of human dry eyes syndrome. There were used 9 New Zealand rabbits in this project. After MGD induction right eye of rabbits developed inflammation which caused symptoms similar to dry eyes. After 3 weeks post inductions rabbits were randomised in to 3 groups which received liposomal solution with different active substances as eyedrops. During experiment tear production, tear brake up time, clinical evaluation of eyelids and cornea visualization with cobalt blue light was performed. Eye treatment started 21 days post induction. Rabbits were treated for 10 days.

The results showed an improvement of the symptoms of tear brake up time and inflammation of eye lids. In conclusion, liposomal formulation is a promising tool for ophthalmic drugs delivery for the treatment of MGD.

[1] Gyan P.Mishra,Mahuya Bagui et al., *Journal of Drug Delivery, 2011;2011:863734.*

Co-culture of human pancreatic organoids with cells of the peripheral nervous system.

Parfejevs Vadims[1], Goluba Karina[1], Pleiko Karlis[1], Pcolkins Andrejs[2], Vilmanis Janis[3], Terjajevs Igors[4], Riekstina Una[1]

[1]University of Latvia, Faculty of Medicine, Jelgavas iela 3, Riga, Latvia
[2]Riga East Clinical University Hospital, Department of Abdominal and Soft Tissue Surgery, Hipokrata 2, Riga, Latvia
[3]Pauls Stradins Clinical University Hospital, Surgery Clinic, Pilsonu iela 13, Riga, Latvia
[4]Hospital of Traumatology and Orthopaedics, Traumatology Center, Duntes iela 22, Riga, Latvia

vadims.parfejevs@lu.lu

The public need for therapies to treat pancreas-related conditions like diabetes, exocrine pancreatic insufficiency and cancer is increasing. Protocols to establish human pancreatic organoids (hPO) containing progenitor-like cells have been recently developed [1]. hPOs offer new ways to model pancreatic disorders and study the aspects of development and regeneration of this organ. Organoid cultures can be further complicated by integrating other cell types. Such co-culture approaches can help to dissect the function of the cells in the progenitor niche or tumour stroma [3]. The role of the peripheral nervous system (PNS) in such contexts has often been overlooked; nevertheless, mounting evidence supports its active involvement [4].

The aim of our work is to establish adult hPOs from healthy and tumour tissue, co-culture them with peripheral nervous system components and study the interaction of the exocrine pancreas with mesenchymal cells, and neural crest-derived glia.

Normal and tumour hPOs are established from donor tissue material. Primary human Schwann cells (SC) and stromal cell lines are used for co-culture with pancreatic organoids. hPO identity is validated using targeted DNA sequencing, while co-culture constructs are characterized using immunofluorescence in gel sections and using whole-mount approaches.

We report successful derivation of nine normal and tumour hPO lines, as well as primary human SC cultures. hPOs express various markers of the pancreatic ducts and ductal progenitors including CK19, SOX9, PDX1, but no acinar markers, like PTF1a. SCs and mesenchymal cells are identified in co-cultures by vimentin and p75 expression. Both cell types survive in various co-culture setups and media formulations. SCs have a tendency to associate with pancreatic cells and form network-like structures around hPOs. Both SCs and mesenchymal cells support growth of organoids in depleted co-culture medium.

Successful hPO derivation and co-culture with SCs and other stromal cells offers opportunity to study the role of the PNS in pancreatic deficiencies and physiology.

Acknowledgements. Authors declare no conflict of interest. The study is funded by Postdoctoral research project no. 1.1.1.2/VIAA/4/20/623.

1. Georgakopoulos N, Prior N, Angres B, et al. *BMC Dev Biol*. 2020.
2. Driehuis E, Gracanin A, Vries RGJ et al. *STAR Protoc*. 2020; 1(3):100192.
3. Seino T, Kawasaki S, Shimokawa M, et al. *Cell Stem Cell*. 2018; 22(3)
4. GolubaK, Kunrade L, Riekstina U, Parfejevs V. *Cells*. 2022;11(5).

Effect of 2-acetylfuran on smooth muscles in rat prostate and aorta

Irma Martišienė[1], Vilma Zigmantaitė[2], Jonas Jurevičius[1]

[1]Laboratory of Membrane Biophysics, Institute of Cardiology, Lithuanian University of Health Sciences, Sukilėlių Ave. 15, LT50162 Kaunas, Lithuania
[2]Biological Research Center, Lithuanian University of Health Sciences, Tilžės St. 18/7, LT47181 Kaunas, Lithuania
irma.martisiene@lsmuni.lt

A variety of furan ring containing compounds are found in food, including herbs, and are used in the production of synthetic and herbal medicines. Being aromatic, they are abundant in various industrial processes and the environment. Many of furan-containing compounds are known as toxic but some of them are used in medical practice, such as antihypertensive drug prazosin, diuretic agent furosemide used to treat hypertension and edema [1].

A recent *in vivo* study in pigs showed that essential oil of the flowering plant *Elsholtzia ciliata* has a hypotensive effect, reducing arterial blood pressure possibly by modulating peripheral vascular resistance [2]. The study showed that dehydroelsholtzia ketone and elsholtzia ketone were proportionally the highest amount of all organic components found in *E. ciliata* essential oil. These ketones contain furan ring in their structure therefore it encouraged us to examine the effect of other furan-containing compounds on smooth muscles. One of them is 2-acetylfuran (2-Furyl methyl ketone) which is known as flavour compound or intermediate in foods, is isolated from essential oils, sweet corn products, fruits, and flowers. 2-Acetylfuran can be used to synthesis of antibiotic cefuroxime. To date, no data available about the effect of this compound on smooth muscles.

The aim of our study was to evaluate the effect of 2-acetylfuran on smooth muscle in rat prostate and aorta. Male Wistar rats weighing 600-800 g were used. Tension measurements were performed on isolated prostate strips (1.5-2 mm in width, 2-3 mm in length) of ventral lobe and intact aortic rings (~2 mm in length). Preparations were mounted in the chamber of a constant perfusion system, stretched to a resting tension of 1 g, and equilibrated for 60 minutes. To obtain a maximal contractile response, preparations were exposed twice to 100 mM KCl containing Tyrode‘s solution. Before beginning measurements of exposure to 2-acetylfuran, the preparations were washed with normal Tyrode solution until the basal tone level was restored. First, prostate strips and aortic rings were precontracted with 10^{-6} M or 3×10^{-7} M phenylephrine, respectively. After steady state was reached, 2-acetylfuran was cumulatively added to the solution starting from 0.01 µl/mL to 3 µl/mL. The maximal concentration used corresponded to 3×10^{-2} M. The change in tension was evaluated in respect to the phenylephrine-induced contraction. Data were fitted to the Hill equation.

Increasing concentrations of 2-acetylfuran starting from 0.01 µl/mL to 0.03 µl/mL, 0.1 µl/mL, 0.3 µl/mL, 1 µl/mL, 3 µl/mL caused gradually decrease of tension in both preparations. In prostate, the relaxation effect was significantly induced starting from 0.03 µl/mL of 2-acetylfuran, the contraction decreased to 89.27±2.73 % (n=4, $p<0.05$). At highest applied concentration, i.e., 3 µl/mL, the tension of prostate strip decreased to 15.14±4.7 % (n=4, $p<0.05$) *vs* phenylephrine-induced contraction. Half inhibition value K_B for prostate was 0.6±0.1 µl/mL, the Hill coefficient – 1.2±0.2 (n=5). In aortae, the tension significantly decreased starting from 0.3 µl/mL of 2-acetylfuran, i.e., to 77.36±9.05 % (n=5, $p<0.05$), and at 3 µl/mL – reduced to 7.44±2.09% (n=4, $p<0.05$) *vs* phenylephrine-induced contraction. K_B of 2-acetylfuran for aortae was 0.8±0.2 µl/mL, the Hill coefficient – 1.8±0.3 (n=5).

In conclusion, our study shows that 2-acetylfuran decreased phenylephrine-induced contraction of both prostate strips and aortic rings in concentration-dependent manner. Results suggest that 2-acetylfuran has a relaxation effect on smooth muscles.

[1] L. A. Peterson, *Chem. Res. Toxicol*. **26(1)**, 6–25 (2013).
[2] V. Zigmantaitė, E. Jonušaitė, R. Grigalevičiūtė et.al., *Pharmaceuticals (Basel).* **15(8),** 982 (2022).

Electrophysiological and antihypertensive action of *Elsholtzia ciliata* essential oil in large animal model

Rimantas Treinys[1], Vilma Zigmantaitė[2], Ramunė Grigalevičiūtė[2], Audrius Kučinskas[2], Antanas Navalinskas[1], Lauryna Pudžiuvelytė[3,4], Jurga Bernatonienė[3,4], Eglė Jonušaitė[1], Regina Mačianskienė[1], Jonas Jurevičius[1]

[1]Lithuanian University of Health Sciences, Institute of Cardiology, Laboratory of Membrane Biophysics, Sukilėlių ave. 15, LT50162 Kaunas, Lithuania
[2]Lithuanian University of Health Sciences, Biological Research Center, Tilžės st.18/7, LT47181 Kaunas, Lithuania
[3]Lithuanian University of Health Sciences, Faculty of Pharmacy, Institute of Pharmaceutical Technologies, Sukilėlių ave. 13, LT50162 Kaunas, Lithuania
[4]Lithuanian University of Health Sciences, Medical Academy, Department of Drug Technology and Social Pharmacy, Sukilėlių ave. 13, LT50162 Kaunas, Lithuania
rimantas.treinys@lsmuni.lt

Cardiovascular diseases are rising burden in all the world [1], therefore the need of new medicine is growing. New pharmaceutical remedies often have side effects and herbal medicines might be an alternative to treat cardiovascular diseases due to minimal side effects and wide field of physiological targets. Herbal essential oils are volatile liquids which contain many chemical compounds and have various valuable properties [2]. We performed an *in vivo* analysis of the effects of *Elsholtzia ciliata* essential oil on the cardiovascular system to clarify the newly discovered antiarrhythmic effect of this substance [3, 4].

For the study the big animal model was developed. Eight local crossbreed pigs (32 ± 1.9 kg) were used in experiments. All experiments were performed in accordance with the EU Directive 2010/63/EU and permitted by State Food and Veterinary Service of Lithuania. Animals were premedicated intramuscularly using xylazine hydrochloride 3 mg/kg, ketamine hydrochloride 20 mg/kg and fentanyl citrate 3 µg/kg. Pigs were anaesthetized intravenously using 8 mg/kg thiopental sodium and intubated using a 6-in tracheal cuffed tube. During all procedures, analgesia was infused continuously using a pump. General anaesthesia was maintained via inhalation of sevoflurane. Anaesthesia was monitored every 5 min during the procedure. The test substance (*Elsholtzia ciliata* essential oil – EO) using same dose 30 µg/kg was injected into ear vein as bolus. T0 – control value, T1, T5, etc. – number indicates minutes after injection of the bolus.

Vital sign monitoring was performed to monitor pulse oximetry, capnography, blood preasure measurements. ECG parameters were recorded using 5-lead electrocardiography. Paired and two-tailed distribution t test was used for statistical evaluation.

After the bolus, heart rate (HR) increased significantly ($p < 0.05$) to 114.82 ± 8.73 bpm at T2 versus a control value of 92.02 ± 4.53 bpm. Thereafter, HR started to decrease and approached the control value at T10.

The bolus of EO significantly shortened the QT interval during the study and prolonged the QRS complex. After bolus of EO, at T3, the QRS complex reached a maximum value of 0.0565 ± 0.0037 s compared with the control value of 0.0531 ± 0.0031 s ($p < 0.05$). After T7, the QRS complex gradually shortened but remained non-significantly longer than control value.

Following bolus of EO, a significant reduction in arterial blood pressure ($p < 0.05$) was observed. From a control value of 80.47 ± 5.54 mmHg, mean arterial blood pressure (MAP) decreased to 50.90 ± 8.32 mmHg at T1. At T3 MAP increased to 67.80 ± 7.24 mmHg, and a delayed lower hypotensive effect of 65.83 ± 9.74 mmHg was subsequently measured at T7.

In this study we show that *Elsholtzia ciliata* essential oil expresses similar properties to class 1B antiarrhythmics and has a hypotensive effect in pigs; the arterial blood pressure is reduced possibly by modulating peripheral vascular resistance.

[1] G. A. Roth, G. A. Mensah, C. O. Johnson et al., *J. Am. Coll. Cardiol.* 76(25):2982-3021 (2020).
[2] A. Brochot, A. Guilbot, L. Haddioui et al., *Microbiologyopen* 6(4) (2017).
[3] R. Mačianskienė, L. Pudžiuvelytė, J. Bernatonienė et al., *Biomolecules* 10(6) 1-15 (2020.)
[4] V. Zigmantaitė, E. Jonušaitė, R. Grigalevičiūtė et al., *Pharmaceuticals (Basel)* 10;15(8):982 (2022).

Evaluation of the *Elsholtzia ciliata* essential oil effect on heart rate variability and blood composition in a large animal model

Vilma Zigmantaitė[1], Ramunė Grigalevičiūtė[1] , Audrius Kučinskas[1], Rimantas Treinys[2], Antanas Navalinskas2, Regina Mačianskienė[2], Jonas Jurevičius[2]

[1]Biological Research Center, Lithuanian University of Health Sciences, Tilžės st. 18/7, LT47181, Kaunas, Lithuania;
[2]Laboratory of Membrane Biophysics, Institute of Cardiology, Lithuanian University of Health Sciences, Sukilėlių ave. 15, LT50162, Kaunas, Lithuania
vilma.zigmantaite@lsmuni.lt

The demand for the development of new and safer drugs is rising. Extensive research on herbal extracts has been conducted in hopes that the compounds will exert their precise effects without harmful side effects. Essential oils from herbal plant are volatile liquids that contain many chemical compounds, such as oxygenated monoterpenes, monoterpene hydrocarbons, oxygenated sesquiterpenes, and sesquiterpene hydrocarbons. It is already known that essential oils (EO) possess antibacterial, antioxidant, anti-inflammatory, antiviral, and antifungal etc. activities. Previously, our team analysed and patented the antiarrhythmic effects of whole plant extracts of *Elsholtzia ciliata* in isolated rabbit hearts. The purpose of this study was to investigate the effects *of E. ciliata* EO on the cardiovascular system in vivo in anesthetized pigs. All animal usage was organized in accordance with the EU Directive 2010/63/EU permitted by Ethics Commission. Animals were maintained in Lithuanian Health Science university Biological research. Lithuanian local breed pigs n=8, weighted 32 kg ± 1.9 were used in following experiments. During procedure animals were anesthetized. The test substance using same dose 30 µl kg-1 was injected intravenously using 1 ml syringe per 10 seconds. Heart rate variability (HRV) were measured using 5 leads ECG. To calculate HRV frequent domain was used for each time segment normalized to LF and HF; LF:HF ratio. Frequency ranges used to determine low frequency (LF) 0.01 – 0.07 Hz and high frequency (HF) 0.07 – 1.0 Hz. Blood samples was taken under sterile condition from common jugular vein in different experiment times: before experiment T0, after injection 1 min, 5 min and at the end of experiment after 30 minutes.

In this study we managed to measure and evaluate HRV in anesthetized pigs, in order to evaluate the effects of EO on the autonomic nervous system. We think that intravenous injection of EO altered the activity of the autonomic nervous system through mechanisms that are may be related to an increase in the sympathetic tone dominance. Higher sympathetic tone and activity are also reflected in the increased LF/HF ratio of HRV and the predominance of the LF component of the HRV frequency domain. Finally, we suggest that after the administration of an EO bolus, the activity of the nervous system is altered, possibly due to an increase in the dominant role of sympathetic tone as a secondary reflection. Most same acting drugs have been found to modulate the autonomic nervous system and improve sympathetic function in patients by increasing catecholamine (noradrenaline and adrenaline) production, possibly through baroreflex associated sympathetic activation. Changes in blood parameters after *EO* administration were evaluated in venous blood. We revealed that *EO* reduces the number of leukocytes and platelets and increases potassium concentration. In conclusion we think that alterations in the autonomic nervous system are the response of an organism to the other effects of an *EO* bolus. After the injection of the EO, blood parameters changed within the limits of clinical normal values, but this had no effect on the condition and health status of the animals.

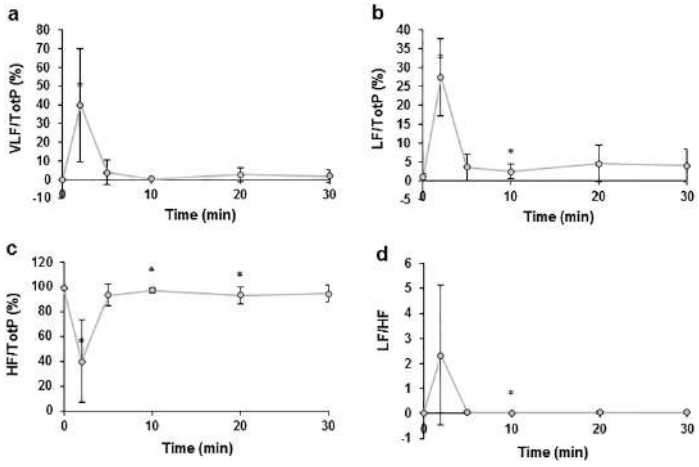

Figure 1. The effects of *EO* on the frequency domain of pig HRV

[1] R. Mačianskienė, L. Pudžiuvelytė, J. Bernatonienė et al., Biomolecules. 10, 1 -14 (2020)
[2] V. Zigmantaitė, E. Jonušaitė, R. Grigalevičiūtė et.al., Pharmaceuticals (Basel). 15(8), 982 (2022)

What can $\delta^{13}C$ Reveal About Plant Fitness? A Primary Investigation of a Lycophyte, *Spinulum annotinum*

Anita Elizabeth Clarke[1], Radvilė Rimgailė-Voicik[1], Ričardas Paškauskas[2], Jonas Mažeika[3]

[1]Vilnius University, Life Sciences Centre, Institute of Biosciences, Sauletekio Av. 7, 10257 Vilnius, Lithuania
[2] Laboratory of Algology and Microbial Ecology, Nature Research Centre, Akademijos Str. 2, 08412 Vilnius, Lithuania
[3] Laboratory of Nuclear Geophysics and Radioecology, Nature Research Centre, Akademijos Str. 2, 08412 Vilnius, Lithuania
anita.e.clarke@gmail.com

The ratio of stable carbon isotopes ($^{13}C/^{12}C$), which can be indicated using the $\delta^{13}C$ (delta) notation, is a tool to analyse ecophysiological processes in plants. Understanding $\delta^{13}C$ differences which occur between heterotrophic and autotrophic (photosynthetic) tissues in plants stands as a vaguely investigated aspect, especially among the lycophytes, most ancient extant plants. In this study, $\delta^{13}C$ in different organs of the clubmoss *Spinulum annotinum* (L.) A.Haines was explored. The aims of our study were to evaluate the isotopic composition of *S. annotinum* parts and to provide possible hypotheses to explain differences in ^{13}C abundance. To hypothesize about the cause of differences, we evaluated the size of *S. annotinum* outgrowths, distance from a body of water and vegetation diversity.

Plant material was collected from 12 different locations situated in two different sites (forest of Nemenčinė and Valakupiai geomorphological reserve). Both sites included a body of water (lake). Specimens had to include seven organs (roots (R), plagiotropic stems (PS) and leaves (PSL), running stems (RS) and leaves (RSL), orthotropic stems (OS) and leaves (OSL)) which were separated after collecting them. Samples were prepared and analysed as described in Clarke et al. [1]. Stable carbon isotope ratio was presented as $\delta^{13}C$ values per mil (‰) deviations from Vienna Peedee Belemnite standard. R (ver. 3.6.2) [2] was used for statistical analysis. Vegetation diversity was evaluated using package BiodiversityR Vegan [3].

There were significant differences between $\delta^{13}C$ in different *S. annotinum* organs. $\delta^{13}C$ varied by about 2.4‰. The highest $\delta^{13}C$ mean was – 29.98‰ (in roots) and the lowest was −32.41‰ (in plagiotropic shoot leaves) (Fig. 1). The distance to a body of water had no significant effect on $\delta^{13}C$ values in *S. annotinum*. Outgrowth size did not have a clear relationship with $\delta^{13}C$ in *S. annotinum*. Shannon Diversity Index was a significant predictor for $\delta^{13}C$ values in *S. annotinum* (Fig. 2). These findings provide a base for future lycophyte ecophysiology research.

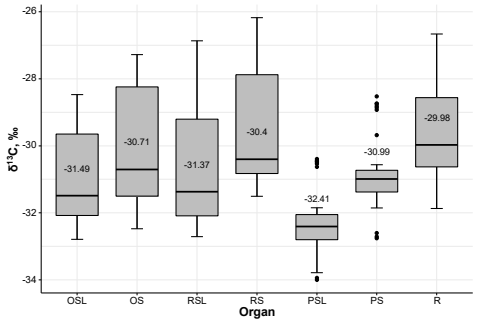

Fig. 1. $\delta^{13}C$ in different *Spinulum annotinum* organs. Boxes represent the interquartile range (IQR) between the 1st (Q1) and the 3rd (Q3) quartiles. The line in the middle of the box shows the median, along with the median value. The lower whisker marks Q1–1.5IQR, the upper whisker – Q3+1.5IQR. Dots represent outliers.

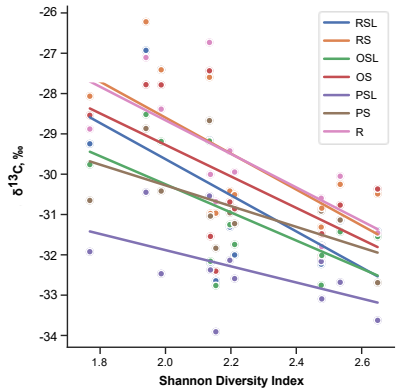

Fig. 2. Multiple regression (Shannon index, $\delta^{13}C$ in different organs of *Spinulum annotinum*.

[1] A.E. Clarke, R. Rimgailė-Voicik, R. Paškauskas, J. Mažeika, 2022. $\delta^{13}C$ in above-ground and below-ground organs of *Spinulum annotinum* (Lycopodiaceae). Flora, 294: 152119.
[2] R Core Team, 2019. R: A Language and Environment for Statistical Computing. R Foundation for Statistical Computing, Vienna, Austria. https://www.R-project.org/ (accessed 2021-05-20).
[3] J. Oksanen, F. G. Blanchet, R. Kindt, P. Legendre, P.R. Minchin, R.B. O'Hara, G.L. Simpson, P. Solymos, M.H.H. Stevens, H. Wagner, 2016. Vegan: Community Ecology Package. R package version 2.5.7. https://cran.r-project.org/web/packages/vegan/index.html (accessed 2021-05-21).

Valuable Compounds Extraction From Microalgae Using Cold Plasma and Pulsed Electric Fields

Gintarė Dalmantaitė[1,2], Kamilė Jonynaitė[2], Liutauras Marcinauskas[3], Arūnas Stirkė[2]

[1] Vilnius university, Life Sciences Center, 7 Saulėtekio Ave, Vilnius, Lithuania
[2] Laboratory of Bioelectrics, Center for Physical Sciences and Technology, Saulėtekio av. 3, Vilnius, Lithuania
[3]Plasma Processing Laboratory, Lithuanian Energy Institute, Breslaujos st. 3, Kaunas, Lithuania
gintare.dalmantaite@gmc.stud.vu.lt

Microalgae are a source of protein and other highly valuable compounds, which are used in various industries. However, rigid cell wall hinders extraction of intracellular compounds, hence researchers are looking for effective and eco-friendly extraction methods. One of the most effective methods to extract these compounds is high-pressure homogenization technology. Different fractions of algae compounds are mixed during this process, thus there is a need for an additional purification step. Therefore, other effective extraction methods are investigated [1].

Pulsed electric fields (PEF) is a promising cell disruption method, which is based on usage of short (µs-ms) and strong (5-80 kV/cm) electric pulses, which cause an increase of cell membrane permeability. Advantages of this method are selectiveness and purity of extracted substances [2]. However it is not effective enough for protein extraction. Combination of PEF and cold plasma could be a potential solution to this problem. During plasma treatment, generated radicals may cause lipid oxidation, leading to membrane weakening and pore formation [3]. A combination of these techniques could be useful strategy to increase extraction yields of valuable compounds from microalgae. Moreover, they could be adapted to an industrial scale.

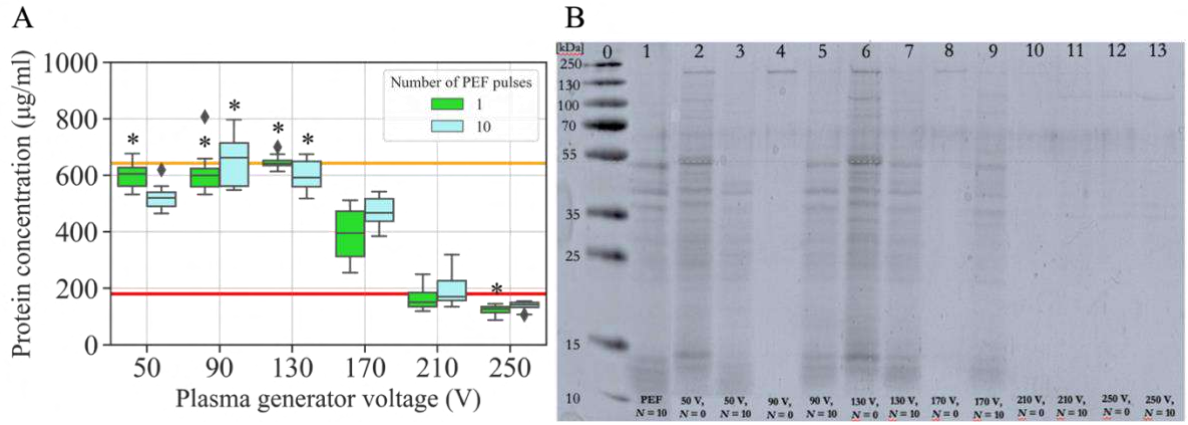

Fig. 1. A – protein concentration extracted from *C. vulgaris* after cold plasma and PEF treatment. Red line represents negative control, orange line – median protein concentration after one PEF pulse. B – visualization of the protein extracts obtained by treatments by SDS-PAGE.

For protein extraction experiments, suspension of *Chlorella vulgaris* microalgae was concentrated up to 5 g/L dry biomass with BG-11 medium (σ = 1,87 mS/cm). Then they were treated with cold plasma or PEF only, or firstly by cold plasma and then by PEF. Cold plasma treatment lasted for 5 minutes, plasma generator voltages were 50 - 250 V and the distance between the sample and electrodes was 3 cm. PEF parameters were U = 3,5 kV, t = 10 µs, f = 1 Hz, N = 1;10, d = 0,1 cm. Conductivity and pH of the suspensions were measured after cold plasma or PEF treatment. Chlorophyll was extracted with ethanol and its concentration was measured spectrophotometrically. Protein concentration in the supernatant was determined with a commercial kit. Finally, protein qualitive analysis was conducted with SDS-PAGE.

The results showed that PEF treatment induces the rise of suspension's conductivity (up to 66 %) and the decrease of pH (up to 8 %). Combination of 50 V plasma and 1 PEF pulse was the most effective for chlorophyll *a* extraction from *C. vulgaris* - obtained value was 23 % higher compared to PEF treatment only. Nevertheless, impact of high plasma generator voltages (170 V – 250 V) was not significant. Protein concentration measurements showed that PEF treatment increased protein extraction yield 3,57 times, compared to untreated samples. However, cold plasma or synergistic effect of selected treatments led to protein yield decrease by 80 % and 29 %, compared to PEF treatment and untreated samples. Moreover, qualitative analysis with SDS-PAGE showed that cold plasma processing induced extraction of higher molecular mass proteins (130 kDa – 250 kDa), compared to PEF and synergistic treatments (10 kDa – 55 kDa). Therefore, further investigation on how cold plasma and PEF together affect microalgae cells is needed.

[1] Han, P., Lu, Q., Fan, L., & Zhou, W. (2019). A Review on the Use of Microalgae for Sustainable Aquaculture. *Applied Sciences*, *9*(11), 2377.
[2] Zocher, K., Banaschik, R., Schulze, C., Schulz, T., Kredl, J., Miron, C., Schmidt, M., Mundt, S., Frey, W., & Kolb, J. F. (2016). Comparison of Extraction of Valuable Compounds from Microalgae by Atmospheric Pressure Plasmas and Pulsed Electric Fields. *Plasma Medicine*, *6*(3–4), 273–302.
[3] Gururani, P., Bhatnagar, P., Bisht, B., Kumar, V., Joshi, N. C., Tomar, M. S., & Pathak, B. (2021). Cold plasma technology: Advanced and sustainable approach for wastewater treatment. *Environmental Science and Pollution Research International*, 1–21

Comparison between titanium and stainless-steel electrodes on electroporation and gene transfer efficiency

Dominyka Gabulaitė[1], Baltramiejus Jakštys[1], Saulius Šatkauskas[1]

[1]Faculty of Natural Sciences, Vytautas Magnus University, Vileikos g., 8, Kaunas, Lithuania
dominyka.gabulaite@vdu.lt

By using short, high-voltage electrical pulses, an electric field is created that permeates the plasma membrane of cells. This process is known as electroporation (EP). Electroporation is commonly applied to deliver materials into cells or tissues and is used in practical applications such as antiviral or anticancer vaccination [1]. Moreover, EP is practiced in gene transfer *in vitro* level to genetically modify cells. Nevertheless, gene electrotransfer (GET) still needs to be improved. One of the problems is low cell viability using GET. Studies have noted that after using different electrodes, such as gold, aluminum, copper, stainless steel, platinum, or carbon, electroporated cellular responses and viability vary according to the material of the electrodes [2]. However, no studies could be found on titanium electrodes, which are more inert than the golden standard - stainless steel electrodes. More electrodes that are inert should reduce sample contamination with metal ions that negatively affect cell viability and gene transfer [3]. In our study, we wanted to determine whether more inert titanium electrodes could improve cell viability and gene transfection compared to stainless steel electrodes.

Chinese hamster ovary (CHO) cells were used in our experiments. Cells were treated with titanium (BT-20) and stainless steel (AISI 304) electrodes separated with a 2 mm gap. Low conductivity electroporation medium (0.1 S/m, 270 mOsmol, 7.2 pH) was used. EP parameters were one and nine high voltage (HV) pulses with a duration of 100 µs, repeating at a 1 Hz frequency. Pulse intensity was between 0.6 kV/cm to 2.2 kV/cm. Propidium iodide (PI) was used to determine cell electropermeabilization and irreversibly electroporated cell number with a flow cytometer. Cell viability was assessed with two methods - MTS assay 24 and 48 hours after treatment and colony formation assay 6 days post EP. pEGFP plasmid was used for transfection efficacy evaluation.

Results revealed that EP with titanium or stainless-steel electrodes permeates the same amount of CHO cells. By increasing electric field intensity intracellular PI fluorescence and the number of PI^+ cells increased similarly comparing both electrodes. A similar impact after EP was observed on cell viability with some exceptions using colony formation assay, where cell viability after 9 HV pulses of 0,8 kV/cm was significantly lower using titanium - 19,96 % ± 21,86 % electrodes compared with stainless steel - 46,23 % ± 29,9 %. MTS assay demonstrated significantly lower viability of cells electroporated with titanium electrodes 24 hours after treatment with 0,8 kV/cm 9 HV pulses and 48 hours after EP with 1,8 kV/cm 1 HV, 0,6 kV/cm 9 HV, and 0,8 kV/cm 9 HV pulses. By measuring irreversibly electroporated CHO cells, we determined that cell viability did not depend on pore resealing. In all conditions using both types of electrodes, irreversibly electroporated cell amount did not exceed 30 %. Furthermore, gene transfection results showed that plasmid electrotransfection efficiency was alike with titanium and stainless steel electrodes. Cell viability with both electrodes after transfection was identical.

To sum up, using titanium and stainless steel electrodes in EP have a similar effect on CHO cell permeabilization, viability, pore resealing, and gene transfection. At the same time, titanium electrodes at some EP parameters revealed lower cell viability and gene transfection compared with stainless steel electrodes. In conclusion, stainless steel electrodes are a better choice concerning price and GET efficiency compared with titanium electrodes.

[1] A. M. Bodles-Brakhop, R. Heller and R. Draghia-Akli, *Electroporation for the Delivery of DNA-based Vaccines and Immunotherapeutics: Current Clinical Developments,* Molecular therapy: the journal of the American Society of Gene Therapy, **17**(4), 585-592, 2009.

[2] A. Vižintin, J. Vidmar, J. Ščančar, D. Miklavčič, *Effect of interphase and interpulse delay in high-frequency irreversible electroporation pulses on cell survival, membrane permeabilization and electrode material release,* Bioelectrochemistry, 134, 2020.

[3] R. R. Rodaitė, R. Saulė, V. Snitka, G. Saulis, *Release of Iron Ions from the Stainless-Steel Anode Occurring During High-Voltage Pulses and Its Consequences for Cell Electroporation Technology*, IEEE Transactions on Plasma Science, **42**, 249-254, 2014.

Emulsifying Properties of PEF-treated BSA/Soluble Starch Conjugates

Ahmed Taha[1], Federico Casanova[2], Povilas Šimonis[1], Arūnas Stirkė[1]

[1] Center for Physical Sciences and Technology, Department of Functional Materials and Electronics
Saulėtekio av. 3, LT-10257 Vilnius, Lithuania
[2] Food Production Engineering, National Food Institute, Technical University of Denmark
2800 Kgs. Lyngby, Denmark
ahmed.taha@ftmc.lt

Pulsed electric field (PEF), as an emerging eco-friendly technology, has been used in the food industry for the inactivation of enzymes and microorganisms [1]. During PEF treatment, pulses of high voltage electric field for a short time (from nanoseconds to milliseconds) were applied to the material between two electrodes [2]. PEF technology offers several advantages over traditional pasteurization methods in the food industry, such as shelf-life extension, nutrient retention, quality preservation, and cost-effectiveness [3]. Besides, PEF was utilized to change the structural and techno-functional properties of food proteins. In this study, PEF treatment (at electric field strengths from 3.5-8.1 kV/cm, pulse duration (τ) = 50 µs) employed to facilitate the glycation between BSA and soluble potato starch. The physiochemical and emulsifying properties of the conjugates were investigated.

Electroporation at 3.5-5.7 kV/cm decreased fluorescence emission intensity, and improved protein solubility of BSA/soluble starch conjugates (fig. 1A and B). Furthermore, PEF-treated (3.5-5.7 kV/cm) BSA/soluble starch conjugates had better emulsifying properties (lower droplet size of emulsions) compared to native BSA and untreated BSA/soluble starch mixtures (fig. 1C). Diffraction scanning calorimetry confirmed that emulsions stabilized by PEF-treated conjugates had better freeze-thaw stability.

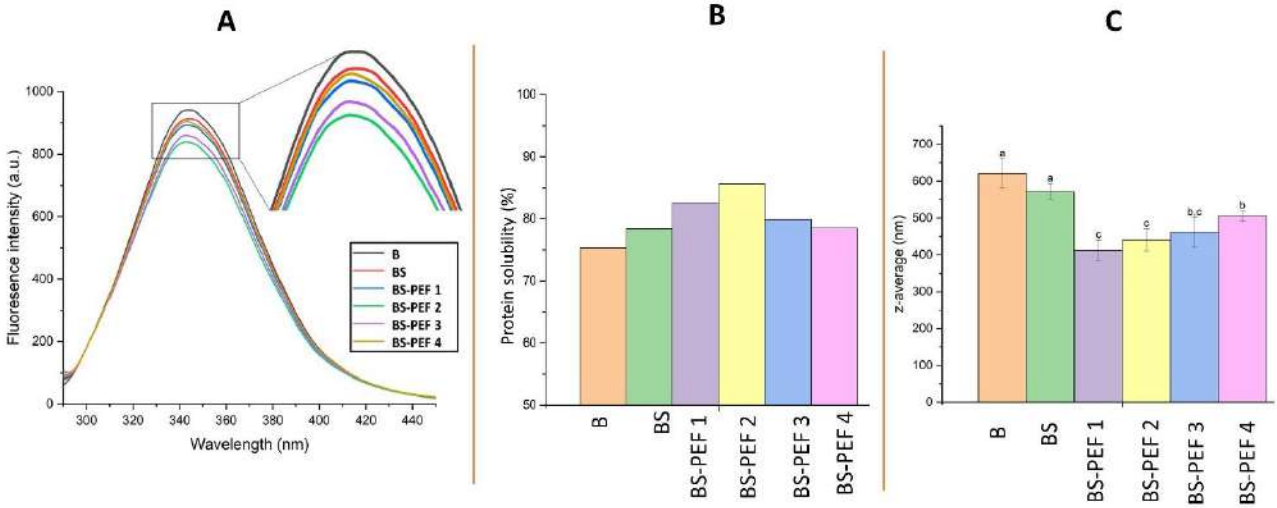

Fig. 1. A) fluorescence spectra B) protein solubility of BSA and BSA/Starch conjugates with and without PEF treatment and C) droplet size (z-average) of BSA and BSA/starch conjugates (with and without PEF treatment)-stabilized emulsions. B; native BSA, BS; BSA/starch mixture without PEF, BS-PEF 1- 4; PEF treated conjugates at 3.5, 4.5, 5.7 and 8.1kV/cm).

In conclusion, it is recommended to apply low-moderate PEF treatment to improve the emulsifying properties of BSA/starch complexes. These findings could promote the application of PEF technology in the food and pharmaceutical sectors.

[1] H. Jaeger, N. Meneses, and D. Knorr, Elsevier, *Innov Food Sci Emerg Technol.,* **10**, 470–480 (2009).
[2] A. Taha, F. Casanova, P. Šimonis, V. Stankevič, M. A. E. Gomaa, and A. Stirkė, *Foods*, **11**, 1556 (2022).
[3] R. N. Arshad et al., *Trends Food Sci Technol*, **104**, 1–13 (2020).

Investigation of oligonucleotide, propidium iodide and plasmid DNA electrotransfer efficiency into cells

Aras Rafanavičius[1], Saulius Šatkauskas[1]

[1]Vytautas Magnus University, Faculty of Natural Sciences, Vileikos st. 8, Kaunas, Lithuania
aras.rafanavicius@vdu.lt

Electroporation is a technique used to increase cell plasma membrane permeability by application of short (µs-ms in duration) electric pulsation [1]. The method is used to effectively deliver substances such as oligonucleotides, plasmid DNA and small molecules into cells. Electroporation protocols are relatively simple and the method is a fast, inexpensive and effective way of transporting target substances to cells. The aim of this work was to study the character of electrotransfer of propidium iodide (PI), oligonucleotides and plasmid DNA by using different electroporation parameters: voltage, duration and number of pulses, in order to determine the basis of transport of molecules of different molecular mass and to identify optimum parameters for effective transport.

The experiments were conducted with Chinese hamster ovary (CHO) cells by using stainless steel electrodes to administer pulses. The cells were suspended in electroporation medium (0.1 S/m, pH 7.3) and placed in a 2 mm gap between the electrodes. Oligonucleotide electrotransfer was measured after the cells were treated with 1 pulse of varying voltage and duration (500 V/cm 5 ms, 1200 V/cm 250 µs, 1400 V/cm 100 µs). Oligonucleotide transport dependency on total pulse duration was further examined by applying 1-10 500 V/cm 5 ms pulses at 1 Hz frequency. For PI and plasmid DNA transfer, the cells were treated with either 1, 5 or 10 500 V/cm 5 ms 1 Hz pulses or 1 1400 V/cm 100 µs pulse. Expression of green fluorescent protein (GFP) encoded by the plasmid was measured 24 h after the experiment. Electrotransfer efficiency was examined via flow cytometry by assessing fluorescence of the cells. In addition, transport of PI was inspected via fluorescence microscopy, and electroporation was performed by using coplanar copper electrodes with a 2 mm gap on a glass slide and the previously established pulse parameters. Images were captured digitally and a timescale of 15 min was created.

It was determined that the electrophoretic force created by the external electric field was especially significant for the delivery of oligonucleotides, and an increase of total pulsation time increased the amount of transported oligonucleotide molecules. Propidium iodide transport was not affected by duration of pulsation and occurred after the external electric field had been removed and until the pores had closed off. Moreover, after applying 10 500 V/cm 5 ms pulses, 15 min later 73.00 % ± 4.97 % of cells remain permeable. This signifies that the plasma membrane of a portion of the cells does not recover after being affected by a long pulsation. High pulse voltage is the most suitable for plasmid DNA electrotransfer, whereas several pulses of a short duration did not cause a significant change in fluorescence of GFP and severely decreased viability of the cells.

[1] Teissie, J., Golzio, M., & Rols, M. P. (2005). Mechanisms of cell membrane electropermeabilization: a minireview of our present (lack of ?) knowledge. *Biochimica et biophysica acta*, 1724(3), 270–280.

Bleomycin Electrotransfer or Irreversible Electroporation between different Cell Lines: An Investigation of the Bystander Effect

Ugnė Borinskytė[1], Neringa Barauskaitė[1], Paulius Ruzgys[1], Saulius Šatkauskas[1]

[1] Biophysical Research Group, Faculty of Natural Sciences, Vytautas Magnus University, Kaunas, Lithuania
ugne.borinskyte@vdu.lt

A total of almost 2 million cases of cancer are predicted to be diagnosed in 2022, which equates to approximately 5,250 new cases each day [1]. It is known that many cancer treatments have been developed, one of them being radiation therapy, which uses ionizing radiation. However, new, more effective methods are needed due to the inhomogeneous and difficult to predict tumor growth. Therefore, safe, effective and alternative methods of cancer treatment are being sought. One alternative is electrochemotherapy, a method of delivering anticancer drugs to tumor cells based on electrical impulses [2].

Electrochemotherapy is based on the phenomenon of electroporation, when cells in tumor tissues are exposed to electric fields and the transmembrane potential of their membranes increases. When the potential exceeds a critical value, hydrophilic pores are created in the cell membrane through which various water-soluble molecules, such as the anticancer drug bleomycin (BLM), can enter the cell. Electroporation can be either reversible or irreversible. After reversible electroporation, the cell membrane is restored, and the cells are not killed. Meanwhile, irreversible electroporation is used when cells exposed to electrical pulses are destroyed without damaging nearby blood vessels or healthy tissue [3]. The cancer treatment method affected by irreversible electroporation is called electroablation. Both of these electroporation-based methods are already applied in clinical practice, but the phenomenon of electroporation, the electrotransfer of various molecules, and the secondary processes caused by these processes have not been fully investigated.

Bystander effect has been observed to be induced in ionizing radiation therapy. Although the effect has been observed for some time after radiotherapy, it has not been studied when cells are exposed to the electric fields applied during electrochemotherapy. To date, only a few publications have been found showing that the bystander effect is possible after electrochemotherapy or electroablation [4], [5]. Also, there are still no data on how the bystander effect affects different types of cells, and in particular, how this effect affects the viability of different cells among themselves. The study investigated the bystander effect after BLM electrotransfer and irreversible electroporation *in vitro*. Five cell lines are used for experiments: chinese hamster ovary cells (CHO-K1), human adenocarcinoma alveolar basal epithelial cells (A-549), human mammary carcinoma cells (MX-1), murine melanoma cells (B16-F10), mice murine mammary carcinoma cells (4T1). A similar methodology is used to induce the bystander effect after both irreversible electroporation methods. BLM (20 nM) electrotransfer is induced using a single 100 µs electrical pulse of 1400 V/cm amplitude. After irreversible electroporation, the cells are exposed to one electric pulse of 2800 V/cm amplitude lasting 100 µs. After electroporation, wait 10 min for cell pores to close. Cells are plated in a 6-well plate with the addition of 1 ml of RPMI culture medium and incubated for one or several days at 37°C. After incubation, the medium is centrifuged twice and transferred onto 400 cells completely unaffected by electric fields. After the colonies have grown, a colony test is performed using crystal violet dye.

From the obtained results, we found that the cells were divided into three groups when studying the bystander effect: insensitive, moderately sensitive and highly sensitive. Insensitive cells include CHO-K1 cells, moderately sensitive cells include 4T1 and B16-F10 cells, and highly sensitive cells include MX-1 and A-549 cells. Interchanging the media of the five cells showed different viability results. When using CHO-K1 cell culture, no significant changes were observed compared to untreated media, but the effect of bystander media from different cells was separated into two groups: the first CHO-K1, MX1 and 4T1, and the second B16-F10 and A-549. Bystander medium from the first group slightly affected CHO-K1 cells, but the second group completely killed those CHO-K1 cells both after BLM electrotransfer and irreversible electroporation.

[1] R. L. Siegel, K. D. Miller, H. E. Fuchs et al., *Cancer statistics, 2022,* CA: A Cancer Journal for Clinicians. **72,** 7–33 (2022).
[2] Y. Peng, H. Tao, Y. Gao et al., *Review and Prospect of Tissue-agnostic Targeted Strategies in Anticancer Therapies*, Curr. Top. Med. Chem. **21**, 404–425 (2020).
[3] N. Jourabchi, K. Beroukhim, B. A. Tafti et al., *Irreversible electroporation (NanoKnife) in cancer treatment,* Gastrointestinal Intervention. **3**, 8–18 (2014).
[4] A. Prevc, A. B. Zavec, M. Cemazar et al., *Bystander Effect Induced by Electroporation is Possibly Mediated by Microvesicles and Dependent on Pulse Amplitude, Repetition Frequency and Cell Type,* The Journal of Membrane Biology. **249**, 703–711 (2016).
[5] P. Ruzgys, N. Barauskaitė, V. Novickij et al., *The Evidence of the Bystander Effect after Bleomycin Electrotransfer and Irreversible Electroporation,* Molecules. **26**, 6001 (2021).

Electrotransfection of Cancer and Primary Murine Dendritic Cells

Eivina Radzevičiūtė[1], Veronika Malyško-Ptašinskė[2], Jurij Novickij[2], Vitalij Novickij[2], Irutė Girkontaitė[1]

[1]State Research Institute Centre for Innovative Medicine, Department of Immunology, 08406 Vilnius, Lithuania;
[2]Faculty of Electronics, Vilnius Gediminas Technical University, 03227 Vilnius, Lithuania.
eivina.radzeviciute@imcentras.lt

One of the well-known forms of nonviral gene transfection is electroporation (EP). EP is defined as a method where a pulsed electric field (PEF) induces transient alteration of cell membrane permeability to introduce various molecules, including plasmid DNA [1]. For decades used long micro–millisecond-range electric field pulses (ESOPE*) now can be replaced by shorter, nanosecond pulsed electric fields (nsPEFs) [2,3]. Studies show that the treatment with nsPEF significantly increased the transfected cell viability and enhanced gene expression [4].

In this study, we used Chinese Hamster Ovary cells (CHO-K1), murine mammary carcinoma cell line (4T1), and primary murine dendritic cells (DC's) for nano and microsecond range electrotransfection protocols comparison. For microsecond (µsPEF) 1.2 kV/cm × 100 µs × 8, 1 Hz protocol was used. The nanosecond (nsPEF) protocol involved sequences of 100 pulses delivered at 1 MHz frequency (7 kV/cm ×300 ns ×100). Also, the efficiency of electrotransfection was evaluated using two different sizes and different detectable proteins encoding plasmids: green fluorescent protein (GFP) encoding plasmid (4.7 kbp; p-EGFP-N1) and a plasmid expressing firefly luciferase and red fluorescent protein (tdTomato) (8.5 kbp; pcDNA3.1(+)/Luc2=tdT). Permeabilization with green-fluorescent stain Yo-Pro1 and transfection efficiency was assessed with flow cytometry. Also, cell viability after EP treatment was evaluated using Alamar blue reagent.

First, we checked that both µsPEF and nsPEF electrotransfection protocols trigger permeabilization. Results showed that the sensitivity to PEF of all the cell lines involved in the study was similar. Therefore, both protocols can be used in further studies. Initially, we used CHO-K1 cell line, as a model cell line, to determine the optimal concentration of used plasmids for further studies. The plasmids concentration was limited to the 0.2 µg/µL due to minor differences in transfection efficiency when compared to the higher 0.3 µg/µL concentration. Surprisingly, electrotransfection efficiency of CHO-K1 cells was similar for both plasmids even though the size of the fluorescent tdTomato protein-encoding plasmid was almost two times larger than the GFP-encoding plasmid. Also, nsPEF and µsPEF protocols showed comparable results. But it was not the case with 4T1 cell line and primary DCs. The transfection rate with bigger pcDNA3.1(+)/Luc2=tdT plasmid was reduced several-fold and at the same time nanosecond protocol ensured significantly better transfection efficiency than µsPEFs. In order to increase primary DCs transfection efficiency we used immature (iDC) and mature (mDC) dendritic cells. However, there were no significant differences in transgene expression DCs electroporated either before or after maturation.

Our study has shown that the used nanosecond electrotransfection protocol ensured similar or even better transfection efficiency compared to µsPEFs. However, the size and concentration of the plasmid as well as the cell type significantly affect the transfection efficiency even though the sensitivity to electroporation itself was comparable. These results suggest that nsPEFs range protocols can be applied for gene electrotransfection experiments.

Acknowledgement: The project was funded by the Research Council of Lithuania (No. S-MIP-19-22).

---

* European Standard Operating Procedures for Electrochemotherapy (1.3 kV/cm x 100 ms x 8 /1 Hz).

[1] Carlsten, M.; Childs, R.W. Genetic Manipulation of NK Cells for Cancer Immunotherapy: Techniques and Clinical Implications. Front. Immunol. 2015, 6, 266.
[2] Desai, P.; Yagnik, B.; Sharma, D.; Khan, A.; Desai, N.; Padh, H. Transfecting CHO-K1 Cells: Comparison of CaPO4, Electroporation and Lipoplex Method with In-house Prepared Polyplex. Indian J. Pharm. Sci. 2017, 79, 655–662.
[3] Čegovnik, U.; Novakovic´, S. Setting optimal parameters for in vitro electrotransfection of B16F1, SA1, LPB, SCK, L929 and CHO cells using predefined exponentially decaying electric pulses. Bioelectrochemistry 2004, 62, 73–82.X,
[4] Guo, S.; Jackson, D.L.; Burcus, N.I.; Chen, Y.-J.; Xiao, S.; Heller, R. Gene electrotransfer enhanced by nanosecond pulsed electric fields. Mol. Ther. Methods Clin. Dev. 2014, 1, 14043.

Influence of Oxygen Concentration on the Effectiveness of Electrochemotherapy *in vitro*: Modeling and Experiments

Rita Saulė, Mantas Šilkūnas, Danutė Batiuškaitė, Gintautas Saulis

Department of Biology, 58 K. Donelaičio str., Kaunas, Lithuania
rita.saule@vdu.lt

Electrochemotherapy (ECT) combines tumour exposure to high-voltage pulses and cytotoxic drug, the most popular of which is bleomycin. Despite that standard operating procedures for ECT have already been defined, a meta-analysis of ECT effectiveness has shown that some tumours respond only partially to treatment, and others are not responsive at all. Thus, there is still a need for further optimization of treatment.

Bleomycin causes single- and double-strand DNA breaks only when the drug forms a complex called "activated bleomycin". Both routes of the formation of activated bleomycin require oxygen: either directly or as a source for the formation of H_2O_2 [1]. Meanwhile, tumour development *in vivo* is often accompanied by dysregulated angiogenesis, which leads to an uneven blood supply and differential oxygen availability to tumour cells, and causes the existence of hypoxic regions. The concentration of oxygen in tumours can be lower than 1%. The aim of this study was to find out whether oxygen concentration in the medium in which cells loaded with bleomycin are incubated, affects the effectiveness of electrochemotherapy *in vitro*.

Experiments were carried out on mouse hepatoma MH-22A cells. Cells were loaded with bleomycin by using a single square-wave electric pulse with the amplitude of 2 kV/cm and the duration of 100 μs under normoxic conditions, seeded into Petri dishes, and grown under normoxic and hypoxic conditions. Cell viability was determined by means of a colony-forming assay. The kinetics of the changes of the oxygen concentration in the cell culture medium was measured using Clark-type oxygen electrode.

We have demonstrated that when cells loaded with bleomycin were incubated in hypoxia (0.2% O_2), up to 5.3-fold higher concentrations of bleomycin were needed to kill them in comparison with cells grown in normoxia (18.7% O_2) [2]. It can be concluded from the experiments that: i) the effectiveness of electrochemotherapy with bleomycin *in vitro* depends on the oxygen concentration of the cell culture medium, ii) a time window of about 1–2 h post-electroporation defines the duration throughout which the concentration of available oxygen is essential for bleomycin cytotoxicity *in vitro*.

To understand the reasons of the occurrence of the differences between bleomycin cytotoxicities against intact and electroporated cells exposed to bleomycin in the cell culture medium with high and low levels of oxygen in the cell culture medium, the model *in* silico has been created. The following processes occurring during experiments have been taken into account [2]: 1) transmembrane transport of bleomycin into the cell; 2) inactivation of bleomycin by intracellular bleomycin hydrolase; 3) changes in oxygen concentrations of the system occurring as a result of: 3.1) the evaporation of oxygen from the medium, 3.2) transmembrane transport of oxygen into and out of the cell, 3.3) the consumption of oxygen within the cell, and 3.4) the efflux of oxygen from the bottom of the Petri dish. 4) the formation of the activated bleomycin complex; 5) creation of single- and/or double-strand DNA breaks by activated bleomycin; 6) the repair of DNA single- and/or double-strand breaks and 7) cell death. The model has been drawn following Systems Biology Graphical Notation (SBGN) format [3] and stored using the Systems Biology Markup Language (SBML) [4].

The analysis of the kinetics of various processes have shown that taking into account at least the first three processes listed above is already sufficient to understand the appearance of the time window of about 1–2 hours during which the concentration of available oxygen is essential for bleomycin cytotoxicity *in vitro*. The results of this study might allow increasing of the effectiveness of electrochemotherapy procedure *in vivo* and *in clinics*.

[1] R.M. Burger, K. Drlica, B. Birdsall, *J. Biol. Chem*. **269**, 25978-25985 (1994).
[2] M. Silkunas, M. Bavirsa, R. Saule, et al., *Bioelectrochemistry*, **137**, 107636 (2021).
[3] N. Le Novère, M. Hucka, H. Mi et al., *Nat. Biotechnol*. **27**, 735-741 (2009).
[4] M. Hucka, H. Bolouri, A. Finney, et al., *Bioinformatics* **19**, 524-531 (2003).

Tumor Elimination *In Vivo* Using Combined Calcium Electroporation

Augustinas Želvys[1], Austėja Balevičiūtė[2], Vitalij Novickij[3], Eivina Radzevičiūtė-Valčiukė[1]

[1]State Research Institute Centre for Innovative Medicine, Department of Immunology, Santariškių g. 5, Vilnius, Lithuania
[2]Institute of Environmental Medicine, Toxicology Unit, Karolinska Institutet, Stockholm, Sweden
[3]Faculty of Electronics, Vilnius Gediminas Technical University, Saulėtekio al. 11, Vilnius, Lithuania
augustinas.zelvys@gmail.com

The aim of this study was to find out whether combined treatment of calcium electroporation with dendritic cell or bezafibrate injections would be a viable treatment for tumor ablation. Two systems were chosen to evaluate the efficacy of such combination treatments: the BALB/cJ mouse line and SP2/0 myeloma, also the C57BL/6J mouse line and LLC1 carcinoma model systems. In all experiments, mice survival, tumor luminescence and volume dynamics were monitored. The blood was collected and the relative amount of antitumor IgG antibodies produced in the serum was determined by flow cytometry. Combined calcium electroporation with mature dendritic cells for *in vivo* tumor elimination showed no statistically significant differences between treatment groups. However, regardless of the combination, calcium electroporation significantly reduced tumor volumes (SP2/0 and LLC1) and prolonged mice lifespan. From relative amount of antitumor IgG antibodies, it was concluded that injection of mature dendritic cells induces a more rapid humoral immune response, compared with only calcium electroporation treated group. But the efficacy of the treatment varies between different cancer models. Combining calcium electroporation with bezafibrate for tumor elimination *in vivo* showed no statistically significant differences between treatment groups. Regardless of the combination, calcium electroporation significantly reduced tumor volumes (SP2/0 and LLC1) and prolonged mice survival.

$CaCl_2$ influence on the electrotransfection potency of pDNA and cell viability

Rūta Palepšienė[1], Saulius Šatkauskas[1]

[1] Biophysical Research Group, Faculty of Natural Sciences, Vytautas Magnus University, Vileikos str. 8, Kaunas, LT - 44404, Lithuania
ruta.palepsiene@vdu.lt

Calcium (Ca^{2+}) ions are associated with a variety of different processes including cell proliferation, developmental processes and cellular motility. Therefore, the level of intracellular free Ca^{2+} is strictly controlled and varies depending on the cellular localization. Experiments using calcium and electroporation - a physical delivery method that increases the permeability of cell membranes – combination already proved as a novel anti – cancer treatment strategy that can induce both apoptotic and necrotic cell death [1].

Electroporation applicability for nucleic acid electrotransfer also known as electrotransfection have been extensively studied in both *in vitro* and *in vivo* systems. However, the exact mechanism by which DNA enters the cell, travels to the nucleus and what factors affect this process is still under investigation. To this date, according to generally accepted DNA electrotransfer mechanism, due to negative charge of DNA it moves electrophoretically after electric field is applied. After reaching the membrane, DNA forms aggregates that are translocated to the cytoplasm within minutes after electric field application. Experimental data also suggested that divalent cations like Ca^{2+} can abolish the electrostatic repulsion between the plasma membrane and DNA and therefore enhance the nucleic acid absorption and aggregates formation levels [2]. However, less is known how specifically low calcium concentration in the medium can influence the electrotransfection efficacy or how this simultaneous electrotransfer of DNA and Ca^{2+} can affect cell viability dynamics. Thereby, the aim of this study was to evaluate the effect of different extracellular $CaCl_2$ concentrations (0 – 1mM) on the pDNA transfection efficiency and cell viability tendencies. Experiments were conducted using two sets of electroporation parameters: 1400V/cm, 100 μs, and 1200V/cm, 250 μs. Electrotransfection efficiency and green fluorescence protein (GFP) fluorescence intensity were evaluated using flow cytometry 24h after electroporation. For the evaluation of cell viability patterns, FCA and MTT methods were used. Results revealed that as low as 0,1mM Ca^{2+} concentration in the electroporation medium negatively effects electrotransfection efficiency while the higher Ca^{2+} (> 0.25mM) concentrations are associated with significantly decreased pDNA transfection efficiency and cell viability. Moreover, results also showed that phenomenon is not present when different cations are used suggesting calcium significance in the process of DNA electrotransfection.

[1] J. Dudek, S. Pfeffer, R. Zimmermann et al., *J. Mol. Biol.* **427**, 1159-1175 (2015).
[2] P. M. Boersenberger, D. S. Weiss, *Organic Photoreceptors for Imaging Systems*, CRC Press, 1993.

DAMPs Obtained from Irreversibly Electroporated Cells Prevent Cell Death After Electroporation

Baltramiejus Jakštys[1*], Rūta Palepšienė[1], Salvijus Vykertas[1], Dovilė Uždavinytė[1], Ingrida Šatkauskienė[1], Saulius Šatkauskas[1]

[1]Research on Delivery of Medicine and Genes Cluster, Faculty of Natural Sciences, Vytautas Magnus University, Vileikos str. 8, Kaunas, LT - 44404, Lithuania.

*Presenting author baltramiejus.jakstys@vdu.lt

Cells exposed to electric fields experience reversible electroporation (EP) irreversible electroporation (IRE) leading to immediate cell death, or no electroporation if pulses used were too low intensity [1]. The interplay of cell death and plasma membrane permeabilization is modulated by pulse parameters as pulse strength, duration, pulse number and frequency. IRE uses brief pulsed electric fields to damage cell plasma membrane irreversibly and is applied for tissue ablation. Irreversible electropermeabilization subsequently leads to instant cell death and inflammation due to released DAMPs [2].

The model to investigate the impact of intracellular DAMPs on electroporated cell viability was based on cell electroporation in the EP supernatant, which was the same EP medium that contained the IRE-extracted intracellular molecules. Cell viability was assessed using clonogenic and MTT assays. Flow cytometry and Trypan Blue exclusion assays were used to evaluate cell number and plasma membrane integrity of the electroporated cells. BCA and SDS-PAGE assays were used to assess EP-extracted protein amount and size in samples. Gel electrophoresis analysis were used to assess DNA and RNA content in EP supernatants.

Intracellular DAMPs get released from cells after IRE, however, the influence of IRE extracted intracellular compounds (ICs) on cancer cell viability has never been studied. We created an in vitro model to investigate the ICs influence on cancerous cell viability. We determined that ICs significantly increased the viability of reversibly electropermeabilized cancer cells compared to noncancerous cells. Furthermore, results demonstrated no observable cell lysis after ICs acquisition. Next, we assessed that 60 % of total intracellular proteins could be extracted after IRE. Afterward, the main amounts of extracted RNA were 26S and 18S ribosomal RNA subunits with some messenger RNA. Interestingly, we obtained only slight amounts or no DNA in EP supernatants.

In conclusion, the levels of extracted proteins and RNA directly corresponded to increasing intensity of electric pulses, subsequently leading to elevated cell viability after electroporation.

Keywords: DAMPs (Damage Associated Molecular Patterns), electroporation, extraction, cell viability, cancer

[1] B. Jakstys, M. Jakutaviciute, D. Uzdavinyte, I. Satkauskiene, S. Satkauskas, *Bioelectrochemistry* **135**, 107550 (2020).

[2] M. B. Sano, C. B. Arena, K. R. Bittleman, M. R. Dewitt, H. J. Cho, C. S. Szot, D. Saur, J. M. Cissell, J. Robertson, Y. W. Lee, R. V. Davalos *J. Sri. Rep.* **5**, 14999 (2015).

Pulsed electric field (PEF) treatment of marine microalgae

Kamilė Jonynaitė[1], Valentina Kavaliauskaitė[3], Rolandas Uscila[2], Skirmantas Keršulis[1], Žydrūnas Kavaliauskas[2], Liūtauras Marcinauskas[2], Arūnas Stirkė[1], Voitech Stankevic[1]

[1]Department of Functional Materials and Electronics, State Research Institute Center for Physical Sciences and Technology, Saulėtekio ave. 3, Vilnius, LITHUANIA
[2]Plasma Processing Laboratory, Lithuanian Energy Institute, Breslaujos str. 3, Kaunas, LITHUANIA
[3]Life Sciences Center, Vilnius University, Saulėtekio ave. 7, Vilnius, LITHUANIA
kamile.jonynaite@ftmc.lt

Microalgae are rapidly growing photoautotrophic microorganisms, which can help to tackle important challenges, like greenhouse gas emission, shortages of sustainable food, bioactive compounds and energy. Most part of valuable algae compounds are accumulated inside the cell. Organelles, like oil droplets, or membranes rich in bioactive molecules are surrounded by strong, rigid cell wall or extracellular protective layers. Therefore, various chemical, biological, and physical pre-treatment methods have been employed to disrupt the cells. One of the most promising alternatives for disruption of cell is treatment by pulsed electric field (PEF), where strong and short electrical pulses cause an increase in the transmembrane potential. This effect leads to the formation of pores in the cell membrane and the release of intracellular compounds. Compared to conventional methods, PEF is also characterised by the absence of side effects such as heating, additional product purification steps, availability to operate on large scale etc.

From PEF processing point of view, the intensity of induced membrane potential change generally depends on generated electric field strength (E), which refers to the field strength present in the treatment chamber during the sample treatment. It depends on the voltage (U) applied between the electrodes, geometry of the treatment chamber (surface area of electrodes (A), distance between electrodes (d)), and the spatial distribution of dielectric properties of the material (resistance of the conductor (R), conductivity of the conductor (σ)) between the electrodes [1]. According to electrical laws (Eq. 1-3, where I represent current though the conductor), there are two possible solutions, which can increase E and the efficiency of the electroporation. Firstly, the electrode area and the geometry of the cuvette can be changed. However, this approach is not entirely practical, as changes in the properties of the object (e.g., cell concentrations, medium conductivity or sample volume) require a different treatment chamber. The second and more commonly implemented is changing the conductivity of the medium. Unfortunately, no PEF studies have so far been found that have determined the effect of changes in conductivity on the physiological state of marine algae.

$$E = \frac{U}{d} \quad (1) \qquad U = I \times R \quad (2) \qquad R = \frac{1}{\sigma} \times \frac{d}{A} \quad (3)$$

Nevertheless, efforts have been made to show that change in salinity (which directly affects conductivity) can affect the growth rate, motility, actin filament structure, cell permeability and even cytotoxicity of *Dunaliella tertiolecta*, *Tetraselmis suecica* or *Heterosigma akashiwo* [2,3]. Therefore, the main aim of this study is to determine whether the PEF treatment efficiency of *Isochrysis galbana* and *Porphyridium purpureum* depends on the change of the algae suspension.

In order to achieve the objective, the PEF treatment were applied on *Isochrysis galbana* and *Porphyridium purpureum* cultivated in the F medium under 21 ± 1°C with fluorescent lamps at a photosynthetic photon flux density of 90 µmol/s/m^2, 12: 12 hours light: dark cycle and shaking at 140 rpm till harvest. Before PEF treatment, algae samples were 3 times washed with F-growth medium of a specific salinity and suspended to a final optical density of 1 at 750 nm. After 30 min incubation, the samples were treated with a PEF high-voltage exponential wave electrical pulse generator (developed at the Center for Physical Sciences and Technology, Lithuania). The PEF treatment parameters used were 1-10 pulses at 1 Hz and the applied electric field strength ranged from 20-60 kV/cm. Afterwards, changes in the electrical conductivity, cell permeability, extracted protein content of untreated and treated algae suspension were determined. For cell permeability assays, samples were incubated for 5 min with the fluorescent dye SYTOX green (final concentration 1 µM) and the fluorescence intensity was determined using a luminescence spectrometer (excitation at 490 nm, emission at the range 500-550 nm). Furthermore, extracted protein content in the untreated and treated algae suspension was determined using a commercial BCA Protein Assay Kit and Bovine Serum Albumin standard curve.

The results obtained on the efficiency of PEF to induce pore formation in seaweeds and the physiological changes in cells caused by changes in the conductivity of the medium will be presented and discussed in a poster presentation.

[1] J. Raso, W. Frey, G. Ferrari, G. Pataro, D. Knorr, J. Teissie, D. Miklavčič, *Innovative Food Science & Emerging Technologies*. **37** 312–321 (2016).
[2] C.E. Ikeda, W.P. Cochlan, C.M. Bronicheski, V.L. Trainer, C.G. Trick, *Journal of Phycology*. **52** 745–760 (2016).
[3] N. Novosel, T. Mišić Radić, M. Levak Zorinc, J. Zemla, M. Lekka, I. Vrana, B. Gašparović, L. Horvat, D. Kasum, T. Legović, P. Žutinić, M. Gligora Udovič, N. Ivošević DeNardis, *J Appl Phycol.* **34** 1293–1309 (2022).

The Influence of Bystander Effect to the Viability of Directly Unaffected Cells After Electroporation Based Treatments

Neringa Barauskaitė[1], Paulius Ruzgys[1], Saulius Šatkauskas[1]

[1] Biophysical Research Group, Faculty of Natural Sciences, Vytautas Magnus University, Kaunas, Lithuania
neringa.barauskaite@vdu.lt

Cancer research is one of the leading research topics worldwide. Therefore, alternative anticancer treatments are being developed alongside to the conventional ones. One of most promising novel anticancer therapies are electrochemotherapy (ECT) and electroablation [1]. Both therapies are based on the electroporation (EP) phenomenon. Such process occurs as a result of electric field triggered increase of transmembrane potential (TP). After reaching threshold level of TP the formation of transient electropores is initiated. If the electric field triggered TP does not deviate far from the EP threshold, then cells reseal the pores and not die, thus reversible electroporation (RE) is in action. If the TP greatly exceeds the EP threshold irreversible electroporation (IRE) is induced and cells die. This is the main mechanism of electroablation anticancer therapy.

ECT is based on (RE), when created transient hydrophilic electropores act as a bridge for various water-soluble molecules, such as the anticancer drug bleomycin (BLM). If BLM is replaced to Ca^{+2} ions, then this EP based treatment is termed calcium electroporation (CaEP).

All EP based anticancer therapies are local i.e., a well-defined tumour area of treatment effect is present. Naturally, there will be a part of the tissue in between area of affected and unaffected areas of the tumour. The effect of such area in EP based anticancer therapies is not defined well. However, in radiotherapy as another local anticancer treatment method, the therapeutic effect of such area is termed as bystander effect [2]. Although the effect has been observed for some time after radiotherapy [3], it has not been studied when cells are exposed to the electric fields applied during ECT, CaEP or electroablation. However, studies used different viability methods, hence it is hard to compare the published data [4,5]. Therefore, here we present results that are evaluated using clonogenic (ability to form colonies), flow cytometry (real number of cells that remain after the treatment), and Alamar blue (metabolic activity) assays.

4T1 (mouse breast cancer) cells were used in the experiments. A single electrical pulse with an amplitude of 1400 V/cm and a duration of 100 µs was used to electrotransfer $CaCl_2$ and the anticancer drug BLM. A single electrical pulse with an amplitude of 2800 V/cm and a length of 100 µs was used to accomplish irreversible electroporation.

Following electroporation, the cells were cultured in a 24-well plate with 0.2 ml of RPMI growth media for 48 hours. The medium is collected after incubation and centrifuged twice. Finally, the Bystander effect was created by adding the conditioned media on the untreated cells. To imitate the expressed molecule gradient the conditioned media was diluted with fresh media (FM) in a way that conditioned media had 10, 30, 50, 70, 90 and 100 % of total applied media. Depending on experiment this media was put on cells as conditioned media. In the case of Alamar Blue assay, conditioned media (200 µl) was put on 8000 cells, then incubated for 48 hours. Afterwards, 20 µl of Alamar Blue dye was put on the conditioned media, incubated for two hours and then fluorescence was measured. In the case of flow cytometry assay conditioned media (200 µl) was put on 15000 cells, then incubated for 48 hours. Then cells were detached from the surface with TrypLE and measured with flow cytometry. In the case of clonogenic assay conditioned media (2000 µl) was put on 400 cells that were put in 40 mm petri dish 24 hours prior to addition of conditioned media. After 6 days colonies were stained, imaged and ability to form colonies was determined.

Results show that CaEP, ECT has similar tendencies when measuring ability to form colonies, real number of cells that remain after the treatment and metabolic activity. Nevertheless, when conditioned media used form ECT and CaEP was diluted in ratio (9 CM to 1 FM) cell number and colony formation decreased to around 60 %, yet metabolic activity stayed at 100 %. However, the main differences occurred with IRE at diluted ratios 7 CM to 3 FM, 9 CM to 1 FM and 10 CM to 0 FM the viabilities were accordingly 55,65±3,81%, 17,44±0,71% and 24,96±1,36% with flow cytometry assay, 81,40 ±3,92 %, 64,99 ±7,09 % and 2,36 ±0,73 % with clonogenic assay, and 96,63±4,02%, 71,92±3,92% and 56,20 ±5,19 % with Alamar Blue assay.

Conclusions. Here we have showed that bystander effect has decreased the ability to form colonies, real number of cells that remain after the treatment and metabolic activity with similar tendencies after CaEP, ECT. However, the same viability measurements do not correlate when bystander effect is triggered by IRE.

[1] U. Probst, I. Fuhrmann, L. Beyer and P. Wiggermann, Electrochemotherapy as a new modality in interventional oncology: A review, *Technol. Cancer Res. Treat.* **17** (2018).
[2] A. Prevc, A. B. Zavec, M. Cemazar et al., Bystander Effect Induced by Electroporation is Possibly Mediated by Microvesicles and Dependent on Pulse Amplitude, Repetition Frequency and Cell Type, *The Journal of Membrane Biology*. **249**, 703–711 (2016).
[3] N. Jalal, S. Haq, N. Anwar, S. Nazeer and U. Saeed. Radiation induced bystander effect and DNA damage. *J. Cancer Res. Ther.* **10,** 819–833 (2014).
[4] E. Pirc, C. Federici, M. Bošnjak, B. Perić, M. Reberšek, M., L. Pecchia, L, N. Glumac, M. Čemažar, M. Snoj, G. Serša, Early Cost-effectiveness Analysis of Electrochemotherapy as a Prospect Treatment Modality for Skin Melanoma, *Clin. Ther*. **42**, 1535–1548 (2020).
[5] P. Ruzgys, N. Barauskaitė, V. Novickij et al., The Evidence of the Bystander Effect after Bleomycin Electrotransfer and Irreversible Electroporation, *Molecules*. **26**, 6001 (2021).

The differences between viability evaluation by using colony formation and metabolic activity methods of *Streptococcus Thermophilus* after application of pulsed electric field

Simona Gelažunaitė[1], Paulius Ruzgys[1], Saulius Šatkauskas[1]

[1]Biophysical Research Group, Vytautas Magnus University, Vileikos st. 844404, LT-44001, Kaunas, Lithuania
simona.gelazunaite@vdu.lt, paulius.ruzgys@vdu.lt, saulius.satkauskas@vdu.lt

According to the Centers for Disease Control and Prevention (CDC), each year 48 million people get sick from a foodborne illness. This indeed shows the urgent need to control the amounts of bacteria in the food. To date, the pasteurization of food is divided into thermal (T) and nonthermal (NT) treatments [1]. Usually, the NT treatment is more desirable since the bioactive compounds are not deformed, hence their biological activity is unaffected. Such biologically active thermally degradable compounds can be also found in raw milk [2]. In order to leave those molecules unharmed, conventional NT milk pasteurization methods (e.g., filtration) are used. However, such NT pasteurization has high economical cost. Therefore, novel and unconventional methods like pulsed electric fields (PEF) have high application potential [3]. The main mechanism of PEF pasteurization is electroporation (EP) [4]. EP is a process when external electric fields increase bacterial transmembrane potential to form transient pores in the membrane. If the pores are properly formed, then the bacterial homeostasis is disrupted and lead to inactivation of affected bacteria [4]. Even though PEF is a promising NT pasteurization technique, the processes that occur during bacterial inactivation is not fully understood. One of such, is the capability of the affected microorganism to maintain metabolic activity in comparison to the ability to form colonies after PEF treatment. Here, we compare viability differences obtained with colony formation with metabolic activity methods of *Streptococcus Thermophilus* (ST) after application of pulsed electric field.

Streptococcus Thermophilus was used for experiments. ST was grown to 0.5 OD, centrifuged, and put in electroporation media to concentrate the ST to 1 OD. Applied electric field number was from 1 to 99, with pulse amplitude from 8 - 24 kV/cm and pulse duration from 10 to 80 µs. After PEF application and 10 min incubation the metabolic activity was measured using Alamar Blue assay. Also, colony formation assay was performed.

The results showed that bacteria can be inactivated after electroporation. The best effect for PEF inactivation when measuring with colony counting method was observed at the highest parameters 24 kV/cm, 80 µs, 99 pulses (Fig. 1 A, B, C). However, when measuring metabolic activity for optimal viability decrease and applied lowest energy, the electric field parameters were 16 kV/cm, 30 µs, 99 pulses. (Fig. 1 D, E, F).

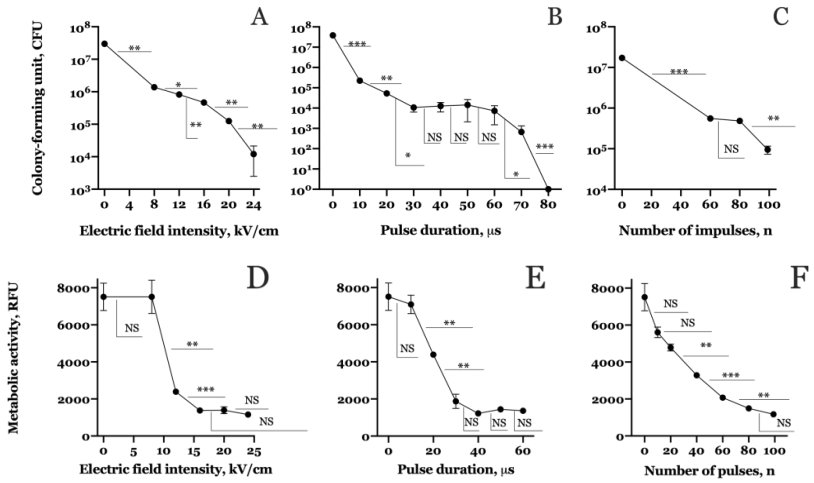

Fig. 1. Dependence of the electric field intensity of The *Streptococcus Thermophilus* bacteria viability dependence on PEF field intensity (A), duration (B) and number of pulses (C) when evaluating colony-forming units and PEF field intensity (D), duration (E) and number of pulses (F) when evaluating metabolic activity. Graphs show means ± SEM. Statistical significance was evaluated using Student's t test. NS - results does not significantly differ, *$p < 0.05$, **$p < 0.01$, ***$p < 0.001$.

Conclusions: Here we indicate that *Streptococcus Thermophilus* (ST) loss of metabolic activity does not correlate with ability to form colonies. That, in turn, can dictate that ST can withstand huge metabolism deviations form homeostasis without being irreversibly damaged.

Acknowledgments: This work was supported by grant (BiPyCellDeath) from funds of Kaunas University of Technology and Vytautas Magnus University.

[1] D. Jacobo-Velazquez, J. Benavides et al., *Foods.* **10(12)**, 2904 (2021).
[2] L. Tiantian, M.Meletharayil, K. Rohit et al., *J Nutrition Reviews.* **79**, 48-69 (2021).
[3] K. Nowosad, M.Suika, U. Pankiewicz et al., *J Food Sci Technol.* **58(2)**, 397-411 (2021).
[4] A. Salasevicius, D.Uzdavinyte, M. Visockis et al., *J Applied Sciences.* **11(23)**, 11281 (2021).

Cell size change after electroporation and its influence to triggered electrotransfer

Paulius Ruzgys[1], Neringa Barauskaitė[1], Saulius Šatkauskas[1]

[1] Biophysical Research Group, Faculty of Natural Sciences, Vytautas Magnus University, Kaunas, Lithuania
paulius.ruzgys@vdu.lt

When cells are exposed to a pulsed electric field with a sufficient amplitude, their transmembrane potential (TP) increases. If the TP increase surpasses the threshold, then pores start to form in an affected membrane. This phenomenon is termed as electroporation (EP). The pores that are induced by EP are hydrophilic and act as a bridge for exogenous molecules. This way, the intracellular electrotransfer (ET) of such molecules is initiated [1]. This technique can be applied as a local cancer treatment (electrochemotherapy, calcium electroporation) as well as for gene transfer to cells and tissues.

The electric field triggered TP (U_{tp}) can be counted by simplified Schwan equation shown in Eq. 1 [2].

$$U_{tp} = 1.5ErCos\Theta \quad (1)$$

Were, E is external electric field strength, r is the radius of the cell and Cosθ is the angle between electric field line in between the electrodes that passes through the centre of the cell and the area on the cell membrane were the TP will be counted. From the Eq. 1 one can already observe that the radius of the cell is directly proportional to the induced TP values. However, due to the processes of molecule ET, diffusion and then induced osmose the size of the cell can change, hence changing the sensitivity to future induction of EP and ET [3]. Here we tested the hypothesis of cell size change after EP and its influence on efficiency of molecule ET.

CHO cell line was used for experiments. Cells were electroporated in these different mediums using 1, 2, 4, 8 impulse sequences of 100μs duration (1Hz frequency), and amplitude of 1400V/cm. 10 minutes after electroporation cells were transferred to a hemocytometer and imaged using light microscope. The sizes of the cells were measured by using open-source ImageJ software. The experiment was conducted in triplets, each time 300 cells were measured, and the average is derived.

For propidium iodide (PI) electrotransfer efficiency experiments we used 2 or 8 HV, 1400 V/cm pulses and after 5, min time interval PI (40 μM) was put with an application of an additional 1 HV pulse (1400 V/cm). Then, cells were plated for flow cytometry measurements that was performed 10 min after the incubation procedure.

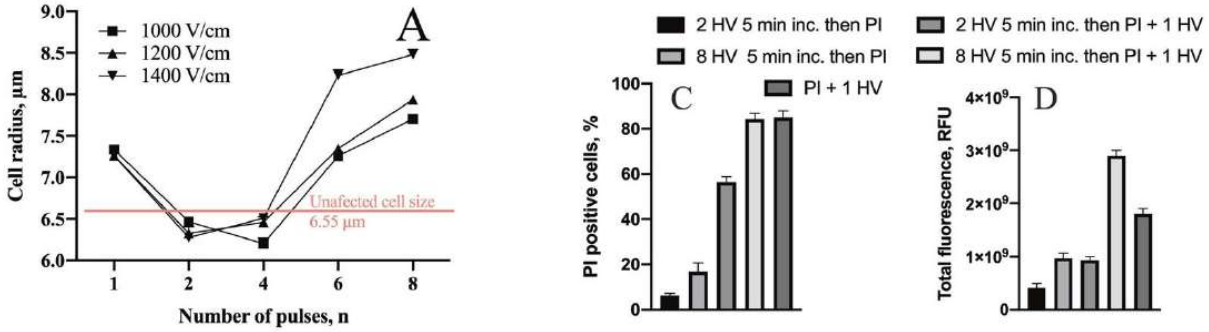

Fig. 1. A) Cell radii change after EP with 1-8 pulses at amplitude 1000 to 1400 V/cm for 100 μs. B) The scheme of used experiment setup. C) and D) PI positive cells and total PI fluorescence after ET using scheme as shown in part B. HV is coded as 1400 V/cm 100 μs pulse.

The results show that normal CHO cell size (6.55±0.02μm) cell size change in between 6.27±0.08μm after 2 pulses with 1400 V/cm and 8.48±0.06μm after 8 pulses with 1400 V/cm. This changes PI ET after the first EP (see fig. 1 B) from 85.02±2.93% of PI positive cells to 56.35±2.44% after desensitization with 2 pulses and 84.35±2.49% after effect with 8 pulses.

Here we show that CHO cell size change after electroporation. Also, we indicate that PI ET is affected but not according to Schwan equation.

Acknowledgments: This work was supported by grant (BiPyCellDeath) from funds of Kaunas University of Technology and Vytautas Magnus University.

[1] K. Balantič, D.Miklavčič, I. Križaj et al., *Acta Chim Slov.* **68(4)**, 753-764 (2021).
[2] X. Li, F. Yang, B. Rubinsky, *IEEE Trans. Biomed Eng.* **67(9)**, 2594-2602 (2020).
[3] S.M. Becker, *Int J Number Method Biomed Eng.* **38(3)**, e3564 (2022).

Functional activity of L-type Ca^{2+} channels in bone marrow-derived human mesenchymal stem cells during chondrogenic differentiation and in chondrocytes.

Anastasiia Shelest[1], Raminta Vaičiulevičiūtė[2], Eiva Bernotienė[2], Aidas Alaburda[1].

[1]Vilnius University, Institute of Biosciences, Life Sciences Center, Lithuania
[2]Department of Regenerative Medicine, State Research Institute Centre for Innovative Medicine, Lithuania
anastasiia.shelest@gmc.stud.vu.lt

Bone marrow-derived human mesenchymal stem cells (BM hMSCs) play an important role in tissue repair and engineering. They have a multipotent capacity to give rise to osteoblasts, adipocytes, and chondrocytes. BM hMSCs can be induced to differentiate into chondrocytes under special cultivating conditions. These conditions include using the chondrogenic medium and can be enhanced by transforming growth factor – β (TGF) or Interleukin [1].

According to the current literature, L-type Ca^{2+} channels play a crucial role in cell differentiation [2]. Also, it is known that an inward L-type calcium current was observed in 15% of undifferentiated hMSCs [3] and that the L-type Ca^{2+} channels family is expressed in chondrocytes [4]. But it remains unclear how the functional activity of L-type Ca^{2+} channels changes in BM hMSCs during chondrogenic differentiation and in chondrocytes.

In this study, we used the whole-cell patch-clamp to directly investigate the changes in the functional activity of L-type Ca^{2+} channels in BM hMSCs during chondrogenic differentiation and in chondrocytes. BM hMSCs and chondrocytes were obtained after post-trauma surgical procedures. Samples cultured in Dulbecco's Modified Eagle Medium (DMEM) were used as the control group. Chondrogenic differentiation was induced by cultivating BM hMSCs in a chondrogenic medium [5]. We tested the functional activity of L-type Ca^{2+} channels in chondrocytes by adding Nifedipine (a specific antagonist of L-type Ca^{2+} channels) and Bay-K (a specific agonist of L-type Ca^{2+} channels) to the DMEM. Also, we tested if TGF and Interleukin added to the chondrogenic media influence the functional activity of L-type Ca^{2+} channels in BM hMSCs during chondrogenic differentiation.

Our results indicate no significant differences in current in chondrocytes cultivated in control and adding Nifedipine or Bay-K. There wasn`t a noticeable inward current in BM hMSCs in control. The BM hMSCs in chondrogenic media also didn`t have any inward current. Adding TGF to the chondrogenic media activated a noticeable inward current that was blocked by Nifedipine. Adding the Interleukin to the chondrogenic media also induced an inward current, that was blocked with Nifedipine.

We conclude that L-type Ca^{2+} channels of BM hMSCs were activated by TGF or Interleukin during chondrogenic differentiation. In chondrocytes the activity of these channels wasn`t visible.

[1] M. Kondo *et al.*, 'Contribution of the Interleukin-6/STAT-3 Signaling Pathway to Chondrogenic Differentiation of Human Mesenchymal Stem Cells', *Arthritis Rheumatol. Hoboken NJ*, vol. 67, no. 5, 1250–1260, May 2015, doi: 10.1002/art.39036.
[2] N. Ahamad and B. B. Singh, 'Calcium channels and their role in regenerative medicine', *World J. Stem Cells*, vol. 13, no. 4, 260–280, Apr. 2021, doi: 10.4252/wjsc.v13.i4.260.
[3] J. F. Heubach *et al.*, 'Electrophysiological properties of human mesenchymal stem cells', *J. Physiol.*, vol. 554, no. 3, 659–672, 2004, doi: 10.1113/jphysiol.2003.055806.
[4] C. Matta, R. Zákány, and A. Mobasheri, 'Voltage-Dependent Calcium Channels in Chondrocytes: Roles in Health and Disease', *Curr. Rheumatol. Rep.*, vol. 17, no. 7, 43, May 2015, doi: 10.1007/s11926-015-0521-4.
[5] I. Uzieliene *et al.*, 'The Antihypertensive Drug Nifedipine Modulates the Metabolism of Chondrocytes and Human Bone Marrow-Derived Mesenchymal Stem Cells', *Front. Endocrinol.*, vol. 10, 2019, Accessed: Sep. 05, 2022. [Online]. Available: https://www.frontiersin.org/articles/10.3389/fendo.2019.00756

Modulation of TRPM6 and TRPM7 channel expression by experimental conditions (medium ionic composition, acidosis, and TRP channel inhibitors)

Inga Andriulė[1], Regina Mačianskienė[1]

[1]Laboratory of Membrane Biophysics, Institute of Cardiology, Lithuanian University of Health Sciences, Sukilėlių 15, Kaunas, Lithuania
inga.andriule@lsmuni.lt

TRPM7 and its homologue TRPM6 belong to the melastatin subfamily of TRP channels, and both are regulated by intracellular magnesium and are distinguished from other ion channels by unusual bifunctional activities, ion channel and protein kinase. TRPM6 and TRPM7 plays a fundamental role in the cellular uptake of Ca^{2+}, Mg^{2+}, Zn^{2+}, and other divalent cations, but their role in the heart, to date, has been explored in fibroblasts and in pacemaker cells. Recently, we have identified that both of these proteins are present in human cardiomyocytes [1].

The aim of this study was to determine and evaluate various extracellular factors (medium ionic compositions, acidosis, and TRP channel inhibitors) modulating the TRPM6 and TRPM7 expression in native cardiomyocytes.

We investigated the immunofluorescence of TRPM6 and TRPM7 proteins under different ionic compositions of the cell incubation medium (i.e., divalent cation-containing (DV) or divalent cation-free (DVF) extracellular conditions). We measured the immunostaining level of both TRPM6 and TRPM7 proteins of the atrial and ventricular cardiomyocytes, performed at 2 hours or at 12 hours after cell isolation. We found that the immunofluorescence level of both of these channel proteins in cardiomyocytes from all chamber walls was significantly higher following cell incubation in DV extracellular conditions *vs.* the following incubation in DVF conditions. In addition, the expression level for either TRPM6 or TRPM7 was higher when cells were fixed after 12 hours of cardiomyocyte conservation. The results confirm that the immunofluorescence levels are dependent on cell incubation conditions.

Pharmacological drugs known to inhibit TRPM6 and TRPM7 channel function also had an effect on the immunofluorescence levels of TRPM6 and TRPM7. In our study the cardiomyocytes were exposed to 2-APB (500 μM) or carvacrol (CAR; 100 μM). In general, cells treated for 15 min with these drugs displayed weaker TRPM7 fluorescence intensity but stronger TRPM6 intensity [1]. Our finding is the concordance between these changes on TRPM7 and TRPM6 immunofluorescence and the reported electrophysiological effects on the channels [2]: an up-regulation of the TRPM6 current, but the suppression of the TRPM7 current. Since 2-APB at high (2 mM) concentration could have an opposite effect on the TRPM7 channels (increase instead of reduce of current), we also investigated on TRPM7 immunofluorescence levels after 15 min pretreatment with 2 mM concentration in human atrial cardiomyocytes. With 500 μM and with 2 mM 2-APB, two opposite effects on the fluorescence intensity of immunodetected TRPM7 proteins were induced: reduction versus increase of the immunofluorescence level, respectively. With 500 μM 2-APB the immunofluorescence of TRPM7 protein decreased from 0.1492 ± 0.0022 a.u. to 0.0872 ± 0.0015 a.u. ($n = 3–5$, $P < 0.001$), but with 2 mM the fluorescence of TRPM7 markedly increased to 0.1946 ± 0.0019 a.u. ($n = 4$, $P < 0.001$). In contrast, for immunodetected TRPM6 measured under the same experimental conditions, the increase obtained at 500 μM (from 0.064 ± 0.0023 a.u. to 0.1281 ± 0.0016 a.u.; $n = 3$, $P < 0.001$) was further enhanced at 2 mM (increase to 0.1641 ± 0.0031 a.u.; $n = 5$, $P < 0.001$ *vs.* value in the absence of 2-APB), respectively. Again, these new data demonstrate the concordance with the electrophysiological data (decrease of TRPM7 current amplitude at 500 μM, but marked increase at 2 mM). Besides, the reversal of changes in TRPM7 but not TRPM6 immunofluorescences further also supports our the view that both proteins are regulated independently.

Like extracellular divalent cations and pharmacological agents, extracellular pH is known to modulate TRPM6 or TRPM7 channel function [3, 4]. The present study shows that extracellular acidification to pH 5.0 of the cell incubation medium also caused changes in the immunodetected TRPM7 and TRPM6 fluorescence signals (in the DV milieu increased by 1.45 fold and 3.06 fold, respectively, whereas, in DVF mileau suppressed the fluorescence of TRPM7, but consistently increased that of TRPM6 protein. Again, for TRPM7 there is concordance with the electrophysiological data, as extracellular acidification increases current in extracellular solutions containing DV cations, but decreases current in the DVF extracellular solution [4].

In conclusion, the results provide consistent evidence for the extracellular modulation of both TRPM6 and TRPM7 proteins. We found that these channels are not related and may function independently from each other. This might suggest that in cardiomyocytes TRPM6 and TRPM7 compose distinct channels.

[1] Andriulė I, Pangonytė D, Almanaitytė M, Patamsytė V, Kuprytė M, Karčiauskas D, et al. Evidence for the expression of TRPM6 and TRPM7 in cardiomyocytes from all four chamber walls of the human heart. Sci Rep. 2021;11(1):1–14.

[2] Li M, Jiang J, Yue L. Functional characterization of homo- and heteromeric channel kinases TRPM6 and TRPM7. J Gen Physiol. 2006;127(5):525–537.

[3] Gwanyanya A, Amuzescu B, Zakharov SI, Mačianskienė R, Sipido KR, Bolotina VM, et al. Magnesium-inhibited, TRPM6/7-like channel in cardiac myocytes: permeation of divalent cations and pH-mediated regulation. J Physiol. 2004;559(3):761-776.

[4] Mačianskienė R, Almanaitytė M, Jekabsone A, Mubagwa K. Modulation of human cardiac TRPM7 current by extracellular acidic pH depends upon extracellular concentrations of divalent cations. PLoS ONE. 2017;12(1):e0170923.

Towards purification of recombinant TMEM106B

Rokas Bertasius, Lukas Krasauskas, Vytautas Smirnovas.

Institute of Biotechnology, Life Sciences Center, Vilnius University
rokas.bertasius@gmc.stud.vu.lt

Even though neurodegenerative diseases are one of the most widespread in the world, affecting tens of millions of people, medical professionals are predicting numbers will more than triple in the coming 30 years. As the number of people suffering from neurodegenerative diseases is rapidly increasing, each year researchers are finding new clues on how neurodegeneration manifests itself. Usually, amyloid-related brain diseases are grouped by specific proteins that aggregate and cause specific pathologies in these diseases. Recently it was discovered that aggregates of TMEM106B protein are commonly found in some large groups of neurodegenerative diseases, including synucleinopathies, tauopathies, and TPD-43 proteinopathies [1]. TMEM106B is a lysosomal protein highly expressed in neurons and oligodendrocytes. It has 254 amino acid residues and consists of a C-terminal domain that projects into the lysosomal lumen, a single-pass transmembrane domain, and an N-terminal domain extending into the cytosol. Alterations in levels of TMEM106B are intimately linked to neuronal proportions, brain aging, and disorders. Knockdown of TMEM106B can lead to the formation of giant vacuoles near the axon initial segment in neurons due to increased retrograde transport and myelination defects [2]. Currently, almost all knowledge about the aggregation of TMEM106B comes from post-mortem brain research as purification of the protein is proven hard to do [3]. It is hypothesized that in pathology, unknown proteases cut off the C-terminal domain, leaving a couple of different possibilities. Either the C-terminal of TMEM106B aggregates inside lysosomes or it leaves them in an unknown process and forms aggregated structures in the cytosol. Fortunately, the exact structures of TMEM106B aggregates are already determined. Aggregates consist of 18 beta-sheets, have a disulfide bond between C214 and C254 amino acids, and can form butterfly-like doublet fibrils with the still unknown anionic cofactor.

Since *in vitro* studies of TMEM106B are limited due to hard-to-replicate purification protocols, low purity levels, and poor yields it is hard to conduct aggregation tests. Here we aim to create a novel and easier way to purify TMEM106B from genetically modified *E.coli* cells using affinity chromatography and SUMO fusion technology. Fusing SUMO tag to the desired protein is known to promote higher solubility, better folding, and expression of the protein. At the same moment after SUMO cleavage, desired protein results without any additional amino acids at the N-terminus, resulting in the native recombinant protein. To that result, the TMEM106B gene was fused at N-termini with ULP1 protease cleavable His-SUMO tag. His-SUMO-TMEM106B gene was inserted into the pET28A expression vector by restriction cloning using BamHI and NdeI restriction endonucleases. Protein was purified using Ni^{2+} ion affinity and size exclusion chromatography methods. In this work, we purify TMEM106B specific C-terminal fragment (120-254 aa), which was reported to form amyloid structures *in vivo*.

[1] Chang, A., et al. (2022). Homotypic fibrillization of TMEM106B across diverse neurodegenerative diseases. Cell, 185(8), 1346–1355.e15. https://doi.org/10.1016/j.cell.2022.02.026

[2] Feng, Tuancheng, Alexander Lacrampe, and Fenghua Hu. "Physiological and pathological functions of TMEM106B: a gene associated with brain aging and multiple brain disorders." *Acta neuropathologica* 141.3 (2021): 327-339.

[3].Schweighauser, M., *et al.* (2022). Age-dependent formation of TMEM106B amyloid filaments in human brains. Nature, 10.1038/s41586-022-04650-z. Advance online publication. https://doi.org/10.1038/s41586-022-04650-z

Terpenes are Potent Cx43 Gap Junction Inhibitors

Rokas Mickus[1], Vytautas Raškevičius[1], Inga Matulytė[2], Mindaugas Marksa[2], Kęstutis Maciūnas[1], Jurga Bernatonienė[2], Vytenis Arvydas Skeberdis[1]

[1]Lithuanian University of Health Sciences, Institute of Cardiology, Sukilėlių pr. 15, Kaunas, Lithuania
[2]Lithuanian University of Health Sciences, Faculty of Pharmacy, Sukilėlių pr. 13, Kaunas, Lithuania
Rokas.mickus@lsmuni.lt

Physiological and pathological processes such as homeostasis, embryogenesis, development, tumorigenesis, and cell movement depend on the synchronization of cell-to-cell communication. Connexin (Cx)-based gap junction (GJ) channels that provide direct electric and metabolic intercellular communication are formed of two apposing hemichannels between adjacent cells. Each hemichannel is composed of six connexin subunits. The family of connexin genes consists of 21 members in the human genome. Cxs are expressed in all tissues except differentiated skeletal muscle, erythrocytes, and mature sperm cells. Cx43 is the most widely expressed connexin responsible for GJ intercellular communication in the majority of tissues.

Present studies show that essential oils from plants are potential source of molecules having cardiotropic, anticancer, anti-inflammatory, and others activities. Terpenes constitute the largest class of natural products of essential oils. Due to diverse biological activity they are extensively used in anti-cancer research. Despite accumulated evidences of their benefits, the molecular mechanisms of their action are mostly unclear.

In the current study, we: 1) extracted the nutmeg essential oil (NEO) and characterized its composition; 2) performed molecular docking of NEO constituents to Cx43 that is endogenously expressed in Novikoff rat hepatoma cells; 3) examined the effect of NEO and its selected constituents on Cx43 GJ conductance and gating in pairs of Novikoff cells; and 4) using fluorescent dye Lucifer Yellow, examined the effect of NEO on metabolic communication of Novikoff cells in monolayer.

Changes in junctional conductance (g_j) and voltage gating parameters (g_j-V_j) showed that NEO was potent Cx43 GJ channel inhibitor acting via slow gating mechanism. Selected constituents of NEO sabinene, α-pinene and α-copaene inhibited g_j of Cx43 GJ with IC_{50s} of 37.8, 12.3 and 1.4 μM, respectively (Fig. 1).

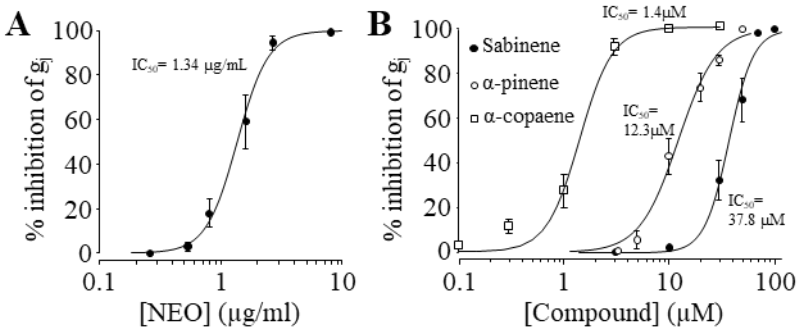

Figure 1. The effect of NEO and its constituents on Cx43 GJ conductance. (A) Dose-response curve for the g_j inhibiting effect of NEO (IC_{50} = 1.34 μg/ml, Hill's coefficient = 3.4). (B) Concentration-response curves for the g_j inhibiting effect of sabinene, α-pinene and α-copaene.

Taken together, our results demonstrate: 1) that NEO itself and its three constituents – monoterpenes sabinene and α-pinene and sesquiterpene α-copaene – can dock to as well as rapidly and reversibly inhibit Cx43 GJ channel conductance by a slow-gating mechanism acting with high potency through more than one active binding site on Cx43 subunits; 2) NEO efficiently inhibits metabolic communication between Novikoff cells.

An efficient rAAV vector for protein expression in cortical parvalbumin expressing interneurons

Gytis Baranauskas[1], Tatiana Tkatch[1,2], Kristina Rysevaite-Kyguoliene[3], Ignas Sabeckis[3], Deimante Sabeckiene[3], Dainius H Pauza[3]

[1]Neurophysiology laboratory, Neuroscience Institute, Lithuanian University of Health Sciences, Kaunas, Lithuania
[2]Anatomy Institute, Lithuanian University of Health Sciences, Kaunas, Lithuania
gytis.baranauskas@lsmuni.lt

Recombinant adeno - associated viruses (rAAV) are extensively used in both research and clinical applications. Despite significant advances, there is a lack of short promoters able to drive the expression of virus delivered genes in specific classes of neurons. We designed an efficient rAAV vector suitable for the rAAV-mediated gene expression in cortical interneurons, mainly in the parvalbumin expressing cells. The vector includes a short parvalbumin promoter and a specialized poly(A) sequence. The degree of conservation of the parvalbumin gene adjoining non-coding regions was used in both the promoter design and the selection of the poly(A) sequence. The specificity was established by co-localizing the fluorescence of the virus delivered eGFP and the antibody for a neuronal marker. rAAV particles were injected in the visual cortex area V1/V2 of adult rats (2 – 4 months old). Neurons expressing the virus delivered eGFP were mainly positive for interneuronal markers: 66.5 ± 2.8 % for parvalbumin, 14.6 ± 2.4 % for somatostatin, 7.1 ± 1.2 % for vasoactive intestinal peptide, 2.8 ± 0.6 % for cholecystokinin. Meanwhile, only 2.1 ± 0.5 % were positive for CaMKII, a marker for principal cells in the cortex. Optogenetic tests confirmed that our vector enables activation of parvalbumin fast spiking interneurons, that leads to elimination of responses to visual stimuli in principal cells. We conclude that our promoter allows highly specific expression of the rAAV delivered cDNAs in cortical interneurons with a strong preference for the parvalbumin positive cells.

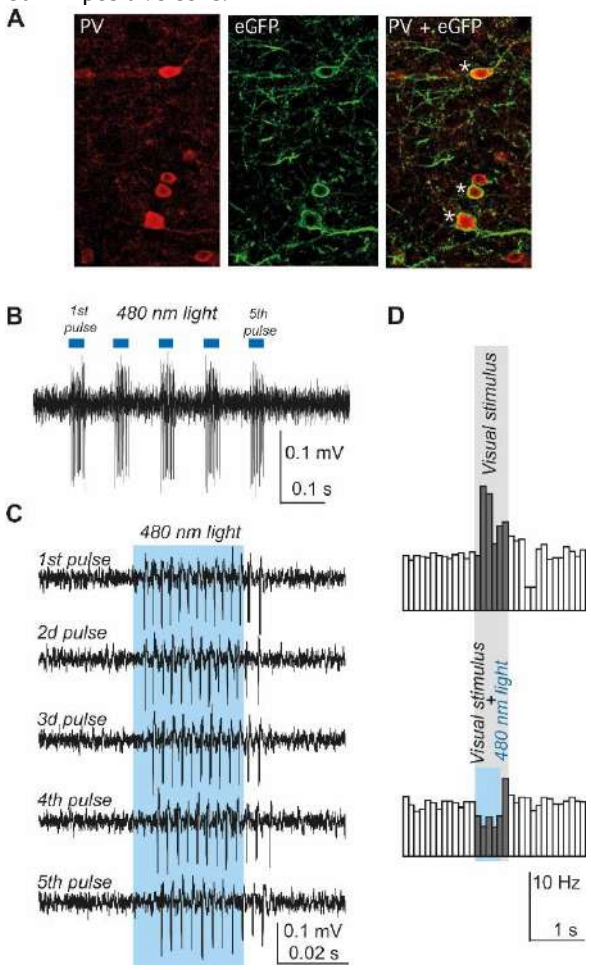

Fig. 1. rAAV vector is suitable for optogenetic experiments. A. Most neurons expressing virus delivered eGFP were also positive for cortical interneuron marker parvalbumin (yellow co-stain, marked with asterisks). B and C. 480 nm blue light evokes high frequency bursts of action potentials, typical for parvalbumin interneurons. D. Activation of parvalbumin interneurons eliminates responses to visual stimuli in principal cells.

Integral actin facilitates connexin-43 hemichannel docking between daughter cells

Vytautas Raškevičius[1], Rokas Mickus[1], Mindaugas Valius[2], Ieva Sarapinienė[1], Vytenis Arvydas Skeberdis[1]

[1]Lithuanian University of Health Sciences, Institute of Cardiology, Sukilėlių pr. 15, Kaunas, Lithuania
[2]Vilnius University, Life Sciences Center, Institute of Biochemistry, Saulėtekio al. 7, Vilnius, Lithuania
vytautas.raskevicius@lsmuni.lt

Gap junction (GJ) channels are composed of two apposed hemichannels of contiguous cells and provide a direct pathway for electrical and metabolic cell-to-cell communication [1]. Six connexin (Cx) subunits oligomerize into a connexon, which after insertion into the plasma membrane is called a hemichannel. The oligomerization of six Cxs into a hemichannel starts in the endoplasmic reticulum and ends in the trans-Golgi network. Then, according to a commonly accepted model, hemichannels-containing vesicles are transported along microtubules and actin filaments to the cell membrane where they are recruited to the outsides of existing GJ plaques. GJ plaques consist of thousands of channels organized in quasi-crystaline arrays; however, for the unknown reason, only a small fraction (~0.1) of them is functional.

Internalization of GJ channels starts from the middle of the plaque via vesicular structures called “annular junctions” [2]. By not well understood mechanism, a whole plaque or a part of it is internalized exclusively into the single cell of the cell pair.

In the present study, we raised a hypothesis that formation of functional GJs during cell division might be coordinated by the integral to both daughter cells microtubule- and actin-dependent delivery system that facilitates docking of apposed Cx43 hemichannels at the interface of the daughter cells (Fig. 1). We propose this hypothesis as an alternative to the generally accepted model because low functional efficiency of GJ plaques suggests that only recruitment of hemichannels to the outsides of the plaques apparently does not guarantee proper docking of apposed hemichannels. In addition, we examined the possibility that the internalization of GJ plaque by the annular junction into the single cell of the pair is preceded by collapse of integral actin filaments in the apposed cell.

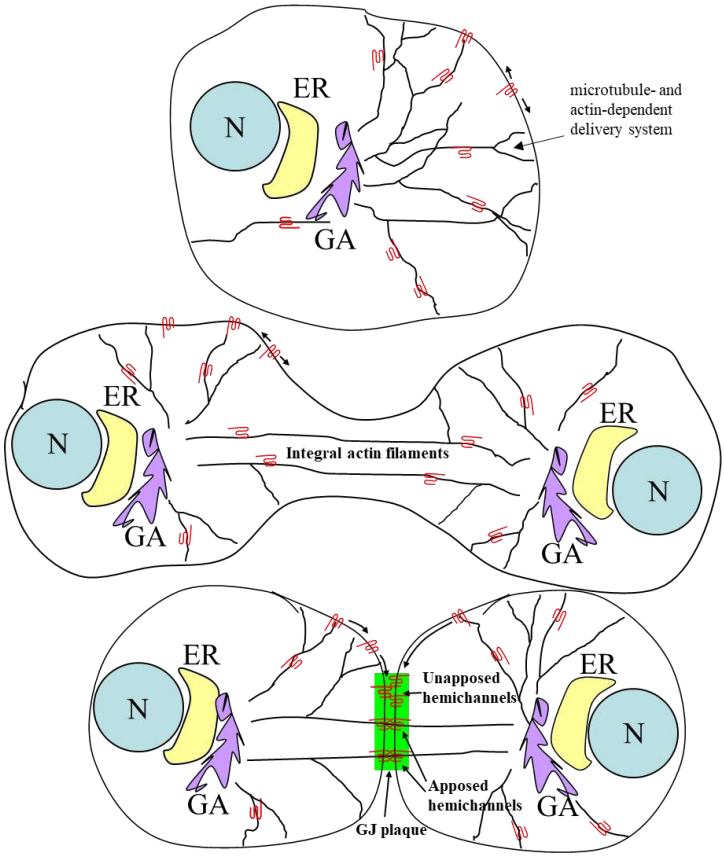

Fig. 1. Formation of functional GJ channels during cell mitosis is coordinated by the integral to both daughter cells microtubule- or/and actin-dependent delivery system. N – nucleus; ER – endoplasmic reticulum; GA – Golgi apparatus.

[1] M. Račkauskas, V. Neverauskas, V. A. Skeberdis. *Medicina (Kaunas)* **46**, 1-12 (2010).
[2] M. M. Falk, C. L. Bell, R. M. K Andrews, S. A. Murray. *BMC Cell Biol.* **17**(Suppl):22 (2016).

Towards Nanomolar Detection of Neurotransmitters: Application of Functionalized Horseradish Peroxidases in Organic Solvents

Diana Macaitytė[1], Vygailė Dudkaitė[1], Audronė Rukšėnaitė[2], Gintautas Bagdžiūnas[1]

[1] Group of Supramolecular Analysis, Department of Bioanalysis, Institute of Biochemistry, Life Sciences Centre, Vilnius University, Saulėtekio av. 7, LT-10257, Vilnius, Lithuania
[2] Institute of Biotechnology, Life Sciences Center, Vilnius University, Vilnius LT-10257, Lithuania
diana.macaityte@chgf.stud.vu.lt

The catecholamine-based neurotransmitters (NTs) such as adrenaline, epinephrine, and dopamine are chemical messengers in the human body. Detection and monitoring of NTs in the brain and blood remains a challenge and continues to garner significant attention because NTs manage the physiological and behavioural state of the neural network [1]. However, NTs concentrations in biological samples are relatively low (from nano- to micro-molar levels) and therefore require highly sensitive sensors to detect these analytes. In our group, the β- or γ-cyclodextrines-based sensors were developed to determine dopamine and adrenaline at these levels [2]. Unfortunately, due to the structural features of the supramolecular sensors, selectivity cannot be achieved for these NTs. On the other hand, enzymatic biosensors based on Horseradish peroxidase (HRP), which can oxidize various organic substrates by hydrogen peroxide, can be applied to selectively analyze the NTs. Moreover, using our developed technology of the functionalization of enzymes in organic solvents, obtained bioconjugates with redox groups can be applied in these biosensors without H_2O_2 [3].

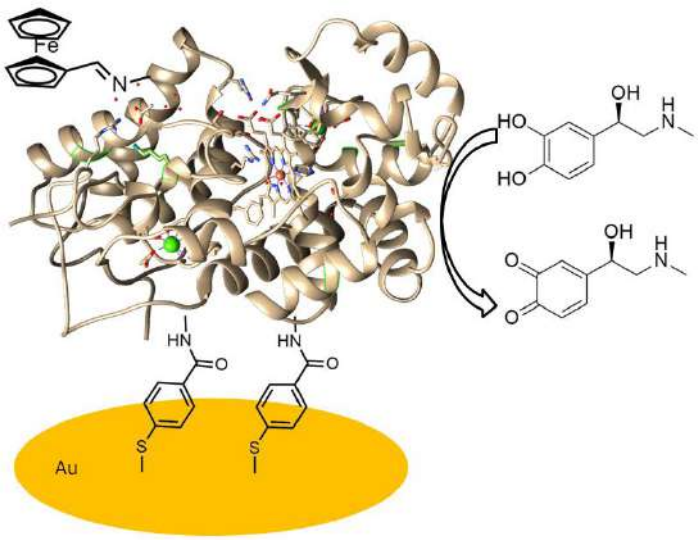

Fig. 1. The Fc-HRP bioconjugate monolayer onto the Au surface for detection of adrenaline.

In this work, I and II type HRPs were functionalized with ferrocenyl aldehyde as the electrochemically active compound to obtain Fc-HRPs. To test and compare the activity of these bioconjugates and starting enzymes, spectrophotometric assays based on 2,2'-azino-bis(3-ethylbenzothiazoline-6-sulfonic acid) (ABTS) as a substrate for a biocatalytic reduction of H_2O_2 was used. We found that HRPs retains their activity after the chemical reaction in chloroform and purification. To prove the ferrocene functional group, buffer solution of these bioconjugates were investigated using electrochemical and optical methods. Monolayers of these bioconjugates were deposited onto gold electrodes to detect adrenaline. The most promising results were achieved using Fc-HRP type I as the electrocatalytic currents up to 100 nM of analyte were higher than those with Fc-HRP type II without H_2O_2. In comparison both type native HRPs and Au electrode, showed almost no response to increasing adrenaline concentration.

Acknowledgments: This work was supported by the European Regional Development Fund under "Promotion of Centers of Excellence and Innovation and Technology Transfer Centers" program No. 01.2.2-CPVA-K-703 (grant No. 01.2.2-CPVA-K-703-03-0010).

[1] Ou, Y. et al., Frontiers in electrochemical sensors for neurotransmitter detection: Towards measuring neurotransmitters as chemical diagnostics for Brain Disorders. *Analytical Methods*, 11(21), 2738 (2019).
[2] Radveikienė, I. et al., Self-assembled cyclodextrins-based nanostructures on indium-tin-oxide for a detection of catecholamine neurotransmitters. *Applied Surface Science*, 600 154170 (2022).
[3] Dudkaitė, V., Bagdžiūnas, G. Functionalization of Glucose Oxidase in Organic Solvent: Towards Direct Electrical Communication across Enzyme-Electrode Interface. *Biosensors* 12, 335 (2022).

Biochemical characterization of SARS-CoV-2 3-chymotrypsin like protease

Kamilė Čerepenkaitė, Aurelija Mickevičiūtė, Asta Zubrienė

Department of Biothermodynamics and Drug Design, Institute of Biotechnology,
Life Sciences Center, Vilnius University, Saulėtekio 7, Vilnius, Lithuania
kamile.cerepenkaite@chgf.stud.vu.lt

In 2020, the world has been shaken up by a global pandemic of COVID-19, a highly contagious disease caused by severe acute respiratory syndrome coronavirus 2 (SARS-CoV-2). Even though the virus causes mild upper respiratory tract illness in most cases, people in high-risk groups and with underlying health conditions often develop severe symptoms that lead to life-threatening conditions. For this reason, the search of chemical substances that would act as antiviral drugs against SARS-CoV-2 has been of great importance.

The 3-chymotrypsin like or main protease (3CLpro or Mpro) is responsible for cleavage of polyproteins during viral replication that are important to assembly of mature viral particles. SARS-CoV-2 3CLpro is intensively explored as a potential target for antiviral drug development[1]. Although the scientific community primarily focuses on newly synthesized compounds, natural substances such as flavonoids are also being investigated as possible antiviral drug candidates using *in silico*-based, *in vitro* and *in vivo* approaches[2].

In this study, two recombinant 3CLpro plasmids were designed, expressed in *E.coli* and the proteins were purified by affinity chromatography. The activity of obtained proteins was measured using FRET-based enzymatic assay and compared with commercially available wild-type 3CLpro. 3CLpro showing the greatest activity has been chosen to screen more than 250 flavonoids as potential 3CLpro inhibitors using fluorescent thermal shift assay, which was also used to examine the effects of pH and NaCl concentration on protein stability. The flavonoids that exhibited stabilizing or destabilizing effect on protein stability were further investigated using *in vitro* enzyme inhibition assay. As a result, three flavonoids were identified as inhibitory compounds and their K_d values were determined by dose-response analysis (Fig. 1). The study suggests that three naturally derived flavonoids could be considered as potential 3CLpro inhibitors.

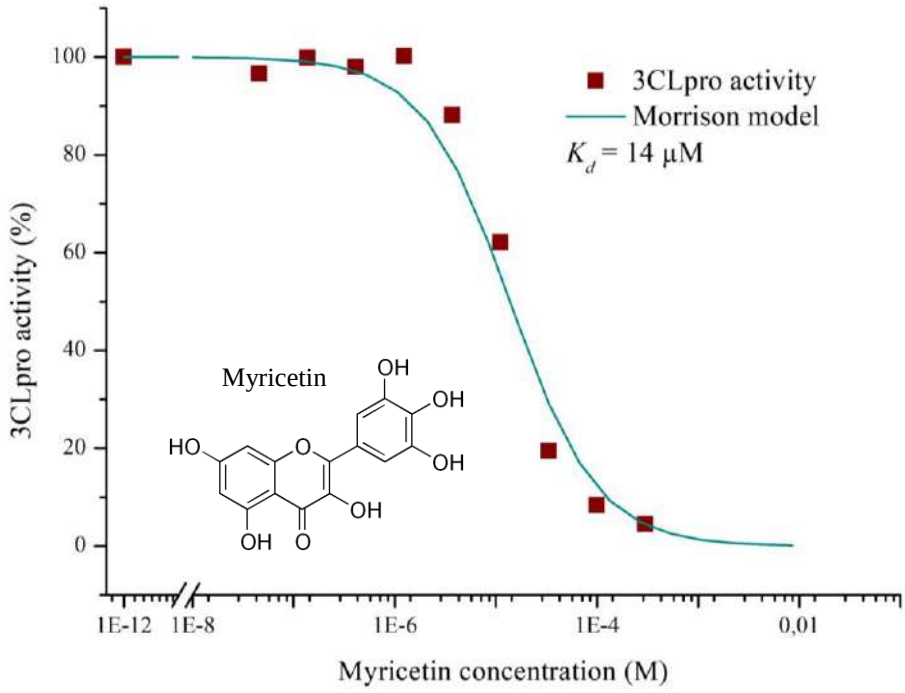

Fig. 1. Dose–response curve of 3CLpro inhibition with myricetin.

[1] Mengist HM, Dilnessa T, Jin T. Structural Basis of Potential Inhibitors Targeting SARS-CoV-2 Main Protease. *Front Chem*. 2021;9. doi:10.3389/fchem.2021.622898

[2] Kaul R, Paul P, Kumar S, Büsselberg D, Dwivedi VD, Chaari A. Promising antiviral activities of natural flavonoids against sars-cov-2 targets: Systematic review. *Int J Mol Sci*. 2021;22(20). doi:10.3390/ijms222011069

Catalytic activity and small molecule binding of cytosolic murine carbonic anhydrases

Tautvydas Kojis, Aurelija Mickevičiūtė, Lina Baranauskienė

Institute of Biotechnology, Life Sciences Center, Vilnius University. Saulėtekio 7, Vilnius, Lithuania
tautvydas.kojis@chgf.stud.vu.lt

Carbonic anhydrases are enzymes that catalyse reversible carbon dioxide hydration. They are essential in many physiological processes, such as pH regulation, ion transport, or metabolic reactions, where bicarbonate is used as a substrate. Thus, carbonic anhydrases are therapeutic targets for diseases which can be controlled by altering pH and bicarbonate homeostasis, such as glaucoma, epilepsy, oedema, some cancer types, etc.

Mammals have multiple carbonic anhydrase isozymes that differ in their cellular localisation, tissue distribution, catalytic activity and link to specific diseases. Therefore, the optimal drug for a specific disease should effectively inhibit the target isozyme(s) and not alter the activity of the off-target ones. However, this task is challenging due to the high structural similarity of the isozymes.

In the preclinical research step, new drug testing is performed on animals. The house mouse (*Mus musculus*) is the most used model organism for preclinical drug testing. While orthologous proteins are highly similar, minor structural differences sometimes result in significant affinity variations toward small molecule inhibitors. There might be significant differences in compound affinity and selectivity profiles of human and mouse carbonic anhydrases, leading to erroneous conclusions. By analysing murine carbonic anhydrases, we will be able to test whether human carbonic anhydrase inhibitors selected using *in vitro* methods have comparable affinity and selectivity to murine carbonic anhydrases, and thus we could expect more accurate results in the preclinical testing.

This study presents catalytic activity and small molecule binding analysis of cytosolic murine carbonic anhydrases: Car I, Car II, Car III, Car VII and Car XIII (Fig. 1).

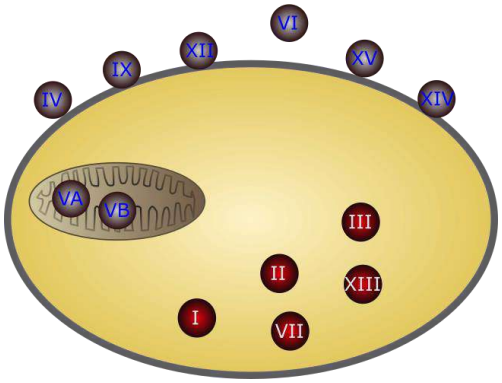

Fig. 1. Cellular localisation of murine carbonic anhydrases. Cellular isozymes (marked in red) were analysed in this study. Others are mitochondrial (Car VA and Car VB), transmembrane, with extracellular active site (Car IX, Car XII and Car XIV), GPI-linked to membrane (Car IV and Car XV), or secreted (Car VI).

[1] Lomelino CL et al. Int J Med Chem. 2018. doi:10.1155/2018/9419521.
[2] J. Smirnovienė et al., *ChemistryOpen* 10(5):567–580 (2021).

Exploring the Effect of Amyloid-Specific Molecules on Protein Aggregation

Kamilė Mikalauskaitė, Mantas Žiaunys, Vytautas Smirnovas

Amyloid Research Sector, Life Sciences Center, Vilnius University, Saulėtekio Ave 7, LT-10257 Vilnius, Lithuania
kamile.mikalauskaite@gmc.vu.lt

Aggregation of amyloid proteins and the resulting amyloid fibrils are associated with various neurodegenerative disorders, such as Alzheimer's, Parkinson's or prion diseases. Although this field has been under intense investigation for many years, only a few effective treatments or drugs have been discovered so far. Often, compounds show potential aggregation inhibitory efficacy during in vitro assays, but fail in clinical trial stages. The effectiveness of inhibitory molecules in vitro is usually analyzed using various fluorescent dyes, such as thioflavin-T (ThT) or 8-anilinonaphthalene-1-sulfonic acid (ANS) [1]. Despite their wide application, the conditions under which amyloid-specific dye molecules are used can vary quite significantly. Studies have shown that increasing the ionic strength of the solution increases the concentration of ThT molecules attached to the fibrils and affects their fluorescence intensity [2]. For this reason, we investigated the influence of ionic strength of the solution or different strains of insulin on the affinity of ANS. For this reason, we investigated how ANS binding and fluorescence parameters are affected by environmental conditions, as well as the surface of different insulin amyloid fibrils.

Different strains of insulin fibrils were obtained under 4 aggregation conditions. Human recombinant insulin powder was dissolved in 20% acetic acid solution, containing 100 mM NaCl (AC conditions), 100 mM phosphate (PH20 conditions), 100 mM phosphate, containing 100 mM NaCl (PH24 conditions) and 1x PBS (PH74 conditions) to a final protein concentration of 200 μM. The prepared AC, PH20 and PH74 samples were incubated at 60 °C for 24 hours without agitation. The PH74 samples were incubated at 60 °C under constant 600 RPM agitation, with two 3 mm glass beads present in the test tube. After aggregation, samples were centrifuged at 12 500 RPM for 10 min and resuspended in MilliQ water (for ionic strength assays) or 1x PBS buffer (for dye affinity assays) to a final fibril concentration of 400 μM. The resulting sample fluorescence intensity, absorbance and excitation-emission matrices were then analyzed.

The results of this work demonstrate that ANS molecules have a higher affinity towards insulin fibrils at low ionic strength conditions. In addition, we show that distinct insulin amyloid fibrils have specific ANS-binding affinities, as well as conformation-specific ANS fluorescence quantum yields.

[1] Gade Malmos, K. et al. ThT 101: a primer on the use of thioflavin T to investigate amyloid formation. Amyloid 24, 1–16 (2017).
[2] Mikalauskaite, K., Ziaunys, M., Sneideris, T. & Smirnovas, V. Effect of Ionic Strength on Thioflavin-T Affinity to Amyloid Fibrils and Its Fluorescence Intensity. Int. J. Mol. Sci. 21, 8916 (2020).

Tool for assisting high-throughput screening of protein-ligand interactions

M. Gedgaudas, E. Kazlauskas, V. Petrauskas, D. Matulis

Department of Biothermodynamics and Drug Design, Institute of Biotechnology,
Life Sciences Center, Vilnius University, Lithuania
marius.gedgaudas@gmc.vu.lt

Differential scanning fluorimetry (DSF; also known as thermal shift assay, TSA) is a quick, easily accessible and inexpensive method to determine protein stability (melting temperature, T_m) at different conditions. This method is often used in drug discovery for high-throughput screening of ligand libraries.

DSF data can be used to quantitatively determine protein-ligand binding affinities (K_b). Despite that, its most common use is limited to only observing a shift in T_m, i.e., only to see whether the ligand binds at all. This is a consequence of a lack of user-friendly software that would perform the necessary regression analysis of complex thermodynamic equations.

For this reason, we developed *Thermott*[1] – a tool capable of performing such analyses from start to finish. From experimental DSF data it can determine protein melting temperatures and subsequently determine protein-ligand binding affinities. *Thermott* is available as a free, open-source online web application and requires no additional setup (https://thermott.com/). We believe that our tool greatly simplifies and streamlines the analysis of DSF data and thus will make this method much more accessible.

[1] M. Gedgaudas, D. Baronas, E. Kazlauskas, V. Petrauskas, D. Matulis, “Thermott: A comprehensive online tool for protein–ligand binding constant determination”, Drug Discovery Today, 2022.

Prion Protein Amyloid Aggregates Associate with Tau Protein Monomers in Conformation-specific Manner

Lukas Krasauskas, Mantas Ziaunys, Kamile Mikalauskaite, Vytautas Smirnovas

Amyloid research sector, Institute of Biotechnology, Life Sciences Center, Vilnius University, Vilnius, Lithuania
lukas.krasauskas@gmc.vu.lt

Protein/peptide aggregation in the form of amyloid fibrils is associated with several amyloidoses, including neurodegenerative Alzheimer's and Parkinson's diseases. These diseases are widely spread, affecting around 50 million worldwide, and these numbers are expected more than triple in 30 years. Despite years of research and numerous studies, the aggregation process is still not fully understood, which significantly impedes the search for potential cures for amyloid-related disorders. Recently, there has been an increase in reports of amyloidogenic protein cross-interactions during the fibril formation process, which further complicates the already intricate process of amyloid aggregation. One of these reports displayed an interaction involving Tau and prion proteins, which prompted a need for further investigation into the matter [1]. Since Tau protein tangles in the brains are one of the two main hallmarks of Alzheimer's disease, a vastly spread form of neurodegenerative diseases, as well as other tauopathies, a new association with prion protein could help to further elucidate mechanisms behind Tau aggregation and related pathologies [2].

In this work, we generated five prion protein fibril types with distinct conformations and examined their interaction with Tau protein by fluorescence spectroscopy using the amyloidophilic dye thioflavin T, also UV/Vis spectroscopy, and by analyzing structures resulting from these interactions with Fourier-transform infrared spectroscopy. We observed that there was a conformation-specific association between Tau monomers and prion protein fibrils, which increased the aggregate self-association and amyloidophilic dye-binding capacity. However, we also determined that the interaction did not induce the formation of Tau protein amyloid aggregates, but rather caused their electrostatic adsorption to the prion protein fibril surface.

[1] Hallinan, G. I., Hoq, M. R., Ghosh, M., Vago, F. S., Fernandez, A., Garringer, H. J., Vidal, R., Jiang, W., & Ghetti, B. (2021). Structure of Tau filaments in Prion protein amyloidoses. Acta neuropathologica, 142(2), 227–241. https://doi.org/10.1007/s00401-021-02336-w
[2] Limorenko, G., & Lashuel, H. A. (2022). Revisiting the grammar of Tau aggregation and pathology formation: how new insights from brain pathology are shaping how we study and target Tauopathies. Chemical Society reviews, 51(2), 513–565. https://doi.org/10.1039/d1cs00127b

Discovery of novel SARS-CoV-2 papain-like protease inhibitors by thermal shift assay

Martynas Bagdonas [1], Kamilė Čerepenkaitė [1], Birutė Grybaitė [2], Vytautas Mickevičius [2], Asta Zubrienė [1]

[1] Department of Biothermodynamics and Drug Design, Institute of Biotechnology, Life Sciences Center, Vilnius University, Saulėtekio 7, Vilnius, Lithuania
[2] Department of Organic Chemistry, Kaunas University of Technology, Radvilėnų pl. 19, Kaunas, Lithuania
martynas.bagdonas@gmc.stud.vu.lt

According to World Health Organization the outbreak of COVID-19 caused by the SARS-CoV-2 virus has resulted in over 6.5 million related deaths by September 2022. Purposely created vaccines have significantly slowed down the spreading of the virus, but have not ensured versatile control of the situation due to the occurrence of viral mutations. For this reason, there is still a need to develop new antiviral drugs for a faster and more efficient treatment strategy. Papain-like protease (PLpro) is one of the two essential proteases encoded by the SARS-CoV-2 genome. PLpro cleaves the peptide bonds in the viral polyprotein to release functional nonstructural proteins (NSPs) responsible for viral replication, transcription, and maturation. In addition, PLpro is involved in the disruption of host antiviral response machinery to facilitate viral proliferation. Therefore, the PLpro is identified as a promising target for antiviral drug development [1,2].

In this study, recombinant full-length SARS-CoV-2 PLpro was expressed in Escherichia coli and purified using affinity chromatography. Our unique library of more than 1000 compounds was screened against PLpro using fluorescent thermal shift assay (FTSA). Six compounds exhibiting a stabilization effect on the protein were identified as potential SARS-CoV-2 PLpro inhibitors. The binding affinities of these compounds were evaluated by FTSA and FRET-based enzymatic assay. Compound BG-84 with a single-digit micromolar dissociation constant was found to be the most potent inhibitor of PLpro (**Fig.1**).

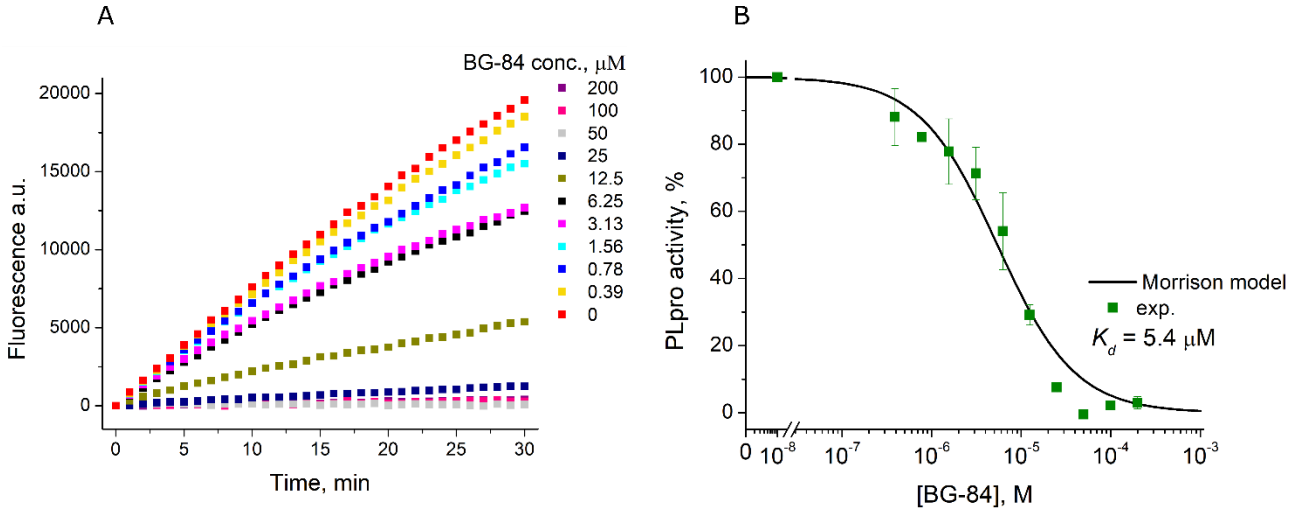

Fig.1. Dose-response curve of PLpro inhibition with compound BG-84. (A) Enzyme activity evaluated according to increase in fluorescence signal due cleavage of fluorogenic substrate by protease. (B) Relative PLpro activity dependence on compound concentration. Dissociation constant calculated according to the Morrison equation.

[1] Shen Z, Ratia K, Cooper L, Kong D, Lee H, Kwon Y, et al. Design of SARS-CoV-2 PLpro Inhibitors for COVID-19 Antiviral Therapy Leveraging Binding Cooperativity. J Med Chem. https://doi.org/10.1021/acs.jmedchem.1c01307
[2] Tan H, Hu Y, Jadhav P, Tan B, Wang J. Progress and Challenges in Targeting the SARS-CoV-2 Papain-like Protease. J Med Chem. 2022 Jun 9;65(11):7561–80.

Influence of Fe(II) on Lipid Orientation in the Lipid Bilayer: Quantum Chemical Simulations

Teresė Kondrotaitė, Alytis Gruodis, Gintautas Saulis

Department of Biology, Faculty of Natural Sciences, Vytautas Magnus University, Kaunas, Lithuania
Alytis.Gruodis@gmail.com

In the cell plasma membrane, phospholipids perform the forming, retaining, labile alteration and the transfer of the barrier layer functions. Under normal physiological conditions, most molecules cannot directly permeate through the membrane without physical or chemical perturbation of the bilayer. Induced effects from outside (uncontrolled discharge of electricity, electroporation, formation of acidic, alkaline media, and localization of aggressive metal ions) allow cell membrane damage through lipid conformational and destructive processes. Since the membrane structure is a layered lipid, it is necessary to evaluate not only the physical but also the chemical aspects: the redox reactions taking place at the membrane create many ionized components that essentially catalyze the above-mentioned factors. Metal ions belong to these factors.

To understand the dynamics of the formation of the pore in the lipid bilaer and its subsequent closure at the molecular level, modeling of the structure of phospholipids and iron ion (Fig. 1) associates by quantum molecular theory methods was performed. Quantum chemical simulations were run using *Gaussian16* [1] package.

Optimization of associate geometry was performed by *Gaussian16* [1] program, using the semi-empirical density function method B3LYP by means of Gaussian basis set 6-31G. Influence of the solvent media (water) was evaluated by Polarized Continuum Model (PCM).

It has been found that metal ion fixation to the lipid chain is insignificant to cause lipid conformational movement. Similarly, metal ion fixation in the case of the $–N–3(CH_3)_3$ head in the lipid head group was not observed. The iron ion binds two lipid molecules in the orthophosphoric region, forming an energetically stable bridge between orthophosphoric fragments. Both saturated and unsaturated phosphatidylserine (PS) have been reported to be similarly resistant to iron-dependent lipid peroxidation. It is believed that the PS head group is responsible for this effect, as it binds the iron ion, reducing the concentration of free iron ions [2]. As a result of this process, the lipid aliphatic chains change their conformation - a curved chain around the metal ion centre is formed from a straight structure.

A typical molecular charge redistribution during excitation was determined and described. It is stated that due to the energetically favorable Fe^{2+} ion position, one lipid becomes a charge donor and the other – a charge acceptor. Fig. 2 represents a typical associate containing two phospholipids bridged by Fe^{2+} ion in the orthophosphoric region, projection XOY. Molecular orbitals correspond a forbidden electronic transition of 0.50 eV from the ground state (MO 210,211) to the first excited state (MO 226). The iron ion binds two lipid molecules in the orthophosphoric region, forming an energetically stable bridge between the orthophosphoric fragments. As a result, the lipid aliphatic chains change the conformation - a curved chain about the centre of the metal is formed from the straight structure.

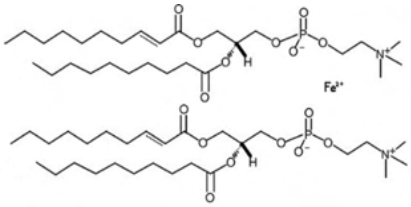

Fig. 1. Associate of Fe^{2+} ion (at centrum) with hydroxyl radicals and ortho-phospholipids.

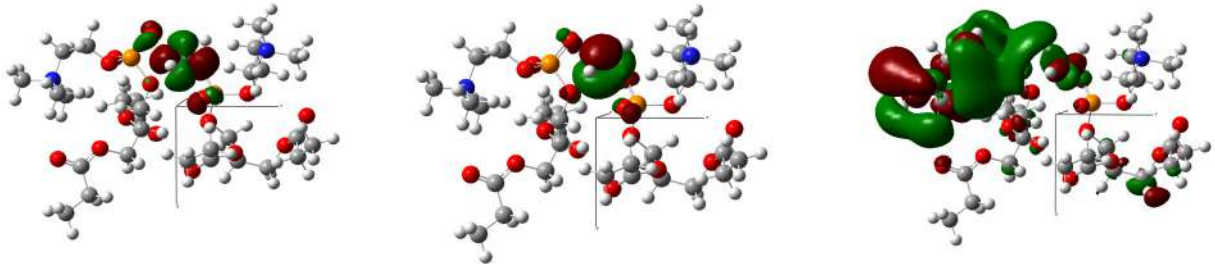

210 211 226

Fig. 2. Associate: two phospholipids bridged by Fe^{2+} ion in the orthophosphoric region, projection XOY. Molecular orbitals (MO) corresponding to a forbidden electronic transition of 0.50 eV from the ground state (MO210,211) to the first excited state (MO226).

[1] M. J. Frisch, G. W. Trucks, H. B. Schlegel et al., *Gaussian 16, Revision B.01*, Gaussian, Inc., Wallingford CT, 2016.
[2] K. Yoshida, J. Terao, T. Suzuki, K. Takama, *Biochem. Biophys. Res. Commun.*, **179**, 1077-1081 (1991).

Bacterial membrane mimicking model and its interaction with antimicrobial peptides

Modestas Mažerimas[1], Rima Budvytyte[1,2]

[1] Life Sciences Center, University of Vilnius, Vilnius, Lithuania
[2]Institute of Biochemistry, Department of Bioelectrochemistry and Biospectroscopy, Life Sciences Center, Sauletekio av. 7, LT-10257, Vilnius
modestas.mazerimas@gmc.stud.vu.lt

Bacteria are the most abundant live organism in the world. Fraction of them is capable of inhabiting a human organism thus risking causing an infectious disease. The introduction of antibiotics, less than a hundred years ago, drastically decreased the possibility of infectious disease complications, however upcoming "post-antibiotics era" when bacteria gain resistance to one or more existing antibiotics creates an emerging threat to the whole health sector [3]. Antimicrobial peptides (AMP) could become an alternative to antibiotics. The fast development of AMPs requires innovative and quick methods of screening for possible preclinical and clinical trial candidates[1].

During this research, tethered bilayer lipid membranes (tBLMs), which are mimicing bacterial membranes were constructed. Using electrochemical impedance spectroscopy (EIS), developed tBLMs were evaluated quantitatively by such parameters as impedance (systems current resistance) and impedance inversely proportional admittance (systems current conductivity), phase shift degree, and systems current capacity [2; 4]. Experiments revealed that selected tBLM were stable over time. By detecting changes in tBLM electrical parameters, we investigated the changes occurring in bilayers when incubated with two different AMPs – colistin and gramicidin.

During the investigation, we noticed that affected with 10-30 μM concentration of colistin bacterial membrane mimicking tBLMs were decreasing in systems current conductivity – the membrane became stiffer, and more tightly packed lipids erased naturally occurring membrane defects. When affected with 1-5 nM gramicidin concentrations bacterial membrane mimicking tBLMs, the conductivity of membrane was increasing rapidly – gramicidin embedded in the lipid bilayer dimerized to form ion-permeable pores in the membrane.

---

[1] Boparai, J. K., ir Sharma, P. K. (2019). Mini Review on Antimicrobial Peptides, Sources, Mechanism and Recent Applications. Protein & Peptide Letters, 27(1), 4–16. https://doi.org/10.2174/0929866526666190822165812

[2] Budvytyte, R., Mickevicius, M., Vanderah, D. J., Heinrich, F., ir Valincius, G. (2013). Modification of Tethered Bilayers by Phospholipid Exchange with Vesicles. Langmuir, 29(13), 4320–4327. https://doi.org/10.1021/la304613a

[3] Davies, J., ir Davies, D. (2010). Origins and Evolution of Antibiotic Resistance. Microbiology and Molecular Biology Reviews, 74(3), 417–433. https://doi.org/10.1128/MMBR.00016-10

[4] McGillivray, D. J., Valincius, G., Vanderah, D. J., Febo-Ayala, W., Woodward, J. T., Heinrich, F., Kasianowicz, J. J., ir Lösche, M. (2007). Molecular-scale structural and functional characterization of sparsely tethered bilayer lipid membranes. Biointerphases, 2(1), 21–33. https://doi.org/10.1116/1.2709308

Effect of pH on tethered Bilayer Lipid Membranes

Shivabalan A.P[1], Gintaras Valinčius [1]

[1]Vilnius University Life Sciences Center, Department of Bioelectrochemistry and Biospectroscopy, Saulėtekio al. 7, Vilnius 10257.

Shivabalan.arun@bchi.stud.vu.lt

Tethered Bilayer Lipid Membranes(tBLMs) are a robust model systems mimicking the lipid bilayer membranes of the biological cells. tBLMs are suitable for studying the biochemical and biophysical properties of lipid bilayer membranes [1]. They are increasingly used for membrane-protein interaction studies including functional reconstitution of the pore-forming proteins and peptides [2]. pH plays a major role in the functioning of membrane proteins. It affects membrane structure and properties such as intactness and fluidity as well as the features of the membrane/protein interactions. The pH induced effects in tBLMs were recently reported [3] and observable phenomena are related to the alteration in packing density in the phospholipid bilayers.

In this communication, we explored the pH effects in the range from pH 4.4. to 7.1. The tBLMs were assembled via multilamellar vesicle fusion onto 30% molecular anchor WC14 and 70% β-mercaptoethanol functionalized thin film gold surface [2]. We studied the pH induced effects on the electrical properties of pristine tBLMs and tBLMs populated with the pore forming toxins: vaginolysin (VLY) assembling into large, >10 nm and mellitin (MEL) into small, ≈2 nm, radius pores. In both cases, the study was performed utilizing the Electrochemical Impedance Spectroscopy (EIS) methodology, and the effect of pH was quantitatively assessed by measuring the impedance phase minimum shift as described in [5].

We found that as the pH increases from 4.4 to 7.1 the EIS phase minimum moves towards higher frequencies, with log Δf_{min} = 0.65± (0.08-0.15) for all compositions of pristine tBLMs. The DOPC:Cholesterol 50:50 membranes populated with VLY exhibited similar phase shift pattern with logΔfmin = 0.38±0.10. DOPC:Cholesterol 70:30 membranes (see Figure below) populated with small MEL pores exhibited phase minimum shift of log Δf_{min} = 0.38±0.17. Taking into account the fact that in the case of DOPC:Cholesterol 50:50 membranes, where the dominant type of defects are large VLY pores, and the modulation of large pore conductivity marginally affects measured position of phase minimum [5], we come up with the hypothesis that the pH affects not only the structural arrangement of tBLMs as suggested in ref [3] but also the properties of the 1-2 nm thick submembrane reservoir separating solid support from the phospholipid bilayer, which significantly affects measured conductivity as well as the position of the EIS phase minimum.

In conclusion, we demonstrated through the interrogation of pH induced effects on EIS response of tBLMs that the submembrane layer may contribute to measured EIS signal and this effect needs to be taken into account when interpreting EIS data of tBLMs. Also, our results demonstrate that the physical properties of the tiny 1-2 thick layer of liquid can be measured by the macroscopic technique like EIS.

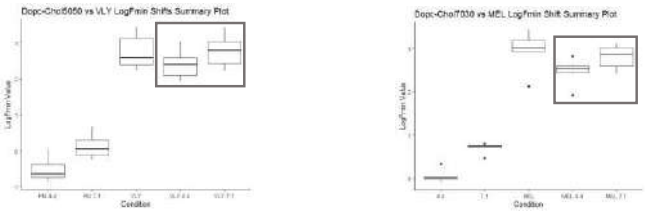

Fig 1. Summary plot indicating similar effect of pH changes (dark grey boxes) on both DOPC – Cholesterol 5050 membranes and DOPC – Cholesterol 7030 membranes populated with VLY and MEL respectively.

[1] Penkauskas, Tadas, and Giulio Preta. "Biological applications of tethered bilayer lipid membranes." Biochimie 157 (2019): 131-141.

[2] Ragaliauskas, Tadas, et al. "Fast formation of low-defect-density tethered bilayers by fusion of multilamellar vesicles." Biochimica et Biophysica Acta (BBA)-Biomembranes 1859.5 (2017): 669-678.

[3] Cranfield, Charles G., et al. "Evidence of the key role of H3O+ in phospholipid membrane morphology." Langmuir 32.41 (2016): 10725-10734.

[4] Raila, Tomas, et al. "Electrochemical impedance of randomly distributed defects in tethered phospholipid bilayers: Finite element analysis." Electrochimica Acta 299 (2019): 863-874.

[5] Raila, Tomas, et al. "Clusters of protein pores in phospholipid bilayer membranes can be identified and characterized by electrochemical impedance spectroscopy." Electrochimica Acta 364 (2020): 137179.

Development of a directed protein evolution method based on droplet microfluidics and DNA microparticles

Simonas Norvaišis[1], Lorenzo Camisi[1], Linas Mažutis[1]

[1] Institute of Biotechnology, Life Science Center, Vilnius University, Vilnius, Lithuania
simonas.norvaisis@gmc.vu.lt

Directed protein evolution remains one of the major techniques for tailoring the catalytic activity or other biochemical properties of biomolecules of industrial or biomedical interest. Most of the strategies for directed evolution of biomolecules rely on screening of mutant libraries by the means of fluorescence readout utilizing microtiter plates. However, limited throughput screening capabilities and large reaction volumes impose constrain when evolving diverse libraries. Droplet microfluidics technology offers significantly higher screening capabilities; over >106 mutant variants can be screened for desirable features thus covering broader combinatorial space. Droplet-based fluorescence-activated sorting enables enrichment of the droplets comprising the desirable protein variants based on catalytic or binding activity. Here, we present a platform for completely in vitro evolution of proteins using DNA microparticle technology. The sub-micron nucleic acid particles consisting of thousands of copies of a single gene are loaded in droplets to achieve an improved yield of proteins by the in vitro transcription/translation. Therefore, water-in-oil droplets having condensed DNA particles and all components necessary for gene expression resemble artificial cells that can be screened under a variety of conditions incompatible with living systems. We show how this novel DNA microparticle technology, when combined with droplet microfluidics and FADS, can be applied for a high-throughput directed evolution of proteins of interest.

Fabrication of microfluidic chip for electroporation of cells

Neringa Bakutė[1], Paulina Kizinievič[1], Elinga Bražionytė[1], Arūnas Stirkė[1,2]

[1]Centre for Physical Science and Technology, Department of Functional Materials and Electronics, Bioelectrics Laboratory, Saulėtekio av. 3, LT-10257 Vilnius
[2]Micro and Nanodevices Laboratory, Institute of Solid State Physics, University of Latvia, Kengaraga str. 8, LV-1063, Riga, Latvia
neringa.bakute@ftmc.lt, arunas.stirke@ftmc.lt

A technology of microfluidics is characterized as engineered manipulation of fluids from nano to micro scale. It is getting more and more potentials in bioscience, as it opens a solution for high-throughput and highly specific analysis for biology, medicine and chemistry[1]. With a microfluidic device, it became possible to integrate a whole laboratory in one simple micro-sized system while consuming only tiny amounts of reagent and a space. In moving from macro- to microscale, there is unprecedented control over spatial and temporal gradients and patterns that cannot be captured in conventional Petri dishes and well plates [2]. Notwithstanding, there is not a single standard microfluidic chip which could be used for all different fields of studies. There are different microchips with certain geometries, inlet/outlet, channel depth and other parameters to precisely regulate the required function. Therefore, the microfluidic chips are mostly custom made.

Since our group is studying an effect of pulsed electric field on cells, thus we are fabricating a continuous-flow microfluidic chip designated for electroporation of mammalian cells, both for the adherent and suspension cells. To realize these materials, we have fabricated microfluidic chip using standard soft-lithography technique with an UV-curable polymer (Fig. 1). In the region of cell culture chamber, there are integrated electrodes for electroporation of cells.

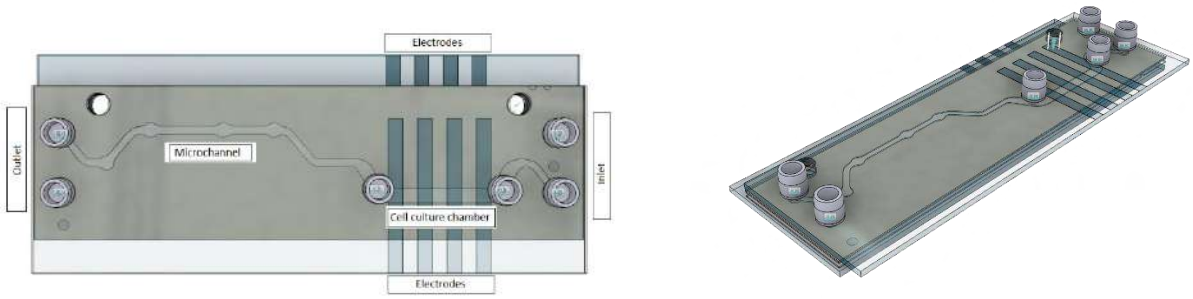

Fig. 1. Scematic presentation of microfluidic chip for electroporation of mammalian cells.

Cell culture chamber of fabricated microchip is divided into two microchannels (upper and lower) with a membrane in-between, thus microchip may be used for high- throughput electroporation of cells in suspension as well as in adherent cells. Both microchannels have their own inlet and outlet, enabling to inject material separately. Our perspectives are electroporation of cells with a fluorescent dye and a plasmid DNA performed in two ways: (1) plasmid is injected in the same chamber together with the cells and (2) plasmid and the cells are be injected into separate channels.

[1] Tabeling P. *Oxford University Press* (2005)
[2] Edmond W. K. Young and David J. Beebe. *J Chem Soc Rev.*; 39(3): 1036–1048 (2010)

Scanning Probe Based Rapid Prototyping of Single Cell Chips

Martynas Gavutis[1], Vytautas Navikas[1], Tomas Rakickas[1], Ramūnas Valiokas[1]

[1]Department of Nanoengineering, Center for Physical Sciences and Technology, Savanorių ave. 231, LT-02300 Vilnius, Lithuania
gavutis@ftmc.lt

We present scanning-probe based techniques for fabrication of sub-micron surface features for single-cell arraying and controlled adhesion. Such rapid prototyping can be implemented by commercial scanning probe (SP) microscopy instrumentation, in the regular chemical laboratory environment. Our key process is direct chemical writing at a speed up to 100 μm s-1, with an SP functioning as a nanofluidic pen for transferring mixtures of surface-selective bifunctional compounds and lipids. We fabricate and subsequently replicate a few mm-sized chip areas, consisting of protein features of virtually any geometry, at a submicron resolution. We demonstrate the utility of the SP nanolithography in the design of subcellular patterns for programming cytoskeletal architectures and developing new single-cell sensing platforms.

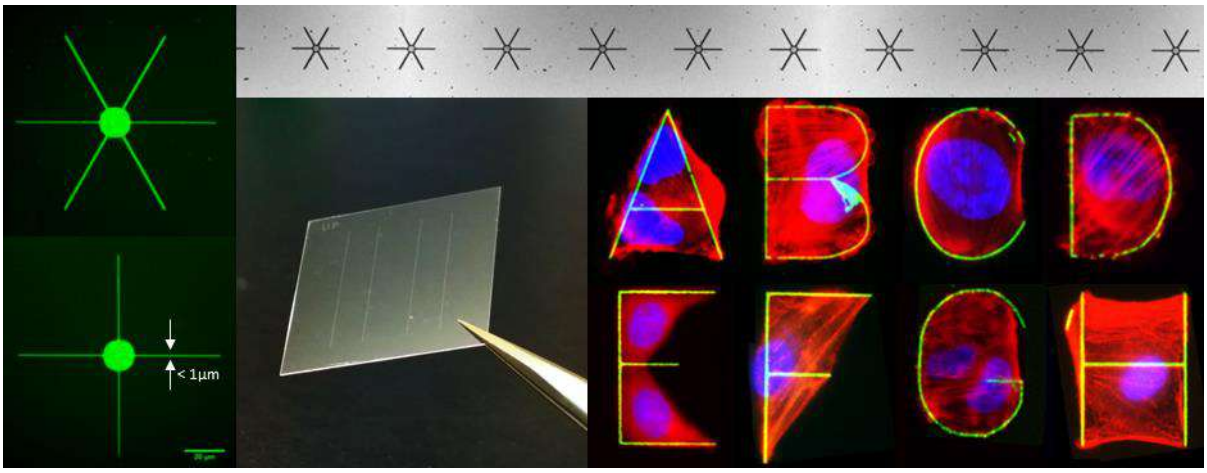

Superlattice Fabrication Employing Multi Exposure Laser Interference Lithography

Gvidas Klyvis[1], Virgilijus Minialga[1], Tomas Tamulevičius[1,2]

[1]Institute of Materials Science, Kaunas University of Technology, K. Baršausko Str. 59, LT-51423, Kaunas, Lithuania
[2]Physics Department, Kaunas University of Technology, Studentų Str. 50, LT-51368, Kaunas, Lithuania
gvidas.klyvis@ktu.lt

Photonic crystals are structures, with periodic feature sizes close to the wavelength of light they are designed for [1]. Such periodic structures enable different spectral and spatial light manipulations that can be utilized in optical light filtering [1], surface-enhanced Raman scattering based sensing [2], etc. Interesting optical properties can be achieved not only from three-dimensional (3D) photonic structures but also from 2D or 2.5D where regular dot or pillar arrays of different symmetries are used [3]. Holographic lithography is a practical alternative to pattern such periodical nanostructures with subwavelength resolution. The period of such a pattern can be changed by varying the angle between two or more incident laser beams while applying multiple exposures even more complex patterns can be imposed. Structure height variation over distances many times larger than the structure pitch [4] can be applied for local electromagnetic field enhancement applications [2].

In this work, Lloyds' mirror interferometer equipped with a 371 nm wavelength laser [5] was used to pattern positive tone photoresist layer with 250 nm, 243.8 nm, and 237.6 nm pitch nanostructures containing superlattice and Moiré features. A code in Matlab was used to simulate the experimentally made superlattices and Moiré lattices where period, rotation, and exposure were varied for analysis of resulting accumulated intensity distributions.

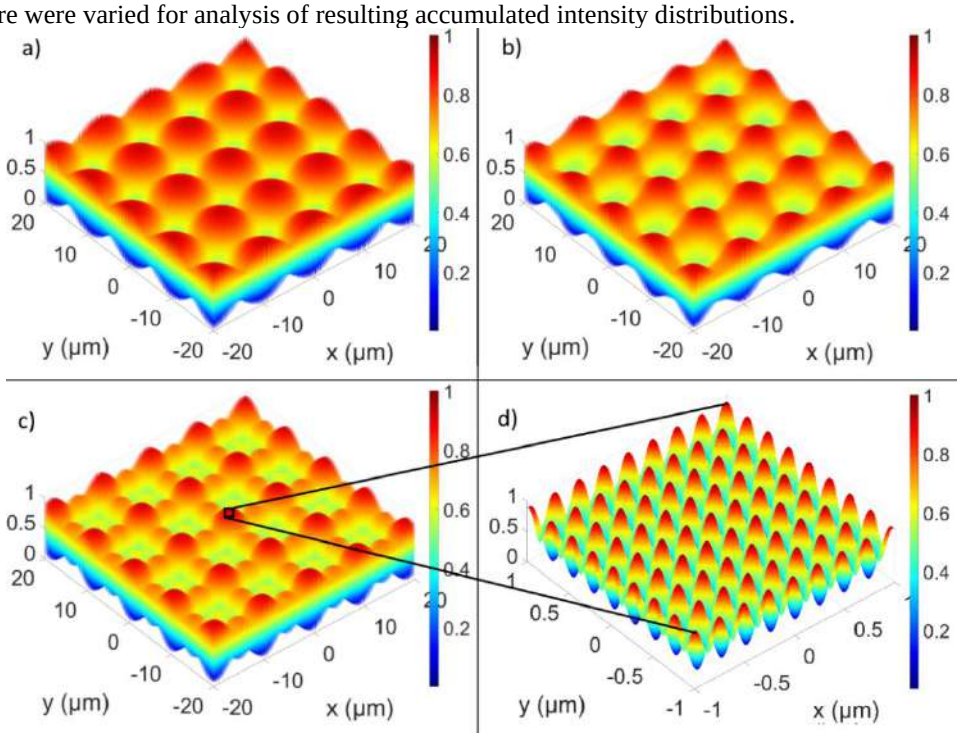

Figure 1. Superlattice simulated using Matlab software where multiple sequential exposures of different periods and intensities, with additional repetition after sample rotation by 90° were accumulated. Set of energy doses for exposures are identical before and after rotation. Used grating periods were 250 nm, 243.8 nm, and 237.6 nm. Applied exposure energies for respective gratings were (a) 5, 5, 0 mJ/cm^2; (b) 5, 5, 1.67 mJ/cm^2; (c) 5, 5, 5 mJ/cm^2. Close up view of the resulting 241 nm period grating in c) is depicted in d). The z-axis is the remaining photoresist thickness.

[1] Joannopoulos, J. D., Villeneuve, P. R., & Fan, S. 1997. „Photonic crystals: putting a new twist on light". *Nature* **386**, 143–149 (1997). https://doi.org/10.1038/386143a0
[2] Seong Jae Kim et al 2021 „Exploring SERS from complex patterns fabricated by multi-exposure laser interference lithography" Nanotechnology **32** 315303. https://doi.org/10.1088/1361-6528/abfb32
[3] Russel et all. 2021 "Creating Two-Dimensional Quasicrystal, Supercell, and MoiréLattices with Laser Interference Lithography: Implications for Photonic Bandgap Materials" ACS Appl. Nano Mater., **4**, 8851−8862. https://doi.org/10.1021/acsanm.1c00210
[4] A. A. Ushkov, I. Verrier, T. Kampfe, and Y. Jourlin, 2020 "Subwavelength diffraction gratings with macroscopic moiré patterns generated via laser interference lithography," Opt. Express **28**, 16453-16468. https://doi.org/10.1364/oe.386699
[5] D. Virganavičius, L. Šimatonis, A. Jurkevičiūtė, T. Tamulevičius, S. Tamulevičius, "Formation of sub-wavelength pitch regular structures employing a motorized multiple exposure Lloyd's mirror holographic lithography setup," Proc. SPIE 9170, Nanoengineering: Fabrication, Properties, Optics, and Devices XI, 91701I (28 August 2014); https://doi.org/10.1117/12.2061191

Towards Supramolecular Neurotransmitters Sensor based on a Dibenzo-18-crown-6 Polymer

Elžbieta Ragauskaitė[1], Gintautas Bagdžiūnas[1]

[1] Group of Supramolecular Analysis, Department of Bioanalysis, Institute of Biochemistry, Life Sciences Centre, Vilnius University, Saulėtekio av. 7, LT-10257, Vilnius, Lithuania
elzbieta.ragauskaite@gmc.stud.vu.lt

Detection and monitoring of neurotransmitters (NTs) such as adrenaline, dopamine, and serotonin at a nanomolar level in the brain and blood remains a challenge and continues to garner significant attention because NTs manage the physiological and behavioural state of the neural network [1]. In many biological systems, selective molecular recognition is based on the formation of intermolecular covalent bonds. Therefore, bioinspired supramolecular recognition systems have intensively been studied and applied for sensors as the artificial molecular recognition devices [2]. In our group, the supramolecular sensors based on β- or γ-cyclodextrines were developed to determine dopamine and adrenaline from nano- to micromolar levels [3]. Due to the low cost and stability of these systems, these sensors can be an excellent alternative to enzymatic devices.

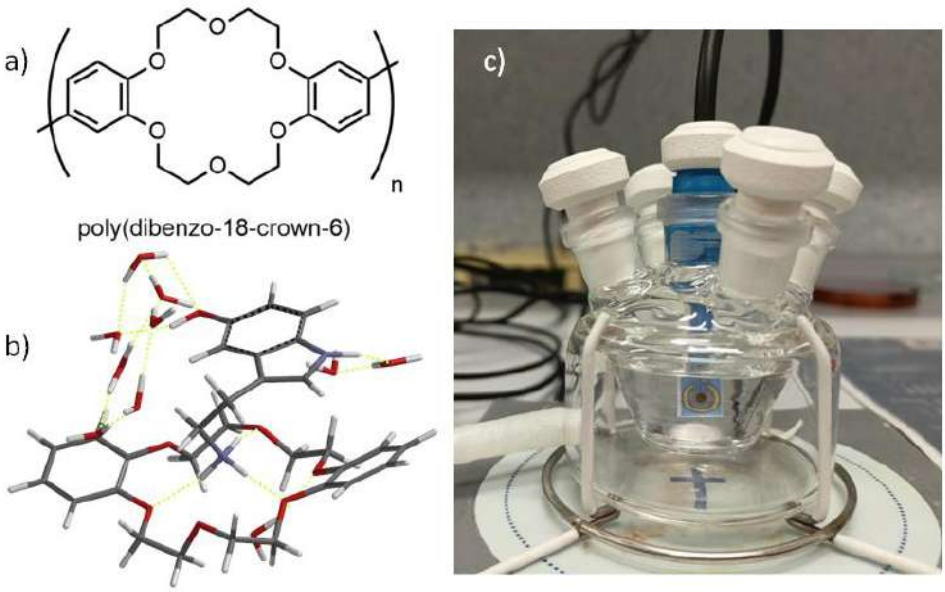

Fig. 1. Structure of the prepared polymer (a), the optimized inclusion complex of serotonin into the cavity (b), and the used electrochemical cell with the screen printed electrode.

In this work, the polymer based on dibenzo-18-crown-6 containing the cavities of 0.6 nm was applied to detect the NTs. Selective recognition of the NTs molecules containing the ammonium groups into the cavities of the dibenzo-18-crown-6 molecules was theoretically established by density functional theory. Therefore, dibenzo-18-crown-6 was electropolymerized onto a screen printed electrode with gold nanoparticles with the diameters of 16 nm. To prove structure of this polymer, vibrational spectroscopy (FT-IR) was used. Solutions in the buffer of pH=7 at nanomolar concentrations of adrenaline, dopamine, and serotonin as the analytes were analyzed using this electrode. In order to elucidate the sensitivity and selectivity, different electrochemical techniques such as cyclic voltammetry and electrochemical impedance spectroscopy were applied.

Acknowledgments: This work was supported by the European Regional Development Fund under "Promotion of Centers of Excellence and Innovation and Technology Transfer Centers" program No. 01.2.2-CPVA-K-703 (grant No. 01.2.2-CPVA-K-703-03-0010).

[1] Y. Zhang, N. Jiang, and A. K. Yetisen, Brain Neurochemical Monitoring, *Biosensors and Bioelectronics* 189, 113351 (2021).
[2] G. T. Williams et al., Advances in Applied Supramolecular Technologies, *Chemical Society Reviews* 50, no. 4, 2737–63 (2021).
[3] I. Radveikienė et al., Self-Assembled Cyclodextrins-Based Nanostructures on Indium-Tin-Oxide for a Detection of Catecholamine Neurotransmitters, *Applied Surface Science* 600, 154170 (2022).

Chirality-Induced Spin Selectivity through an Electrografted Polyaniline

Aida Kamarauskienė[1], Skirmantas Keršulis[1], Gintautas Bagdžiūnas[1,2]

[1] Department of Functional Materials and Electronics, Center for Physical Sciences and Technology, Saulėtekio av. 3, LT-10257 Vilnius, Lithuania
[2] Group of Supramolecular Analysis, Department of Bioanalysis, Institute of Biochemistry, Life Sciences Centre, Vilnius University, Saulėtekio av. 7, LT-10257, Vilnius, Lithuania
aida.kamarauskiene@ftmc.lt

The electron transmission selectivity through chiral molecules depends on the up and down electron spin orientation by quantum mechanics. This phenomenon has been termed the chirality-induced spin selectivity (CISS) effect, and a challenge to theory and perspective for organic molecule–based spintronic devices has recently been provided [1]. To investigate this effect, electrochemistry of self-assembled monolayers of chiral molecules such as biomolecules (peptides, DNA), polymers and coordination complexes have been employed [2].

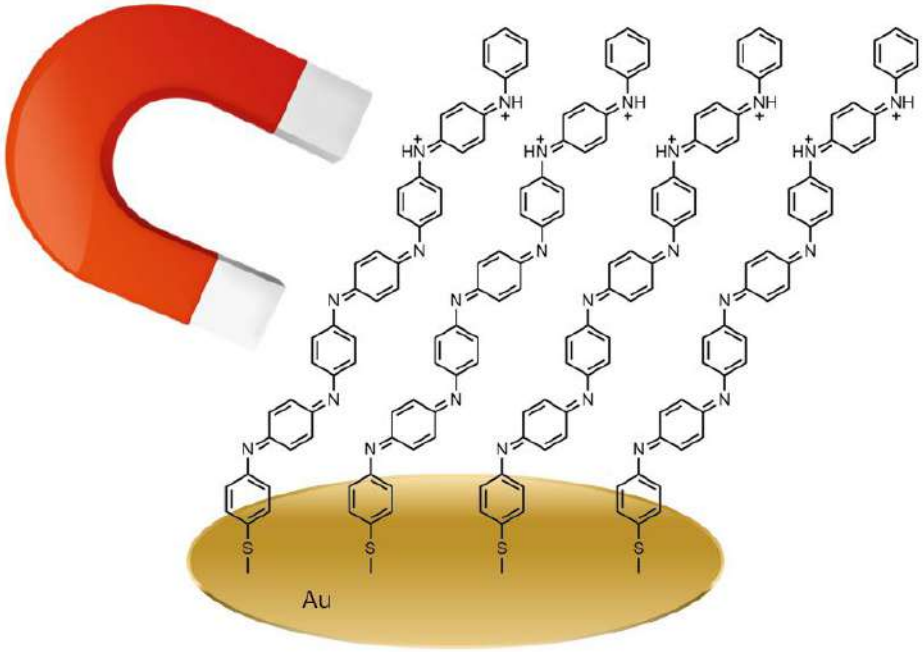

Fig. 1. Structure of the electrografted polyaniline polymer onto a gold surface.

In this work, a chiral polyaniline polymer (Fig. 1) was prepared onto a screen printed gold electrode by electrocrafting of aniline onto a monolayer of 4-aminobenzenethiol. This polymer was characterized using infrared spectroscopy. The (1*R*)- and (1*S*)-10-camphorsulfonic acids were used to induce a chirality of the electrografted polyaniline polymer, respectively. The prepared electrodes were studied by cyclo voltammetry with and without a strong magnetic field of 2.35 T. Moreover, the perpendicular and parallel orientation to the magnetic field was varied. The conductivity of this conducting chiral polymer depended on the magnetic field.

Acknowledgments: This work was supported by the European Regional Development Fund under "Promotion of Centers of Excellence and Innovation and Technology Transfer Centers" program No. 01.2.2-CPVA-K-703 (grant No. 01.2.2-CPVA-K-703-03-0010).

[1] R. Naaman, D. H. Waldeck, Spintronics and Chirality: Spin Selectivity in Electron Transport Through Chiral Molecules (2015).
[2] S. Luo, K. Elouarzaki, Z. J. Xu, Electrochemistry in Magnetic Fields (2022).

Principles of self-assembly and structure of sulfonatophenyl porphine aggregates resembling giant "sea urchin"

Marijus Pleckaitis[1,2,3], Fayez Habach[4], Lukas Kontenis[2,5], Gábor Steinbach[6,7,8], Greta Jarockyte[1,2,3], Agne Kalnaityte[2], Ildikó Domonkos[9], Parveen Akhtar[9], Mehdi Alizadeh[2], Saulius Bagdonas[2], Vitalijus Karabanovas[1,2,10], Győző Garab[8,9,11], Ricardas Rotomskis[1,2], and Virginijus Barzda[2,4,12]

[1]Biomedical Physics Laboratory, National Cancer Institute, P. Baublio str. 3b, Vilnius, LT-08406, Lithuania
[2]Laser Research Center, Faculty of Physics, Vilnius University, Sauletekio av. 10, Vilnius, LT-10223, Lithuania
[3]Life Sciences Center, Vilnius University, Sauletekio av. 7, Vilnius, LT-10257, Lithuania
[4]Department of Chemical and Physical Sciences, University of Toronto Mississauga, 3359 Mississauga Rd, Mississauga, L5L 1C6, Canada
[5]Light Conversion, Keramiku str. 2B, Vilnius, LT-10233, Lithuania
[6]Cellular Imaging Laboratory, Biological Research Centre, Eötvös Loránd Research Network, Temesvári körút 62, Szeged, 6726, Hungary
[7]Institute of Biophysics, Biological Research Centre, Eötvös Loránd Research Network, Temesvári körút 62, Szeged, 6726, Hungary
[8]Biofotonika Research and Development Ltd., Dózsa u. 7, Szeged, 6720, Hungary
[9]Institute of Plant Biology, Biological Research Centre, Eötvös Loránd Research Network, Temesvári körút 62, Szeged, 6726, Hungary
[10]Department of Chemistry and Bioengineering, Vilnius Gediminas Technical University, Sauletekio av. 11, Vilnius, LT-10223, Lithuania
[11]Department of Physics, Faculty of Science, University of Ostrava, Chittussiho 10, Ostrava, CZ-710 00, Czech Republic
[12]Department of Physics, University of Toronto, 60 St. George St. Toronto, Toronto, M5S 1A7, Canada
marijus.pleckaitis@nvi.lt

Molecular self-assembly is spontaneously occurring process that affects the formation of ordered molecular aggregates. It plays a key role in abiogenesis, a natural process that led life arising from simple organic compounds [1].

Meso-tetra(4-sulfonatophenyl)porphine ($TPPS_4$) has been widely studied because it has the ability to form noncovalently bound supramolecular structures [2,3]. However, principles of self-assembly of $TPPS_4$ molecules into complex hierarchical structures is not well understood, therefore it became the aim of this study.

$TPPS_4$ molecules can form several structural types of aggregates in the same solution that interact with each other and assemble into peculiar structures of hundreds of micrometers in size that resemble giant "sea urchin" (GSU) [4]. The $TPPS_4$ aggregates form a central tubular core, which is covered with radially protruding filamentous non-branching aggregates. The filaments cluster and orient at varying angles from the core surface and some filaments form bundles.

Using spectrally resolved fluorescence microscopy we showed that both the central core and the filaments exhibit spectral bands specific to J- and H- bands of $TPPS_4$ aggregates. Even though the fluorescence (FL) of the core was visibly quenched, the filaments showed stronger intensity FL signal. On the other hand, we also noticed that upon drying, the filament fluorescence gets quenched while the core is affected less, demonstrating stronger relative fluorescence. Fluorescence-detected linear dichroism (FDLD) microscopy revealed that absorption dipoles of J-bands were oriented along the filament axis. By comparing the results of FDLD with scanning electron microscopy, we found out that the central core consisted of multilayer ribbons, which wind around the core axis forming a tube.

Polarimetric second-harmonic generation (SHG) and third-harmonic generation (THG) microscopy determined strong signal from the filaments with nonlinear dipoles oriented close to the filament axis. Meanwhile, central core displayed very low SHG due to close to centrosymmetric organization. Large chiral nonlinear susceptibility stresses the helical arrangement of the filaments. Additionally, this study shows that $TPPS_4$ molecules form distinct types of aggregates – chiral nanotubes and nanogranular aggregates. Given enough time, these aggregates associate and self-assemble into the hierarchical GSU structure, which can serve as harmonophores for nonlinear microscopy.

[1] S. Tirard, in Encyclopedia of Astrobiology (Eds.: R. Amils, M. Gargaud, J. Cernicharo Quintanilla, H.J. Cleaves, W.M. Irvine, D. Pinti, M. Viso), Springer, Berlin, Heidelberg, 2014, pp. 1–1.
[2] O. Ohno, Y. Kaizu, H. Kobayashi, J. Chem. Phys. 1993, 99, 4128–4139.
[3] N. C. Maiti, S. Mazumdar, N. Periasamy, J. Phys. Chem. B 1998, 102, 1528–1538.
[4] Pleckaitis, M., Habach, F., Kontenis, L. et al., Nano Res. 2022, 15, 5527–5537.

^{99m}Tc-BSA-Au bioconjugates – potential *in vivo* imaging agents for diagnostics

Kornelija Buivydaitė[1, 2], Greta Jarockytė[1, 2], Marius Stašys[1], Vilius Poderys[1], Danutė Bulotienė[1], Marijus Plečkaitis[1, 2], Vitalijus Karabanovas[1, 3]

[1] Biomedical Physics Laboratory, National Cancer Institute, Vilnius, Lithuania
[2] Life Science Center, Vilnius University, Vilnius, Lithuania
[3] Department of Chemistry and Bioengineering, Vilnius Gediminas Technical University, Vilnius, Lithuania
kornelija.buivydaite@gmc.stud.vu.lt

Clinical imaging techniques now are more precise than ever. However, they still have limited accuracy when applied individually. Combining optical imaging with other techniques may lead to important advances in diagnostics surpassing individual techniques limits. For this purpose, increasingly more attention is shifted to research of novel nanoparticle bioconjugates that could be used as multimodal diagnostic agents. One such combination could be of a biocompatible radionuclide with photoluminescent bovine serum albumin stabilized gold nanoclusters (BSA-Au NCs) previously described by J. Xie et al. [1].

In our study radioactive technetium ^{99m}Tc was attached to BSA-Au NCs to create ^{99m}Tc- BSA-Au bioconjugates. The attachment of ^{99m}Tc to BSA-Au NCs did not affect nanoclusters' photoluminescence suggesting potential detection of these bioconjugates in the body by fluorescence imaging and single photon emission computed tomography. We investigated how ^{99m}Tc-BSA-Au is distributed in Wistar rats after intravenous injection applying computed tomography of single photon emission of organs and confocal microscopy of histological sections of tissues and cell lines. *In vivo* imaging of Wistar rats demonstrated intense cardiac blood pool activity, as well as rapid blood clearance and accumulation in the kidneys, liver and urinary bladder. However, histological sections of kidney, liver and spleen tissue displayed no visible accumulation of ^{99m}Tc-Au-BSA NCs indicating that the bioconjugates possibly circulate in the bloodstream for a shorter period of time than it takes for them to accumulate in tissues. In addition, a study on kidney cells uptake of ^{99m}Tc-Au-BSA NCs revealed that only after 24 hours of cell incubation with bioconjugates their accumulation in cells becomes substantial, further reinforcing our earlier statement. Therefore, ^{99m}Tc- BSA-Au NCs could be used as potential diagnostic agents for bloodstream imaging of excretory organs rather than tissues.

[1] Xie J et al. (2009) J Am Chem Soc, 131, 888-889.

Mesenchymal Stem Cells and Rare Earth Nanoparticles – a Potent Combination for Photodynamic Therapy of Cancer

Alėja Marija Daugėlaitė[1,3], Greta Jarockytė[1,2], Artiom Skripka[4], Vilius Poderys[1], Fiorenzo Vetrone[4], Vitalijus Karabanovas[1,5]

[1]Biomedical Physics Laboratory, National Cancer Institute, Baublio str. 3b, LT-08406, Vilnius, Lithuania
[2]Life Sciences Center, Vilnius University, Saulėtekis Ave. 7, LT-10257, Vilnius, Lithuania
[3]Vilnius University Faculty of Medicine, M. K. Čiurlionio str. 21/27, LT-03101, Vilnius, Lithuania
[4]Centre Énergie, Matériaux et Télécommunications, Institut National de la Recherche Scientifique, Université du Québec, 1650 Boul. Lionel-Boulet, Varennes, QC, J3X 1S2, Canada
[5]Department of Chemistry and Bioengineering, Vilnius Gediminas Technical University, Saulėtekis Ave. 11, LT-10223, Vilnius, Lithuania
aleja.daugelaite@nvi.lt

Among the ongoing developments in cancer treatments, photodynamic therapy (PDT) is a non-invasive and versatile method that exploits interactions between molecular oxygen and photosensitizer molecules under light exposure. In PDT, excited photosensitizers generate reactive oxygen species which are toxic to cancer cells. However, due to the inadequate accumulation of photosensitisers at tumour sites and the low penetration in biological tissue of ultraviolet and visible light needed to excite the photosensitisers, PDT is limited to superficial tumours, such as skin cancer. Limitation imposed by excitation wavelength can be nonetheless solved by using rare earth based upconverting nanoparticles (UCNPs). UCNPs can generate ultraviolet and visible emission under near-infrared irradiation (λ_{ex} = 980 nm), which falls in the so-called biological imaging windows (750-1300 nm) where light can reach deeper tissues. To that end we have previously developed and explored a chlorin e_6 and UCNPs complex (UCNPs-Ce_6) as a deep tissue theranostic platform [1]. However, selective delivery of such a complex to cancer cells remains challenging.

To address this issue, we explore the human skin mesenchymal stem cells (MSCs) as nanoparticle delivery vehicles [2]. MSCs have the ability to migrate towards cancer cells due to chemoattractant gradient, are involved in wound healing, and have anti-tumour and immunomodulatory properties [3]. Thus, nanotechnology and the ability of MSCs to migrate toward the tumour site have been combined to improve the efficacy of PDT in subsurface tumours by using them as Trojan horses [2]. Here we investigate the photodynamic effect of UCNPs-Ce_6 under near-infrared irradiation in 2D cell monolayers and 3D cellular spheroids when MSCs are used to deliver the nanoparticles.

Scanning confocal microscopy demonstrates the accumulation of UCNPs and UCNPs-Ce_6 in MSCs as well as in human breast cancer cell lines MDA-MB-231 and MCF-7. The lactate dehydrogenase cytotoxicity assay shows that UCNPs-Ce_6 are intrinsically non-toxic and do not affect cell viability after 24 h incubation. Next, the photodynamic effect studies were carried out. The generation of singlet oxygen in the colloidal dispersion of UCNPs-Ce_6 under 980 nm laser irradiation was determined using a singlet oxygen sensor green reagent (SOSG). We further investigate the potential efficacy of PDT using the combination of UCNPs-Ce_6 and MSCs in cell monolayers under two-dose irradiation condition. After the 980 nm laser irradiation, cells were stained with the fluorescent viability dyes, calcein-AM and propidium iodide, which stain live and dead cells, respectively. All MSCs incubated with nanoparticles die after the first irradiation with 980 nm, but the co-cultured cancer cells are mostly affected only after the second dose of irradiation. As cell monolayers do not fully reflect the tumour microenvironment, 3D cell cultures were chosen to bring the study closer to natural biological structures. Therefore, a photodynamic effect was demonstrated in triple-negative breast cancer cell spheroids when MSCs were used as nanoparticle carriers. The use of MSCs improves the efficiency of the photodynamic effect and photodrug delivery to 3D cancer spheroids as well.

Overall, the combination of MSCs and UCNPs-Ce_6 with 980 nm irradiation has a phototoxic effect on the cell monolayer as well as on the spheroids of the cancer cells, and is a potential future treatment for cancer.

Acknowledgment

This work is part of a project that was supported by the funds of Lithuania (Grant No. S-MIP-22-31).

[1] A. Skripka, V. Karabanovas, G. Jarockyte, et al., Decoupling Theranostics with Rare Earth Doped Nanoparticles. Adv Funct Mater 29(12), 1807105 (2019).
[2] D. Dapkute, M. Pleckaitis, D. Bulotiene, et al., Hitchhiking Nanoparticles: Mesenchymal Stem Cell-Mediated Delivery of Theranostic Nanoparticles, ACS Appl Mater Interfaces 13(37), 43937–43951 (2021).
[3] I. García-Gómez, G. Elvira, A. G. Zapata, et al., Mesenchymal stem cells: biological properties and clinical applications, Expert Opinion on Biological Therapy, 10(10), 1453-1468 (2010).

Molecular and cellular aspects of intracellular delivery of bacteriophage-derived nanoparticles

Aušra Sasnauskienė[1], Vilmantė Žitkutė[1], Vida Časaitė[2]

[1]Vilnius University, Life Sciences Center, Institute of Biosciences, Saulėtekio av. 7, Vilnius, Lithuania
[2]Vilnius University, Life Sciences Center, Institute of Biochemistry, Saulėtekio av. 7, Vilnius,
ausra.sadauskaite@gf.vu.lt

Nanoparticles are considered to be a promising tool for specific delivery of pharmaceutic compounds. In this study we have analyzed intracellular uptake of nanotubes formed from self-assembled bacteriophage tail sheath protein gp053. For intracellular tracking nanotubes were formed from gp053 proteins fused to SNAP-tag and subsequently labeled with a fluorescent marker. Confocal microscopy was used for nanotube tracking and colocalization analysis in human colorectal carcinoma cells HCT116 and SW480.

We have detected that nanotubes accumulate in lysosomes of colorectal cancer cells. Nanotubes were internalized by endocytosis. HCT116 cell line accumulated nanotubes in the dynamin-dependent endocytosis, while SW480 cells used dynamin- and clathrin-dependent pathway. Incubation of cells with bacteriophage protein gp053 derived nanotubes did not change the extent of autophagy. Nanotubes formed from bacteriophage protein gp053 were not toxic to colorectal cancer cells.

In conclusion, bacteriophage-derived nanoparticles were proven to be potent carriers for intracellular delivery.

PHOTOSTABILITY OF Cd AND Cu BASED QUANTUM DOTS IN DIFFERENT BIOLOGICAL MEDIA

Emilija Januškaitė[1], Agnė Kalnaitytė[1,2], Saulius Bagdonas[1,2]

[1]Biophotonics Group, Laser Research Center, Vilnius University, Saulėtekio 9, bld, 3, LT - 10222, Vilnius, Lithuania
[2]Institute of Ecology, Nature Research Centre, Akademijos str. 2, LT - 08412, Vilnius, Lithuania
emilija.januskaite@gmc.stud.vu.lt

Quantum dots (QDs) are nano-sized semiconductors, which bright photoluminescence (PL) in the visible light range made them useful in many fields of science, especially in biomedicine. The structure of QDs consists of crystalline core (which is responsible for optical properties), surrounded by a shell that protects it from surrounding medium and enhances the photoluminescence quantum yield (QY) of QDs, and a coating of ligands that enables stability and solubility in aqueous media. While the most QDs with high QY are made of toxic metals such as Cd, less harmful elements (e.g., Cu) are taken into consideration, because of environmental issues, that are considered if toxic materials are released when the structure of QDs is damaged [1]. However, a different structure of QDs result in different spectral properties, whose are prone to changes under light exposure [2] and affect the performance of nanoparticles in environment waters. This requires a proper investigation of light induced effects on different type QDs in biological media.

In this work, optical density (OD) and photoluminescence (PL) spectra of CdSe/ZnS-COOH (Invitrogen, USA) and CuInS/ZnS-COOH (Nanooptical materials, USA) QDs in biological media under light exposure were monitored. The samples of QDs (concentration of both QDs was 4 nM unless stated otherwise) were prepared in distilled water (DW), deep well water (DWW), and MWC algae growth medium. During light irradiation, the QDs samples were kept in a 12-well plate, and the collimated violet LED light (404 nm, 30 mW/cm^2) was directed to the sample from 8 cm distance. The fractionated exposures were delivered to obtain the partial cumulative dose up to 36 J/cm^2 (in intervals of 1.8 J/cm^2 and 3.6 J/cm^2) in all media, and later the total dose depended on the decrease of the PL intensity.

The initial OD of Cu based QDs was bigger than the OD of the same concentration Cd based QDs, however, the PL spectrum was narrower, and intensity was bigger of Cd based QDs, thus the QY was bigger for Cd based QDs, too. After being exposed to the light, the PL intensity decreased in all media (Fig. 1). Until an 18 J/cm^2 dose of irradiation was reached the decrease of PL intensity in DW was relativity the same for both QDs, but after bigger doses the PL decrease in Cd based QDs samples were slower than in Cu based QDs samples. After reaching approximately 16.2 J/cm^2 (samples of Cd based QDs) and 36 J/cm^2 (samples of Cu based QDs) the decline slowed down depending on the surrounding medium. The OD decrease and the PL spectra redshift were observed in all samples, after bigger irradiation doses, Cu based QDs samples had PL blueshift as well. In OD spectra of QDs samples in DWW was registered a dispersion, which was bigger than in other samples and indicate bigger aggregation of nanoparticles.

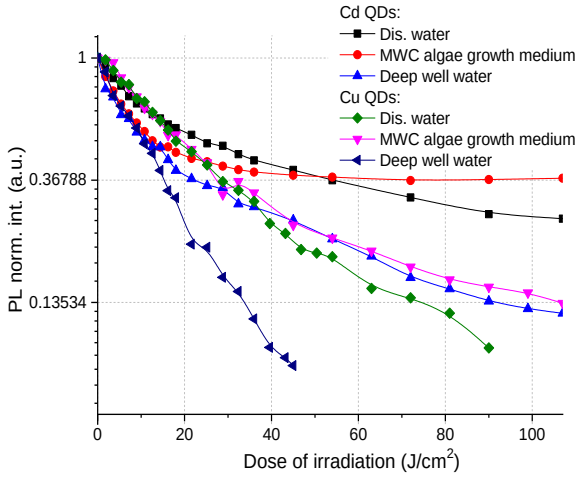

Fig. 1. The decrease in the PL intensity of Cd and Cu based QDs at a spectral peak value (at about 622 nm and 550 nm respectively) depending on the irradiation dose in different media. Excitation wavelength at 405 nm.

Similar patterns of OD and PL intensity decrease were registered during long period illumination. While the PL intensity of Cu based QDs samples under light exposure were registered only from three (in DWW) to five days (in DW), depended on medium, the PL intensity of Cd based QDs also depended on medium, but lasted longer than a week (in DWW and longer in another). Also, it was observed that illumination is more significant for spectral properties of Cu based QDs, while the medium has a greater influence on spectral properties of Cd based QDs.

[1] L. Li, T.J. Daou, I. Texier, T.T.K. Chi, N.Q. Liem, P. Reiss, Luminescent CuInS2/ZnS Core/Shell Nanocrystals: Cadmium-Free Quantum Dots for in Vivo Imaging, Chem. Mater (21), 2009.
[2] A. Kalnaitytė, S. Bagdonas, R. Rotomskis, *The dose-dependent photobleaching of CdTe quantum dots in aqueous media*, Journal of Luminescence, 2018.

Effect of quantum dots on green algae *Scenedesmus quadricauda* in various media

Mindaugas Kazlauskas[1]*, Živilė Jurgelėnė[1], Saulius Bagdonas[2], Agnė Kalnaitytė[2], Nijolė Kazlauskienė[1], Danguolė Montvydienė[1]

[1]Nature research centre, Laboratory of Ecotoxicology, Akademijos 2, Vilnius, Lithuania
[2]Vilnius University, Biophotonics Group of Laser Research Centre, Saulėtekio av. 9, III bld. Vilnius, Lithuania
*Corresponding author: E-mail: kazlauskas.mindaugas@gmail.com, Tel +37069363363

A lot of studies have confirmed the uptake of QDs in mammals and plants cells, demonstrated the translocation of them in plants cells and effects of QDs on various organisms [1]. However, there is a little number of studies related to the investigations of the internalization of QDs into algae cells and their toxicity to algae which become the first target of QDs in the aquatic environment [2]. Due to sensitivity of the spectral properties to environmental factors, hydrophilic QDs can be used as indicators of environmental conditions alterations and become important for monitoring their environmental fate and estimation of the threat of toxicity in various biological environments [3].

Therefore, our study aimed to examine the effects of negatively charged Cd-based QDs (CdSe/ZnS-COOH, 4 nM concentration) on the growth and population structure of green algae (*Scenedesmus quadricauda*) growing in various media (Lake Balsiai water (LBW), deep-well water (DWW), and artificial algal growth media (MWC). The physico-chemical characteristics of tested media with and without QDs were measured. Results obtained indicated that the photoluminescence intensity of QDs in DWW was greatest compared of QDs samples in other studied media.

Obtained data showed that the incubation media modify the toxicity of QDs to *S. quadricauda.* The inhibition of algal growth was markedly dependent on the test medium during the 96-h of exposure and growth of algae in MWC with QD medium was significantly higher compared to LBW and DWW. No significant effects were observed for *S. quadricauda* when exposed to QDs in LBW+QD compared to this LBW without QDs. Algal growth rate increased with increasing exposure duration, and it was evident in LBW, MWC and LBW+QD. The growth of *S. quadricauda* after 72-h and 96-h exposures were markedly inhibited by MWC+QD compared with the MWC medium. When *S. quadricauda* was grown in the absence (control) or presence of QD, the structure of algal colonies was changed drastically in the different incubation's media.

Whereas algae is a key part of the food chain in the aquatic environment, therefore, present study provides a useful information on how nanomaterials can affect the environment and how the environment can affect nanoparticles.

This research received funding from the Research Council of Lithuania under the Project No. S-MIP-20-22.

[1] H.E. Elzorkany, M.A. Farghali, M.A. Hassan et al., *Sci Total Environ.* **20(666)**:480-489. (2019).
[2] F.R. Chen , Z.G. Xiao, L. Yue et al., *Environment Science. Nano*. **6(4)**: 1026–1042 (2019).
[3] A. Kalnaitytė, S. Bagdonas, *J. Photoch Photobio B,* **199**, 111629, (2019).

Accumulation of Quantum Dots and Chlorin e6 Complex in Distinct Phenotypes of Human Colon Cancer Cells

Emile Peciukaityte[1,2], Evelina Voronovic[1,2,3], Austeja Butkute[1,4], Agata Mlynska[4], Simona Steponkiene[1], Vitalijus Karabanovas[1,2], Ricardas Rotomskis[1,5]

[1]Biomedical Physics Laboratory of National Cancer Institute, Baublio 3B, LT-08406, Vilnius, Lithuania
[2]Department of Chemistry and Bioengineering, Vilnius Gediminas Technical University, Sauletekio av. 11, LT-10223, Vilnius, Lithuania
[3]Life Science Center, Vilnius University, Sauletekio av. 7, LT-10257, Vilnius, Lithuania
[4]Laboratory of Immunology, National Cancer Institute, Baublio 3B, LT-08406, Vilnius, Lithuania
[5]Biophotonics Group of Laser Research Centre, Vilnius University, Sauletekio 9, c.3, LT-10222, Vilnius, Lithuania
emile.peciukaityte@stud.vilniustech.lt

Every year, millions of individuals throughout the world are affected by cancer. There are numerous potential treatments for cancer, but the development of more rapid, novel and precise technologies is still needed [1]. Biomedicine-focused research created the idea of integrating therapy and diagnostics, so-called theranostics, in the search for better ways to treat a variety of human illnesses. The area of nanoscience has existed longer than theranostics itself, but the development of nanoparticles with customizable physicochemical properties and subcellular size has made it possible to create multifunctional theranostic nanoplatforms [2]. For instance, quantum dots (QDs), semiconductor nanoparticles with exceptional optical properties, ultrasmall size, and a high surface area to volume ratio, are used for diagnostics, but if QDs are merged with a photosensitizer, it is possible to create an ideal multifunctional complex for theranostics. Chlorin e6 (Ce6) is a second-generation photosensitizer with a high extinction coefficient, which absorbs a wide range of visible light, including absorption at the red side of the spectrum. As is well known, QDs are combined with chlorin e6 (Ce6) and form a complex that is ideal for biomedical applications [3].

Colorectal tumors are among the most heterogeneous cancer types. Consensus classification of molecular subtypes (CMS) in colorectal tumors distinguishes four categories: immune-mediated CMS1, canonical CMS2, metabolic CMS3 and mesenchymal CMS4 tumors [4]. This classification relies on differential gene expression within colorectal tumors and is partially related to pathological and clinical factors. However, to effectively advance tailored management of different disease subtypes, more evidence provided by the fundamental in vitro research of suitable biological models is needed.

This study aimed to investigate the accumulation of QDs-Ce6 complex in different phenotypes of human colon cancer cells. Firstly, it was determined whether the complex (QDs-Ce6) is stable in several media: distilled water and cell growth RPMI medium without phenol red. Moreover, the flow cytometry and laser scanning confocal microscopy revealed the uptake and distribution of the complex within cancer cells. In parallel, cells were screened for the surface expression of selected stemness and immune markers using flow cytometry. The connection between the accumulation of QD-Ce6 complex and the expression of stemness markers had been investigated.

The complex was indicated as stable in distilled water, therefore the experiments were held with the cell culture growth medium. Each of the growth medium components was examined separately to find the best optimal conditions for the stabilization of the QD-Ce6 non-covalent complex. Once the optimal conditions were set, cancer cell lines, representing different CMS subtypes, were chosen as a model system for studying the accumulation of the QDs-Ce6 complex. The surface marker staining showed the inter- and intra-subtype heterogeneity within selected cell lines and allowed for classifying them based on aggressiveness and immunogenicity. Distribution studies of the QD-Ce6 complex revealed rapid accumulation and localization in the perinuclear region.

Obtained results lead to a conclusion that the QDs-Ce6 complex is stable in different biological media and accumulates at a high rate in cells of different phenotypes. Although cancer cells were phenotypically distinct, the QD-Ce6 complex accumulated similarly in all examined cells.

In conclusion, the QDs-Ce6 complex has the potential to overcome phenotype-related accumulation obstacles in cancer cells and should be further used in biomedical research, especially in theranostics.

This study was supported by the funds of Lithuania. Grant No. S-MIP-22-31.

[1] Arranja, A. G., Pathak, V., Lammers, T., Shi, Y. (2017). Tumor-targeted nanomedicines for cancer theranostics, *Pharmacological Research* (Vol. 115, pp. 87–95).
[2] Skripka, A., Karabanovas, V., Jarockyte, G., Marin, R., Tam, V., Cerruti, M., Rotomskis, R., & Vetrone, F. (2019). Decoupling Theranostics with Rare Earth Doped Nanoparticles. In Advanced Functional Materials (Vol. 29, Issue 12, p. 1807105).
[3] Dapkute, D., Pleckaitis, M., Bulotiene, D., Daunoravicius, D., Rotomskis, R., & Karabanovas, V. (2021). Hitchhiking Nanoparticles: Mesenchymal Stem Cell-Mediated Delivery of Theranostic Nanoparticles *ACS Applied Materials & Interfaces*. (Vol. 13, Issue 37, pp. 43937–43951)
[4] Guinney, J., Dienstmann, R., Wang, X., et al. (2015). The consensus molecular subtypes of colorectal cancer. *Ant Med*. (Vol. 21, Issue 11, pp. 1350-1356)

Toxicity of Polystyrene Nanoparticles on Salmonid Fish

Agnė Bučaitė[1,2], Emilija Dešč[1,2], Gintarė Sauliutė[1], Milda Stankevičiūtė[1]

[1]Nature Research Centre, Laboratory of Ecotoxicology, Akademijos Str. 2, LT-08412 Vilnius, Lithuania
[2]Vilnius University Life Sciences Centre, Institute of Biosciences, 7 Saulėtekio Ave, LT- 10257 Vilnius, Lithuania
agne.bucaite@gamtc.lt

Plastic pollution is becoming a serious environmental problem since it accounts for the majority of anthropogenic waste found in the ocean, which includes macro, micro, and nanoscale plastic particles [1]. The term "nanoplastics" (NPs) is newly introduced, and various researchers have established the upper size limit at 1000 nm or 100 nm. A more comprehensive definition was suggested by Gigault and colleagues (2018) who define NPs as ‘particles unintentionally produced (i.e., from the degradation and the manufacturing of the plastic objects) and presenting a colloidal behaviour, within the size range from 1 to 1000 nm’ [2]. Due to a lack of adequate analytical techniques, this is currently the least investigated fraction of plastic littler. Thus, the effects of 25 nm polystyrene (PS) NP on larval stage rainbow trout (*Oncorhynchus mykiss*) were examined using the erythrocytic nuclear abnormalities assay and the analysis of antioxidant biomarkers. For 32 days, fish were exposed to 1000 µg/L PS NPs (PS1000). For erythrocytic nuclear abnormalities assay the formation of micronuclei (MN), nuclear buds (NB), nuclear buds on filament (NBf), blebbed nuclei (BL) cells were assessed as genotoxicity endpoints, and 8-shaped nuclei, fragmented-apoptotic (FA), bean-shaped and bi-nucleated (BN) cells as cytotoxicity endpoints. Meanwhile, as antioxidant biomarkers, changes in catalase (CAT) activity and metallothionein (MT) levels were investigated. R software (version 4.1.1) was used to analyse the data. When compared to the control, significant increase in genotoxicity (MN + NB + NBf + BL) by 8.3-fold and cytotoxicity (8-shaped + bean-shaped + FA + BN) by 10.7-fold were observed. There was also a significant 1.8-fold change in CAT activity, indicating an inhibitory effect induced by PS NPs. Contrariwise, MT level increased 1.2-fold in PS NP-exposed fish. Overall, PS NP had an effect on the frequencies of erythrocytic nuclear abnormalities, CAT activity, and MT levels in *O. mykiss* larvae, indicating increased oxidative stress and genetic damage. Further research should be conducted to investigate a broader range of PS NP sizes, concentrations, and exposure durations in order to get a more precise profile of cytogenetic effects, CAT activity and MT induction in early developmental stages of *O. mykiss*.

This research was funded by the Research Council of Lithuania, Project No. S-MIP-22-51, ARFA.

[1] J. A. Pitt *et al.*, “Uptake, tissue distribution, and toxicity of polystyrene nanoparticles in developing zebrafish (Danio rerio),” *Aquatic Toxicology*, vol. 194, pp. 185–194, Jan. 2018, doi: 10.1016/j.aquatox.2017.11.017.

[2] J. Gigault *et al.*, “Current opinion: What is a nanoplastic?,” *Environmental Pollution*, vol. 235, pp. 1030–1034, Apr. 2018, doi: 10.1016/j.envpol.2018.01.024.

Does morphology matter? Toxicity and magnetic properties of $GdPO_4:Eu^{3+}$ nanoparticles

Augustas Morkvėnas[1], Eglė Ežerskytė[2], Vaidas Klimkevičius[2], Živilė Jurgelienė[3], Vitalijus Karabanovas[1,4]

[1]Biomedicinės fizikos laboratorija, Nacionalinis vėžio centras, Baublio 3b, LT-08406, Vilnius, Lietuva
[2]Chemijos institutas, Vilniaus universitetas, Naugarduko g. 24, LT-03225 Vilnius, Lietuva
[3] Gamtos tyrimų centras, Akademijos st.-2, LT-08412 Vilnius, Lietuva
[4]Chemijos ir bioinžinerijos katedra, Vilnius Gedimino Technikos Universitetas, Saulėtekio al. 11, LT-10223 Vilnius, Lietuva
augustas.morkvenas@vilniustech.lt

The rare-earth (RE) inorganic materials possess outstanding optical and magnetic properties, therefore, such matarials found application in multiple fields such as biomedicine, electronics, catalysis, etc [1]. Scientific literature describes various approaches towards synthesis of multimodal functional inorganic nanomaterials, however, the synthesis of well-defined particles with controlled morphology remains challenging [2].

It is established that the MRI signal intensity depends on the size and shape of nanoparticles (NPs). Due to the ability to produce images of soft tissue with significant spatial and anatomical resolution while releasing no harmful radiation, MRI has proven to be immensely useful in biomedicine. MRI contrast is usually generated by the relaxation of water protons, and this process could be improved by adding a contrast agent (CA) [3].

Morphology is not only a key factor for MRI contrast but also one of the main factors for particle toxicity and the ability to accumulate in biological objects. It has been widely explored how to obtain orthophosphate particles with different morphologies such as nanorods, nanowires, nanofibers, nanocubes, nanoprisms, microspheres, submicrostars, etc [1]. However, toxicological information of orthophosphate particles of various morphology is limited.

It is also important to consider which morphology of RE-orthophosphates ensures optimal relation between magnetic properties and toxicity [4,5].

This study reports the effect of synthesized $GdPO_4:Eu^{3+}$ morphologies on the toxicity and bioaccumulation as well as enhancement of MRI response.

Assessed data showed a direct correlation between particle surface area and MRI capabilities. These tests were conducted using a 1.5T clinical MRI scanner at room temperature. Enhancement ratios and MRI relaxation were calculated using equations (1) and (2), respectively. Gathered data showed that NPs with the largest surface area (nanorods) showed the best results in MRI response enhancement.

$$\beta = \frac{SI_x}{SI_{H_2O}} \quad (1)$$

$$SI(TI) = SI_0\left(1 - 2\left(exp^{\frac{-TI}{T_1}}\right)\right) \quad (2)$$

Toxicological and bioaccumulation tests were conducted on *Daphnia magna*, which is one of the main test objects regarding toxicology. The following advantage of this bio-test object is its transparent superficies, which allows studying nanoparticles' accumulation. Study revealed that there are no relation between the shape of NPs and toxicity. However, the bioaccumulation test showed that the smallest particles (nanorods) were more likely to accumulate in *D.magna* gut if compared to larger ones.

[1] M. Janulevicius, V. Klimkevicius, A. Vanetsev, V. Plausinaitiene, S. Sakirzanovas, and A. Katelnikovas, "Controlled hydrothermal synthesis, morphological design and colloidal stability of GdPO4·nH2O particles," *Materials Today Communications*, vol. 23, p. 100934, Jun. 2020, doi: 10.1016/j.mtcomm.2020.100934.

[2] M. Saraf *et al.*, "Probing Highly Luminescent Europium-Doped Lanthanum Orthophosphate Nanorods for Strategic Applications," *Inorg. Chem.*, vol. 54, no. 6, pp. 2616–2625, Mar. 2015, doi: 10.1021/ic5027784.

[3] R. B. Lauffer, "Paramagnetic metal complexes as water proton relaxation agents for NMR imaging: theory and design," *Chem. Rev.*, vol. 87, no. 5, pp. 901–927, Oct. 1987, doi: 10.1021/cr00081a003.

[4] M. Allegri *et al.*, "Shape-Related Toxicity of Titanium Dioxide Nanofibres," *PLoS ONE*, vol. 11, no. 3, p. e0151365, Mar. 2016, doi: 10.1371/journal.pone.0151365.

[5] J. A. Champion and S. Mitragotri, "Role of target geometry in phagocytosis," *Proc. Natl. Acad. Sci. U.S.A.*, vol. 103, no. 13, pp. 4930–4934, Mar. 2006, doi: 10.1073/pnas.0600997103.

Influence of graphene oxide on the accumulation of metals in *Salmo trutta* at early life stages

Renata Butrimienė[1]*, Živilė Jurgelėnė[1], Danguolė Montvydienė[1], Kęstutis Jokšas[1], Sergej Šemčuk[2], Nijolė Kazlauskienė[1]

[1]Nature Research Centre, Akademijos St. 2, LT-08412 Vilnius-21, Lithuania
[2]SRI Center for Physical Sciences and Technology, Savanorių ave. 231, LT-02300 Vilnius, Lithuania
*Corresponding author: E-mail: renata.butrimiene@gamtc.lt, Tel. +37062581041

Developed industry leads to the entry of heavy metals into the environment and at the same time into water. Heavy metals are non-biodegradable and can bioaccumulate in living organisms [1]. Carbon based nanomaterials like graphene and graphene oxide (GO) are interesting for absorbance's properties [2]. To our knowledge, there are few results that GO dispersion in the aquatic environment may reduce the concentration of metals and eventually affect the biotoxicity of their due to adsorption [3].

This study was undertaken with a view to assess the bioaccumulation GO used in combination with the heavy metal mixture (Cr, Cu, Ni and Zn) to fish (*Salmo trutta*) embryos and larvae as a test organisms. The bioaccumulation of these metals in fish were compared in the presence and absence of GO so as to elucidate potential interactions between GO and metal ions.

Analysis of metal accumulation in *S. trutta* embryos and larvae after the 4-day exposure to MIX, GO and to GO+MIX was performed applying a digestion method [4]. The concentration of Cu, Zn, Ni and Cr in whole bodies of fish embryos and larvae was analysed with a spectrophotometer AAS SHIMADZU AA-7000 (Japan) following the method ISO 15586: 2003.

The amounts of metals determined in fish embryos and larvae after the 4-day exposure to MIX, GO and to MIX+GO were investigated. The obtained results showed that amounts of all the metals present in the mixture (MIX) increased in the MIX-treated embryos compared with those of the control group ($p < 0.05$) (except metal amounts at the lowest concentration of MIX). The accumulated Ni and Zn amounts in larvae after exposure to the lowest concentration of MIX (MIX1) were significantly higher than in the control group ($p < 0.001$). However, the amounts of Cr and Cu in larvae subjected to the 4-day MIX1 treatment (in all cases $p > 0.05$) did not change significantly. The mean values of all the tested metals determined in embryos and larvae after the 4-day exposure to GO (1, 20 and 40 mg/L), did not show significant differences from the control ones. However, under co-exposure to MIX and GO (MIX20+GO20 and MIX40+GO40) ($p < 0.01$), the accumulation of Cr, Cu, Ni and Zn in embryos was found to significantly increase. The accumulation of Cr, Cu and Zn in larvae showed a tendency to increase with the concentrations of the tested substances (MIX40+GO40, $p < 0.001$). Meanwhile, Ni amount significantly increased both in the larvae exposed to MIX20+GO20 and in those exposed to MIX40+GO40 ($p < 0.001$ and $p = 0.001$, respectively).

The impact of GO on metal accumulation in embryos and larvae was assessed by comparing the percentage difference between the amount of metals in the MIX-exposed organisms and that in the organisms co-exposed to MIX and GO. The percentage difference in Cr amount in embryos was not significantly affected by the MIX+GO treatment at all the tested concentrations. However, the amount of Cu in MIX20+GO20-treated embryos decreased approximately by 43 % and in those treated with MIX40+GO40 by 41% compared with the respective MIX20- and MIX40-treatment values, and these changes were significant ($p = 0.001$ and $p = 0.0002$, respectively). These results demonstrate the impact of GO on metal accumulation in organisms.

This study demonstrated that GO can adsorb metals that are present in mixtures (MIX+GO) and modify the accumulation of metals in *Salmo trutta* embryos and larvae.

[1] A. Gupta, V. Sharma et al., *Materials*, 14(16), 4702, (2021).
[2] S.Z.N. Ahmat, V. Salleh et al., *Chemosphere*, 248, 12600811, (2020).
[3] C.B. de Melo, F. Coa et al., *Chemosphere*, 223, 157-164, (2019).
[4] S. Thomas, J.A. Mohaideen, *IJBCS*, 13(1), 53-62, (2015).

Measuring Microviscosity of Lipid Droplets in Human Breast Cancer Cells via Fluorescence Lifetime Imaging

Džiugas Jurgutis[1,2], Greta Jarockytė[1,2], Aurimas Vyšniauskas[3], Ričardas Rotomskis[1], Vitalijus Karabanovas[1,4]

[1]Biomedical Physics Laboratory, National Cancer Institute, P. Baublio St. 3b, 08406 Vilnius, Lithuania
[2]Life Sciences Center, Vilnius University, Saulėtekio Ave. 7, 10257 Vilnius, Lithuania
[3]State Research Institute Center for Physical Sciences and Technology, Saulėtekio Ave. 3, 10257 Vilnius, Lithuania
[4]Department of Chemistry and Bioengineering, Vilnius Gediminas Technical University, Saulėtekio Ave. 11, 10223 Vilnius, Lithuania
dziugas.jurgutis@nvi.lt

Microviscosity is vital in governing the structural and functional balance of subcellular components and regulating diffusion of biomolecules through cells. Abnormal microviscosity of organelles might indicate the onset of diseases, e.g., diabetes or cancer [1]. Recent findings highlight the role of lipid droplets in tumorigenesis and cancer aggressiveness [2]. However, microviscosity of these lipid-rich organelles in human breast cancer cells of different malignancy remains unknown.

In this research, we utilize BDP-H molecular rotor (Fig. 1A), together with fluorescence lifetime imaging microscopy (FLIM) to measure microviscosity of lipid droplets. BDP-H sensitivity to viscosity and compatibility with living cells was confirmed by previous research [3-4]. Intramolecular rotation of BDP-H depends on the microviscosity of the surrounding environment: in a highly viscous cellular compartment (e.g., plasma membrane) the rotation is restrained, leading to a slower non-radiative relaxation from the excited state, thus resulting in a longer fluorescence lifetime, and vice versa in a micro-environment with lower microviscosity (e.g., cytoplasm) [1,3].

The aim of our study was to measure and quantitatively compare microviscosity of lipid droplets in MCF-7 and MDA-MB-231 human breast cancer cells.

Live cancer cells were imaged with a laser-scanning confocal microscope. Fluorescence lifetimes of BDP-H in lipid droplets of live cancer cells were determined using a time-correlated single photon-counting based FLIM. BDP-H calibration curve obtained at 40 °C in toluene-castor oil mixtures of varying viscosity was used to convert fluorescence lifetime values to microviscosity.

Our results demonstrate that BDP-H accumulates in lipid droplets and cytosol of MCF-7 and MDA-MB-231 cells and exhibits monoexponential fluorescence decays. Microviscosity values of 120 ± 9 cP and 195 ± 48 cP were assigned to the lipid droplets in MCF-7 and the more aggressive MDA-MB-231 cells, respectively (Fig. 1B-C). Finally, statistical analysis revealed that the difference between lipid droplet microviscosity in human breast cancer cells of different malignancy is statistically significant (Welch's two-sample *t*-test, $t(20.34) = 6.88$, $p < 0.0001$, $n = 20$) [4]. Collectively, our results provide evidence that lipid droplet microviscosity has a great potential as a biomarker for the identification of the malignancy of cancer cells, and that the BDP-H molecular rotor could be used for this purpose.

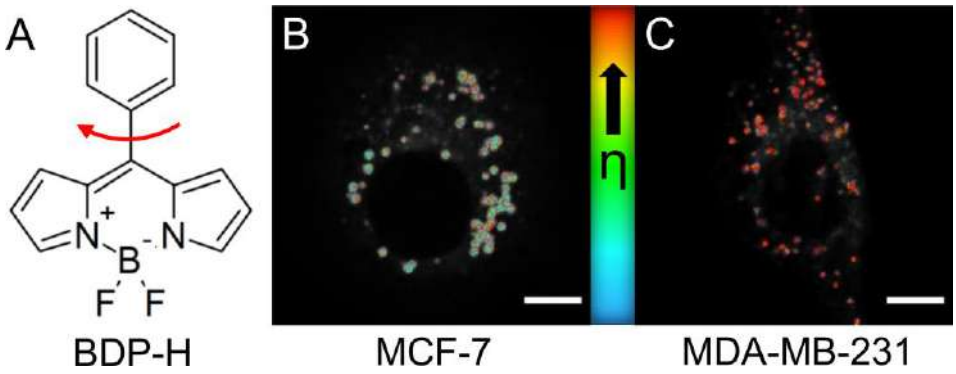

Fig. 1. (A) The structure of BDP-H molecular rotor used in this work. Fluorescence lifetime imaging microscopy images of live MCF-7 (B) and MDA-MB-231 (C) human breast cancer cells; scale bars: 10 μm. Pixel colours indicate BDP-H fluorescence lifetimes and microviscosity (η) values [4].

[1] M.K. Kuimova et al., *Phys. Chem. Chem. Phys.,* **14**, 12671-12686 (2012).
[2] A.L.S. Cruz et al., *Cell Death Dis.,* **11**, 1-16 (2020).
[3] S. Toliautas et al., *Chem. – Eur. J.,* **25**, 10342-10349 (2019).
[4] D. Jurgutis et al., *Int. J. Mol. Sci.,* **23**, 5687 (2022).

Application of Fiber-based FT-IR ATR Spectroscopy for Tissue Diagnostics During Oncological Surgery

Rimantė Bandzevičiūtė[1], Justinas Čeponkus[1], Christian Teske[2], Katja Liedel[2], Gediminas Platkevičius[3], Arūnas Želvys[3], Valdas Šablinskas[1], Gerald Steiner[4]

[1]Institute of Chemical Physics, Faculty of Physics, Vilnius University, Saulėtekio Av. 3, LT-10257 Vilnius, Lithuania
[2] Department of Visceral, Thoracic and Vascular Surgery, University Hospital Carl Gustav Carus Dresden, Dresden University of Technology, Fetscherstr. 74, 01037 Dresden, Germany
[3]Institute of Clinical Medicine, Faculty of Medicine, Vilnius University, Santariškių Str. 2, LT-08661, Vilnius, Lithuania
[4]Clinical Sensoring and Monitoring, Faculty of Medicine Carl Gustav Carus, Dresden University of Technology, Fetscherstr. 13, 01307 Dresden, Germany
rimante.bandzeviciute@ff.vu.lt

Cancer is one of the leading causes of death in the world. Treatment options usually involve surgical resection, chemotherapy, radiation therapy and other treatment types that can be combined together in general. The most applied treatment for various types of solid cancer is surgical operation. The final outcome of the patient, quality of life after the surgery and overall survival highly depends on the resection margin status of the malignant tumor. In order to prevent recurrence of the tumor all cancerous cells have to be resected while as much healthy tissue as possible should be preserved to save vital functions of the organ. In order ensure clearance of microscopic tumor infiltrations not being visible macroscopically, histological frozen section examination is often applied during the surgery. The frozen section examination has some limitations such as prolonged operation and anaesthesia time as well as limited accuracy. Therefore, some additional intraoperative methods for diagnostics of tissue type are required.

Recently, the scope of FT-IR (Fourier transform infrared) spectroscopy studies for tissue examination were reported [1]. Those are usually performed for the processed tissue, such as frozen, dried or formalin-fixed, paraffin-embedded samples. Mostly, the applications cover only the laboratory studies far away from the real clinical applications. In our research, we applied FT-IR fiber probe with germanium ATR (attenuated total reflection) tip attached to the optical fiber for the discrimination of freshly resected human normal and cancerous tissues in various entities. The measuring system contains silver halide ATR fiber probe coupled with a portable compact FT-IR spectrometer thus allows to perform the measurements in the operating room under *ex vivo*, *in situ* or even *in vivo* conditions. The system applied for freshly resected untreated tissues enables to obtain chemical information of the native tissue avoiding the biochemical changes of the tissue due to degradation or contamination with chemical reagents. While applying the described technique, the penetration depth of the infrared radiation into the sample reaches several micrometers. Such spectroscopic approach allows to observe changes in the cells and ECM (extracellular matrix) of the resected tissue samples. The measurements can be performed in a few minutes thus allowing to obtain instant results. The tissue samples were examined immediately after surgical operation in the laboratory or next to the operating room.

Using this method for different tissue types including bladder, pancreas, kidney and liver tissue, spectral tumor markers were identified. In bladder tissue, changes in spectra are related to decreased collagen and increased glycogen levels in the tumorous tissue. Differences between normal and tumorous pancreatic tissue spectra are characterized by a spectral profile change in lipid and protein content (spectra of tumorous and normal bladder and pancreas tissues are represented in Fig. 1). Kidney tumors can be characterized by increased levels of glycogen while liver tumors exhibit different levels of glycogen and collagen depending on the specific tumor type. Successful determination of cancerous tissue areas reveals the potential of the fiber-based FT-IR spectroscopy for the diagnostics during oncological surgeries and brings the method one step closer to clinical applications.

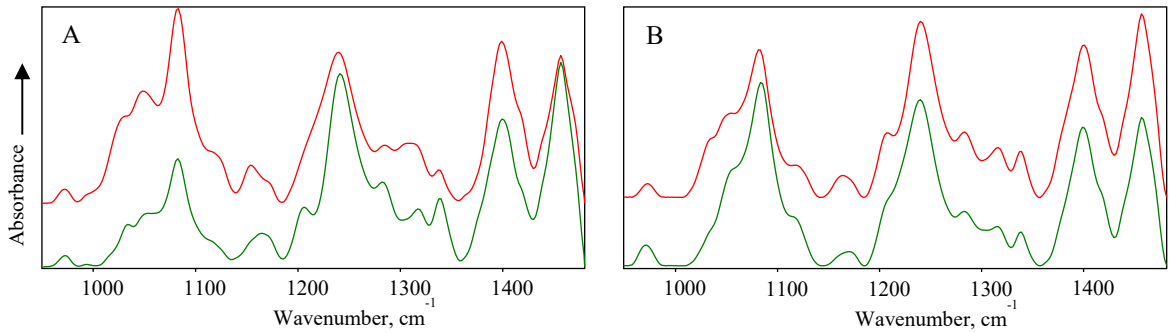

Fig. 1. FT-IR ATR spectra of freshly resected: A – urothelial carcinoma (top, red line) and normal (bottom, green line) human bladder tissue, B – pancreatic adenocarcinoma (PDAC) (top, red line) and normal (bottom, green line) pancreas tissue

[1] G. Bellisola, C. Sorio, Am J Cancer Res **2** (1), 1-21 (2012).

Identification of Pathogenic Bacteria and Fungi by means of ATR-IR spectroscopy

Gerda Anužienė[1], Irmantas Čiužas[2], Rimantė Bandzevičiūtė[1], Eglė Lastauskienė[2], Justinas Čeponkus[1]

[1]Chemical Physics Institute, Faculty of Physics, Vilnius University, Saulėtekio Av. 3, LT-10257 Vilnius, Lithuania
[2]Institute of Biosciences, Life Sciences Center, Vilnius University, Saulėtekio Av. 7, LT-10257 Vilnius, Lithuania
gerda.anuziene@ff.stud.vu.lt

Pathogenic microorganisms such as bacteria and fungi can cause infectious diseases which are currently being treated by prescribing medications. Antibiotics are used for the treatment of bacterial infections, but it is known that bacteria can develop antibiotic resistance while fungi are not sensitive for the treatment by antibiotics so for yeast infections antifungals are used. In mixed infections, only one domain of pathological microorganism (eukaryote or procaryote) can be killed while allowing another to spread even faster. For this reason, it is important to identify the species of microorganisms early to accurately prescribe the treatment. Methods which are used nowadays for pathogenic microorganisms' identification requires sample preparation and/or cultivation and takes a long time until the identification results are obtained, especially in the case of eukaryotic microorganisms. ATR IR spectroscopy is a non-destructive method and often does not require sample preparation. The collection of the ATR IR absorption spectrum takes several minutes therefore the identification of pathogenic microorganisms can be accomplished faster [1-3].

In this work, the method of an attenuated total reflection of infrared radiation (ATR IR) spectroscopy was applied for the analysis. ATR IR absorption spectra of 150 samples of different bacteria (57 samples, 8 different species) and fungi (93 samples, 3 different species) were analyzed.

The main difference between ATR IR spectra of bacteria and fungi were observed in 1183 cm^{-1} – 930 cm^{-1} spectral region which can be associated with carbohydrates that are found in bacterial and fungal cells. Also, a change in the contour of the spectra is observed in the 1360 cm^{-1} – 1280 cm^{-1} spectral region.

In this work hierarchical cluster analysis (HCA) and principal component analysis (PCA) were applied to determine how accurately ATR IR absorption spectra of bacteria and fungi can be identified. HCA was performed by selecting 1800 cm^{-1} – 750 cm^{-1} spectral region while PCA was performed by selecting 1345 cm^{-1} – 930 cm^{-1} spectral region. HCA and PCA showed that ATR IR absorption spectra of fungi can be identified with 100 % accuracy, while ATR IR absorption spectra of bacteria can be identified with 89,9 % and 100 % accuracy respectively. In HCA dendrogram all and in PCA diagram five of the six ATR IR absorption spectra of *Arthrobacter* sp. bacteria were assigned to the fungi group. The main reason for this can be that the ATR IR absorption spectra of *Arthrobacter* sp. bacteria have higher intensity bands at 1183 cm^{-1} – 930 cm^{-1} spectral region.

All in all, ATR IR spectroscopy is a suitable method for the identification of different pathogenic microorganisms. To apply the method for clinical diagnostics it is important to carry out studies with larger sample number and to continue to use both methods of statistical analysis.

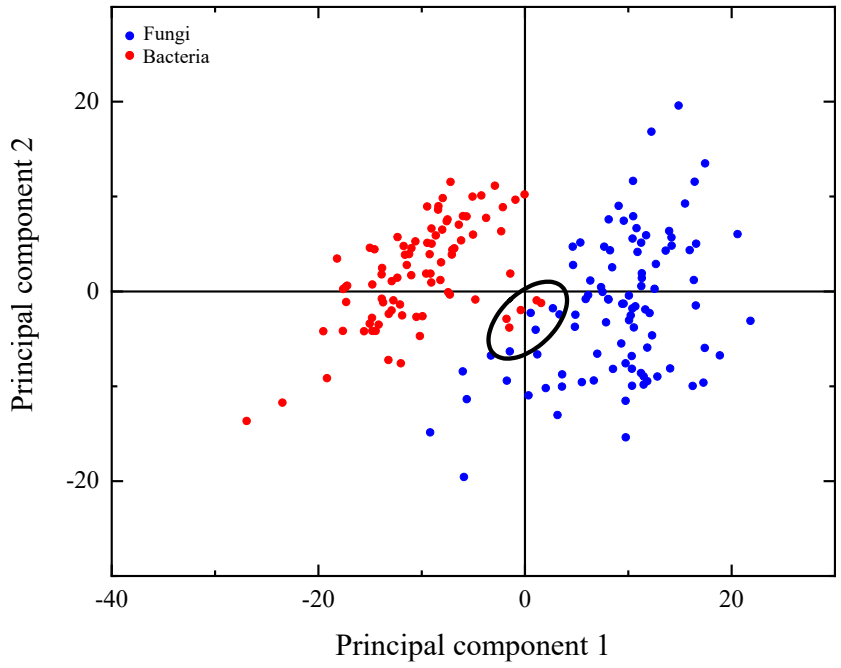

Fig. 1. PCA of ATR IR spectra of pathogenic fungi and bacteria

[1] M. Pigłowski, Int. J. Environ. Res. Public Health **16**, 477 (2019)
[2] M. Harz, P. Rösch, J. Popp, Cytometry **75A**, 104-113 (2009)
[3] B. Buszewski, A. Rogowska, P. Pomastowski, M. Złoch, V. Railean-Plugaru, J. AOAC Int **100**, 1607-1623 (2017)

Use of a laser speckle system in the determination of antibacterial susceptibility by the disc diffusion method

Ilya Balmages[1], Aigars Reinis[2,3], Svjatoslavs Kistkins[1,2], Dmitrijs Bliznuks[4], Emilija Vija Plorina[1], Alexey Lihachev[1], Ilze Lihacova[1]

[1]University of Latvia, Institute of Atomic Physics and Spectroscopy, Jelgavas 3, Riga, Latvia
[2]Pauls Stradins Clinical University Hospital, Pilsoņu 13, Riga, Latvia
[3]Riga Stradins University, Department of Biology and Microbiology, Dzirciema 16, Riga, Latvia
[4]Riga Technical University, Zunda krastmala 10, Riga, Latvia
Ilya.Balmages@rtu.lv

Rapid identification of antibacterial resistance plays a crucial role in treatment of acute infectious conditions, Early identification of infectious agent and its sensitivity to antibiotics can provide targeted pharmacological intervention at the early stage of the disease, increasing patient's survival. The issue has become relevant in the treatment of elderly patients. The empiric antimicrobial treatment must be replaced as soon as possible to reduce the risk of mortality of patients. Phenotypic resistance tests such as disk diffusion and E-test require 16-24 hours to obtain the results [1], while the PCR tests provide only genotypic type of antibacterial resistance.

In previous studies using laser speckle imaging technique, we managed to determine the bacteria growth after 2-3 hours from the beginning of activity [2]. In the laser speckle imaging method, a laser beam is scattered on a Petri dish where the test bacteria and antibiotic discs are located. The laser speckles reflected from the surface are recorded sequentially in time. A sub-pixel correlation analysis was proposed to detect small changes in the sequence of laser speckle images, and the effects associated with changes in bacterial activity can be observed.

Experiments were performed at the Pauls Stradins Clinical University Hospital Joint Laboratory on different bacteria and their corresponding antibiotics [3].

The images captured at 30 second intervals were processed by dividing the experimental field into small sections of NxN pixels. A two-dimensional normalized correlation was performed between consecutive NxN image fragments throughout the experiment. Interpolation around the correlation peak is performed in order to find a more accurate peak position. The correlation peak shift in space characterizes the changes that occur between consecutive images. The offsets obtained between each pair of adjacent images were accumulated and converted to "time signal" [2].

As a result it was obtained that after a few hours from the start of the experiment a disc of the sterile zone begins to form around the antibiotic. The sterile zone becomes clearly visible within a couple of hours after the beginning of formation. The result was obtained significantly earlier than by the disk diffusion method [4] for the same bacterial species [4]. Creating a spatio-temporal image averaging around each radius as it moves away from the centre (from the antibiotic), we can obtain a certain curve, similar to the letter "S", according to which the size of the sterile zone changes over time (Fig. 1). This behaviour has been observed in several different experiments.

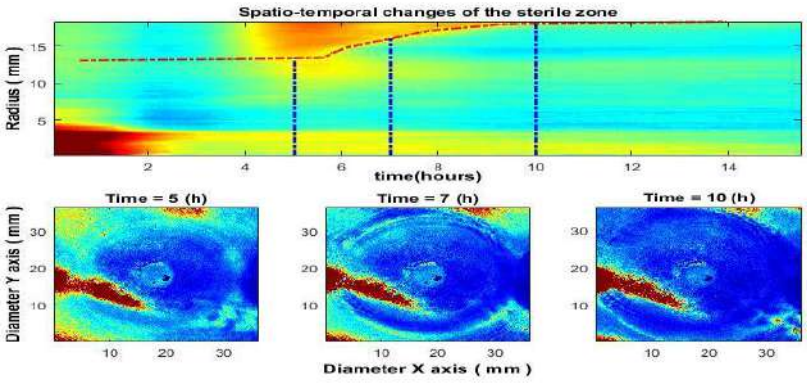

Fig. 1. Spatio-temporal changes of the sterile zone (top), and sterile zone formation in the growth of *Acinetobacter baumanii* around the imipenem disc (bottom).

This work has been supported by the European Regional Development Fund project "Rapid assessment system of antibacterial resistance for patients with secondary bacterial infections" (No. 1.1.1.1/21/A/034).

[1] Tenover F.C. Antimicrobial Susceptibility Testing, Editor(s): Thomas M. Schmidt, Encyclopedia of Microbiology (Fourth Edition), Academic Press, 2019, Pages 166-175, ISBN 9780128117378.
[2] Balmages. I., et al. "Laser speckle imaging for early detection of microbial colony forming units," Biomed. Opt. Express 12, 1609-1620 (2021)
[3] Karlowsky J.A., et al. Comparison of four antimicrobial susceptibility testing methods to determine the in vitro activities of piperacillin and piperacillin-tazobactam against clinical isolates of Enterobacteriaceae and Pseudomonas aeruginosa. J Clin Microbiol. 2003 Jul;41(7):3339-43. doi: 10.1128/JCM.41.7.3339-3343.2003. PMID: 12843088; PMCID: PMC165312
[4] https://www.eucast.org/clinical_breakpoints/

Picosecond-domain Nd: YAG laser in vivo study on tattoo removal and microlesion healing dynamics

Justinas Baleišis[1], dr. Romualdas Rudys[1]

[1]State Research Institute Centre for Innovative Medicine, Department of Biomodels,
Santariskiu st. 5, LT-08410, Vilnius, Lithuania

Picosecond-domain lasers have seen increased use in aesthetic dermatology, with applications ranging from exogenous and endogenous pigment removal to treating acne scars, photoaged, rhytides, photorejuvenation, and skin tightening. Initially, the use of picosecond lasers in dermatology was aimed at improving the removal of unwanted tattoos, which was dominated by Q-switch nanosecond-domain systems. The nanosecond pulse duration, on the other hand, is now thought to be too long to properly fragment ink into small enough particles while minimizing collateral heat injury to adjacent tissue [1]. Therefore, tattoo clearance remains challenging since both temporary and permanent side effects do occur. Temporary side effects include pain, erythema, crusting, pinpoint bleeding, blistering, swelling, infection, and pigmentary disorders. Permanent side effects include scarring, hypo- or hyper-pigmentation, and color change of tattoo pigment [2].

Picosecond (ps) lasers have emerged at the forefront of laser tattoo removal due to their shorter pulse lengths showing better performance and shorter post-treatment downtime in preclinical and clinical studies. The pigment removal approach is based on the photoacoustic effect. The application of energy causes a rapid thermal expansion of the pigment particles, which are then shattered by the generation of acoustic waves. Because pigments break down into smaller granules, macrophages can transport them away via the lymphatic system, thus resulting in the clearance of the tattoos [3].

Fractional laser treatment is a new application of picosecond-domain systems for photorejuvenation and skin tightening that utilizes optical lenses from diffractive beam splitters or microlens array optics. These arrays produce high fluence regions separated by a low fluence background, resulting in focal areas of ablative or non-ablative skin injury. In the high-intensity regions, if sufficient peak power (10^{11}W/cm^2) is generated, plasma formation is initiated due to a non-linear laser-induced optical breakdown process. The induction of micro-injury zones has been shown to stimulate new collagen, mucin, and elastin production in the dermis during the wound healing process [4].

As safety and high efficacy are in high demand, new laser systems for cutaneous interventions are constantly being developed. However, the lack of information regarding crucial parameters is not always described by the authors in published data [4]. Therefore, preclinical in vivo studies are of great importance to assess potential safety concerns and develop protocols that could be used in human and veterinary medicine.

As most available picosecond laser systems excel at 300-600 ps [1], we aimed to investigate the laser-tissue interactions of an Nd: YAG laser, that can generate pulses of 150 ps. The effects of 150 ps ultrashort pulses are not currently described in the literature, and the area is lacking in animal studies that offer great translational value. Thus, we conducted our in vivo study on porcine skin, which is very close to human skin in many regards. By utilizing different beam focusing optics (zoom/fractional), we aimed to analyze the intradermal tattoo ink pigment fragmentation efficiency and healing patterns of laser-induced microlesions, using a non-invasive multispectral imaging technique (SIAscopy) in combination with image processing software and histopathological analysis.

[1] R. Torbeck, L. Schilling, H. Khorasani et al., *Evolution of the Picosecond Laser: A Review of Literature*, Dermatologic Surg. 45-2:183–94 (2019).
[2] P.S. Islam, C. Chang, C. Selmi, et al., *Medical Complications of Tattoos: A Comprehensive Review*, Clinic Rev Allerg Immunol. 50, 273–286 (2016)
[3] O. Reiter, L. Atzmony, L. Akerman, et al., *Picosecond lasers for tattoo removal: a systematic review*, Lasers Med Sci. 31(7):1397–405 (2016).
[4] K. O'Connor, S.B. Cho, H.J. Chung, *Wound Healing Profile After 1064-and 532-nm Picosecond Lasers with Microlens Array of In Vivo Human Skin*, Lasers in Surgery and Medicine. 53, 1059-1064 (2021).
[5] J. Matys, M. Dominiak, R. Flieger, *Energy and Power Density: A Key Factor in Lasers Studies*, J Clin Diagn Res. 9, Zl01-02 (2015).

Spectrophotometric measurements of natural photosensitizers: sodium and copper chlorophyllins

Goda Mažeikaitė[1], Irina Buchovec[1], Pranciškus Vitta[1]

[1]Institute of Photonics and Nanotechnology, Faculty of Physics, Vilnius, Lithuania
goda.mazeikaite@ff.stud.vu.lt

The applications of light, as well as photodynamic therapy, are gaining increasing medical and food safety recognition. The great advantage of these methods is that bacteria have little ability to develop resistance to light. For inactivation of different food pathogens and spoilage bacteria biofilms, blue light is used, but it requires substantially higher light doses for a significant effect, which prolongs treatment procedures. Therefore, blue light is combined with other methods, e.g. with antibiotics or photosensitizers (antimicrobial photodynamic inactivation (API)) [1][2]. API as one of the modern biophotonic technology, is based on the interaction of photoactive agent (non-toxic photosensitizers (PS)), molecular oxygen and light of suitable wavelength to match the PS absorption peak [3]. Usually, after light excitation, the triplet-state of PS interacts with molecular oxygen, electron donors or acceptors and can produce reactive oxygen species (ROS), thereby triggering photo-oxidative reactions that initiate various cellular damages and destroy the bacterial cells. The efficacy of API depends on many factors, but most significantly on the photophysical properties of the used PS. Almost all PSs are degraded during the light illumination through oxygen mediated processes. Therefore, it is important to assess PSs photostability. Fast photobleaching can be a disadvantage in API, as the PS cannot form enough ROS to kill bacteria.

Two natural PSs were used in this work: non-copperized chlorophyllin sodium salt (Na-Chl) (MW = 684.9 g/mol) and copper chlorophyllin sodium salt (Cu-Chl) (MW=724.2 g/mol), manufactured by 'Carl Roth', Germany. Both PS are known as water-soluble, green, negatively charged compounds with the main absorption maximum at 405 nm. Both PSs are known to exhibit optical absorbance reduction after the activation by visible blue light [3]. These changes show the activation dependence on excitation dose and can be used to compare the irradiation efficiency by different spectral components. We primarily studied the absorption characteristics of Na-Chl and Cu-Chl after illumination with an optimal excitation wavelength 402 nm, respectively (Fig. 1).

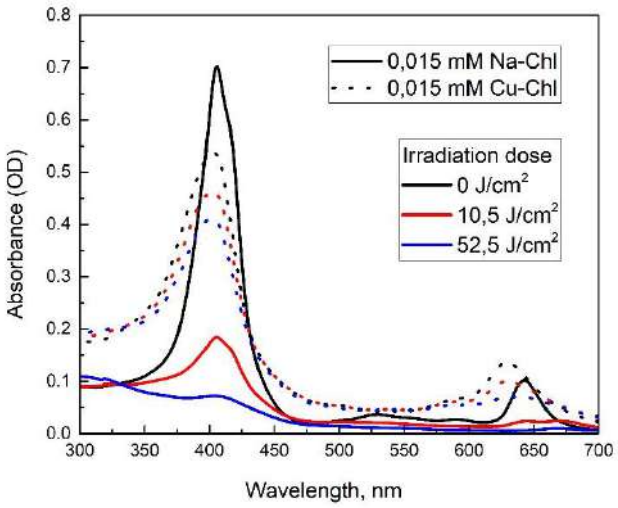

Fig. 1. Photostability as optical absorbance spectra of Na-Chl and Cu-Chl after treatment of different irradiation doses (35 mW/cm^2 irradiance).

Figure 1 shows the spectra recorded after illumination of 0.015 mM Na-Chl and Cu-Chl solutions in distilled water at 35 mW/cm^2 for different time periods (0–25 min). The main absorption peaks of Na-Chl and Cu-Chl decreased to about 26% and 85% after irradiation for 5 min (10.5 J/cm^2) and reached 10% and 77% of its initial magnitude after 25 min (52.5 J/cm^2), respectively. In contrast to Na-Chl photodegradation, the spectroscopic data of Cu-Chl solution revealed the slow photomodification. Therefore, the Cu-Chl was more photostable than Na-Chl, further studies of ROS generation have to be performed.

[1] R. Youf, M. Müller, A. Balasini et al., Antimicrobial Photodynamic Therapy: Latest Developments with a Focus on Combinatory Strategies. *Pharmaceutics* **2021**, *13*, 1995

[2] A. Wozniak, M. Grinholc, Combined Antimicrobial Activity of Photodynamic Inactivation and Antimicrobials–State of the Art. *Front. Microbiol*. 9:930 2018

[3] I. Buchovec, A. Gricajeva, L. Kalėdienė, P. Vitta. Antimicrobial Photoinactivation Approach Based on Natural Agents for Control of Bacteria Biofilms in Spacecraft. *International journal of molecular sciences*. 21 (18). 2020

Photoadaptation of Unicellular Algae Cells: Spectroscopic Studies

Rasa Miliukaitė, Agnė Kalnaitytė

Biophotonics Group of Laser Research Centre, Vilnius University, Saulėtekio ave. 9, III bld. LT-10222, Vilnius, Lithuania
rasa.miliukaite@ff.stud.vu.lt

Light energy that is absorbed by chlorophylls in photosynthetic systems (PS) of plants can undergo three competing fates: it can be used to drive photosynthesis (photochemistry), be dissipated as heat, or re-emitted as fluorescence (FL) [1]. In steady-state emission spectrum algae chlorophylls autofluorescence (AF) occurs in the red light region with a main band at 682 nm, which is mostly from PSII, and a small broad shoulder from 700 nm to 750 nm, due to a contribution of both PSII and PSI. Measurements of chlorophylls FL provide indirect information about the physiological condition of autotrophs and is non-invasive and non-destructive tool for monitoring reactions in the living systems or ecological environment. If stressors are light sensitive (for example quantum dots or photosensitizers), the potential toxicity depends not only on the structure and concentrations of these materials, but also on the species of algae and activated adaptive responses in cells [2].

The aim of this study was to determine spectroscopically how freshwater *Scenedesmus sp*. and *Chlorella sp*. algae cells adapt to violet light irradiation under tested environment conditions. Algae cells were grown in mineral fertilisers dissolved in distilled water (FDW). Samples were prepared with distilled water for final concentration of algae. After preparation samples in plastic cuvettes (10 × 4 mm) were irradiated with violet LED (405 nm, 30 mW/cm^2 at 8 cm distance) for different doses (9 J/cm^2, 36 J/cm^2 and 54 J/cm^2). FL spectra (LS 55 fluorometer, Perkin Elmer, USA) and kinetics of photoinduced changes in peaks AF intensity of algae were measured the first day of the experiment. Kinetics were measured using AvaSpec-3648 spectrometer (Avantes, The Netherlands) with continuously on excitation light source (405 nm) and FL was collected from the bottom of 96-well sample Petri plate during measurements. Then all samples were kept in the plate at room temperature overnight at 8/16 h "light/dark" cycle, which was applied using a combined white LED lamp (6 W). The next day, all samples were adapted in dark for 20 min before measurements of chlorophyll AF induction curves with Pulse-Amplitude-Modulation (PAM) fluorometer. Analysis of AF induction curves allows the evaluation of the physiological condition of PSII and photosynthetic electron transport chain components.

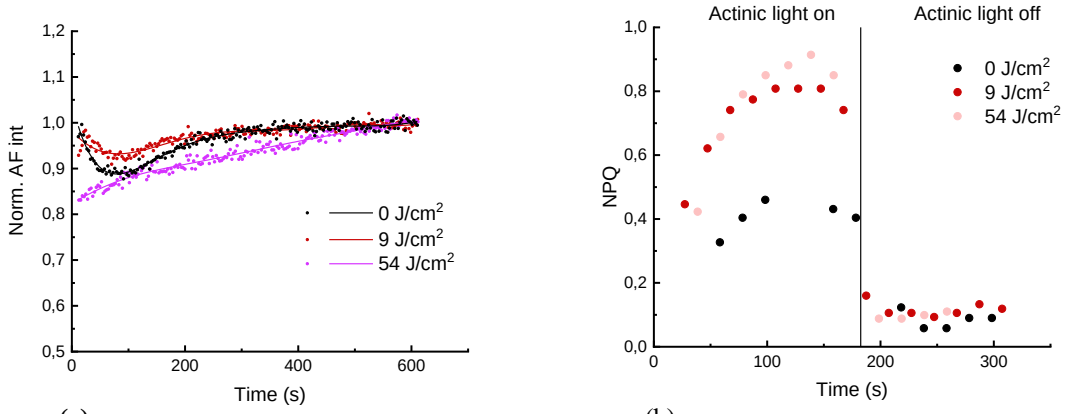

(a) (b)

Fig. 1. The normalised to the final values AF kinetics (at spectrum peak of 682 nm, excitation wavelength 405 nm) of algae cells immediately after irradiation with different doses of violet light (a) and non-photochemical quenching (NPQ) coefficient the next day after exposure (b).

Immediately after irradiation, the AF intensity kinetics of samples affected with 9 J/cm^2 dose were able to maintain a similar pattern as unexposed samples, showing a rapid AF intensity decrease of about 10% from initial value and gradually reached terminal level after 200 s (Fig. 1 (a)). However, in the samples that were exposed to higher doses the AF intensity was about 20% smaller than in control and was recovering during measurement until also reached terminal level. Despite that the second day results of photoinduced changes in peak AF intensity of samples exposed to different doses are all similar, it is seen that NPQ coefficient of irradiated samples is about two times higher than not exposed (Fig. 1 (b)). While the extent of NPQ is proportional to the number of quenching centres in the light-harvesting antenna of PS II, additional irradiation increases the quenching ability in exposed algae samples. These results may imply that *Scenedesmus sp*. and *Chlorella sp*. algae photoadaptation responses immediately after violet light irradiation are dose dependant, yet all doses have a similar impact on photoadaptation in longer periods of time.

[1] A. N. Misra, M. Misra, R. Singh, *Chlorophyll Fluorescence in Plant Biology*, Biophysics, 171-192 (2012)
[2] A. Kalnaitytė, S. Bagdonas, *Light-mediated effects of CdTe-MSA quantum dots on the autofluorescence of freshwater green microalgae: Spectroscopic studies,* Journal of Photochemistry and Photobiology B: Biology, vol. 199 (2019)

Investigation of Autofluorescence of Characean *Nitellopsis obtusa* Cells

Aušrinė Navickaitė[1], Vilmantas Pupkis[1], Saulius Bagdonas[2]

[1]Vilnius University, Department of Neurobiology and Biophysics, Saulėtekio av. 7, LT-10257 Vilnius, Lithuania
[2]Vilnius University, Laser Research Center, Saulėtekio av. 9, LT-10222 Vilnius, Lithuania
ausrine.navickaite@gmc.stud.vu.lt

Chlorophyll fluorescence measurements are frequently used to monitor photosynthetic performance in algae and plants, as emission and photochemical reactions are in direct competition for excitation energy. Consequently, an increase of fluorescence emission indicates disrupted photosynthetic performance [1]. Characean algae provide a unique model system for studying various aspects of photosynthesis. Under constant illumination characean internodes generate alternating acid and alkaline bands along their surface which influence photosynthetic activity of the cell [2]. Nevertheless, many different factors can affect chlorophyll fluorescence in a similar way. Thus, further evaluation of fluorescence parameters is needed.

An optical fiber system paired with a controlled stepper motor enabled registration of chlorophyll fluorescence signals along *Nitellopsis obtusa* internodes in 1 mm intervals. A low intensity (< 1 mW) LED light source emitting at 405 nm was used for excitation. To evaluate the effect of illumination on photosynthetic performance, emission signals were registered in dark-adapted internodes and in cells that underwent no adaptation. Further investigation of light-induced changes was performed by illuminating dark-adapted internodes with an intense (photosynthetic photon flux density of 829 µmol m^{-2} s^{-1}) white LED light source for 15 min. or 30 min.

The fluorescence emission spectrum of *Nitellopsis obtusa* exhibited two peaks around 680 nm and 739 nm (Fig. 1A). Fluorescence intensity values registered at these wavelengths displayed variations along the cell in accordance with changes of fluorescence intensity ratio between 680 nm and 750 nm (F680/F750), regardless of lighting conditions. Additional 15 min. and 30 min. illumination of previously dark-adapted internodes resulted in lower values of fluorescence parameters. Moreover, further investigation of maximum fluorescence intensity and F680/F750 ratio revealed an exponential relationship (Fig. 1B). These results indicate different photosynthetic activity zones along the cell as well as provide a suitable model to predict light-induced changes of fluorescence parameters in algae cells. Hence, the discovered relationship could aid in evaluating the effect of other environmental factors on photosynthetic performance.

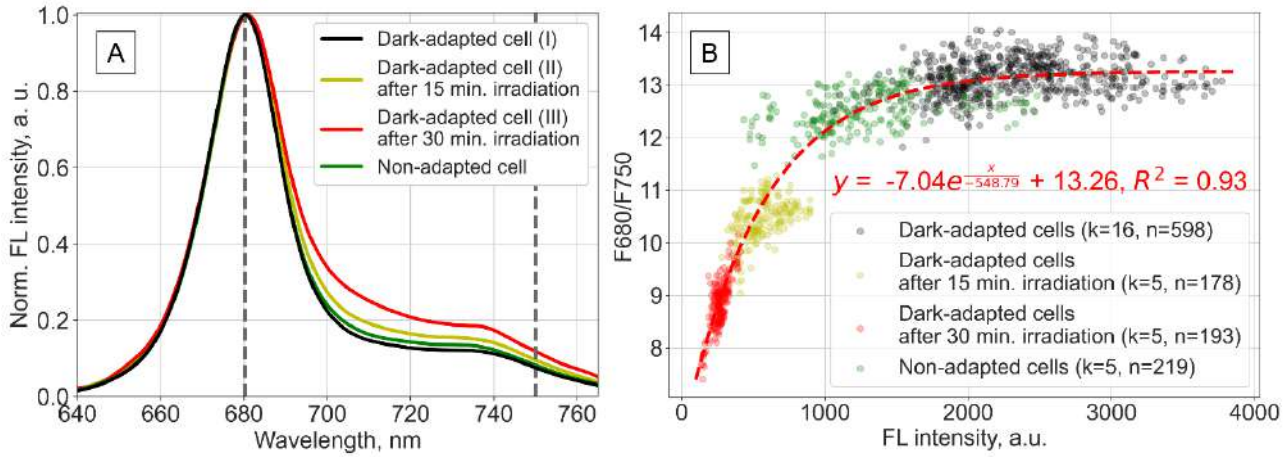

Fig. 1. Fluorescence (FL) spectra (A) and the relationship between peak FL intensity (680 nm) and F680/F750 ratio (B) in *Nitellopsis obtusa* internodes kept under different lighting conditions; k – number of cells, n – number of registered spectra

[1] N. R. Baker, Chlorophyll Fluorescence: A Probe of Photosynthesis In Vivo, Annual Review of Plant Biology 59(1), 89-113 (2008).
[2] A. A. Bulychev, A. A. Polezhaev, S. V. Zykov, et al., Light-Triggered pH Banding Profile in Chara Cells Revealed with a Scanning pH Microprobe and Its Relation to Self-Organization Phenomena, Journal of Theoretical Biology 212(3), 275-294 (2001).

Phototoxicity of CdSe/ZnS-COOH quantum dots with microalgae cells: spectroscopic and microscopic studies

Agnė Kalnaitytė[1,2], Danguolė Montvydienė[2], Emilija Januškaitė[1], Živilė Jurgelėnė[2], Mindaugas Kazlauskas[2], Nijolė Kazlauskienė[2] and Saulius Bagdonas[1,2]

[1] Vilnius University, Biophotonics Group of Laser Research Centre, Sauletekio av. 10, LT-10223, Vilnius, Lithuania
[2] Nature of Research Centre, Institute of Ecology, Akademijos st. 2, LT-08412, Vilnius, Lithuania,
agne.kalnaityte@ff.vu.lt

The increasing applicability of hydrophilic nanoparticles (NPs), for example, quantum dots (QDs), for everyday use also increases the possibility of accidental release of NPs into the natural waters. Various pollutants, such as heavy metals, can accumulate in algae cells, which often serve as model organisms for more complex plants in the studies to assess the toxic effects of substances on ecosystems and global environmental processes. *Scenedesmus sp*. are among the most popular species of green freshwater microalgae used in toxicity studies. The autofluorescence (AF) of microalgae studies have revealed the ability of core QDs to retard the photoadaptation of wild type microalgae under naturally varying illumination conditions [1]. Moreover, different composition of algae growth media has influence on both, algae cells and QDs. It could not only affect the supply of nutrients to cells, but the higher ionic strength in this media than in distilled water facilitates the aggregation of the QDs. However, that does not suppress NPs contacts with algae cells and indicate unpredictable interactions between them.

In this study, optical spectroscopy and microscopy methods were applied to investigate the chlorophylls fluorescence (FL) in *Scenedesmus quadricauda* algae, whose were grown in different natural aqueous media (deep well water (DWW), Lake Balsys water (LW), MWC algae grow media) and exposed with 4 nM or 40 nM final concentration of hydrophilic CdSe/ZnS-COOH quantum dots (625 nm, Invitrogen, USA). Analysis of chlorophyll FL induction curves, measured with Pulse-Amplitude-Modulation (PAM) fluorometer, allows the evaluation of the physiological condition of PSII and photosynthetic electron transport chain components.

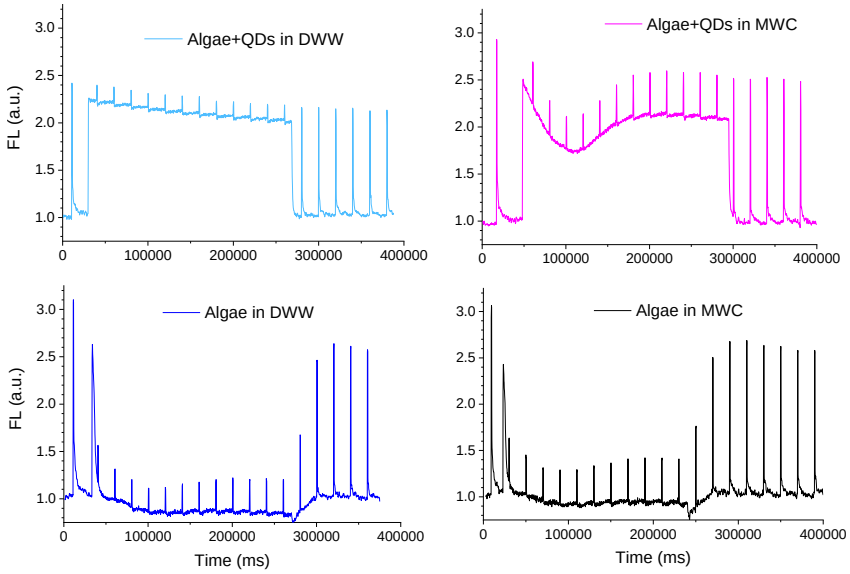

Fig. 1. Algae autofluorescence induction and recovery curves in deep well water (DWW) and MWC grown media after 24-hour incubation with CdSe/ZnS-COOH quantum dots (concentration of 40 nM) and without QDs.

Once in the dark or after adaptation to light conditions all PS II reaction centres are opened, maximal photochemical quenching is reached and FL intensity are reduced. Although, in actinic light the AF of algae in both media (DWW and MWC) decreased during first 20 s, the AF of QDs exposed algae was increased and the fall was reduced (Fig. 1). The non-photochemical fluorescence quenching (NPQ), that dissipate excitation energy and also quench algae AF, was registered higher in algae samples with DWW, then with MWC. The CdSe/ZnS-COOH quantum dots induced the decrease of NPQ in algae samples with both media. During the light periods the photosynthetic electron transport rate (ETR) is increased and this means that virtually PS II reaction centres are in the closed state and not able to convert excitation energy into photochemical energy with maximum efficiency. However, the ETR of algae was reduced by QDs two times in MWC and even four times in DWW. Thus, CdSe/ZnS-COOH QDs affect the PSII of *Scenedesmus quadricauda* microalgae, but the magnitude of the effect also depends on the composition of the surrounding medium.

[1] A. Kalnaitytė, S. Bagdonas, *Light-mediated effects of CdTe-MSA quantum dots on the autofluorescence of freshwater green microalgae: Spectroscopic studies,* Journal of Photochemistry and Photobiology B: Biology, vol. 199 (2019)

Dynamic laser speckle imaging for estimation of microbial growth activity

Alexey Lihachev[1], Ilya Balmages[3,4], Janis Liepins[2], Ilze Lihacova[1], Dmitrijs Bliznuks[4]

[1]University of Latvia, Institute of Atomic Physics and Spectroscopy, Jelgavas 3, Riga, Latvia
[2]University of Latvia, Institute of Microbiology and Biotechnology, Jelgavas 1, Riga, Latvia
[3]LTD Laboratorija Auctoritas, Ciekurkalna 1.līnija, Riga, Latvia
[4]Riga Technical University, Zunda krastmala 10, Riga, Latvia
aleksejs.lihacovs@lu.lv

Microbial colony growth on the agar media is a technique widely used in microbiology to perform routine tests to analyze microbial contamination of environmental, food or to perform antimicrobial susceptibility tests. Usually, the colony growth on a solid medium represents a circle striving to increase in diameter during the incubation. The size of diameter of the outer zone of the colony is often included in the mathematical models to simplify the calculation of colony growth dynamics [1]. However, the experimental data on the actual size of the activity zone of the growing colony are scarce and requires additional studies. Currently, microbial activity within colonies can be explored only with invasive procedures – colony cross-sectioning and viability staining. In this study, the speckle imaging technique was used to record the growth and structural features of the microbial colony. The following microbial strains were used in the experiments: Escherichia coli ATCC® 8739 (E. coli), Vibrio natriegens DSM 759 (V. natriegens), and Staphylococcus aureus ATCC® 6538P (S. aureus). Bacterial cultures were maintained on agar plates. The experimental laser speckle imaging system was used for capturing macro scale images under white light LED and red laser illumination [2].

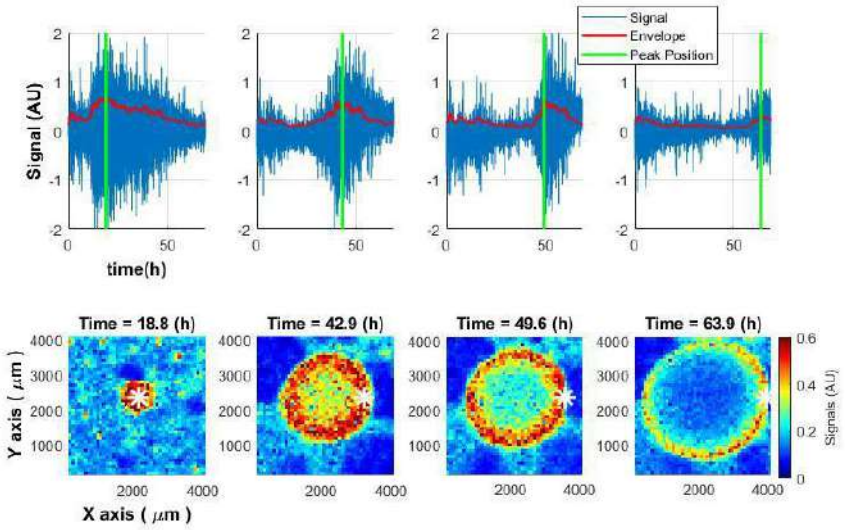

Fig. 1. Spatiotemporal distribution of the speckle signal across S. aureus colony. Upper row: signal dynamics over time at different points within the colony (white star in the bottom graphs). The green line marks the maximum activity, after which the signal decreases. Bottom row: changes in the activity during colony growth.

The obtained results demonstrate that the developed speckle analysis system is capable to record the growth of a microbial colony and to visualize microbial growth activity in the different parts of the colony (Fig.1.). The speckle imaging technique reveals that colony growth is driven by cell proliferation on its edges rather than its center. The results confirm the accuracy of the previous models of colony growth and provide algorithms for microbial activity analyses within the colony.

This research is funded by the ERDF project “Fast and cost-effective machine learning based system for microorganism growth analysis” (agreement No.1.1.1.1/19/A/147).

[1] Rivas, E. M. et al., *Lett. Appl. Microbiol.* **59(6)**, 594–603 (2014).
[2] Balmages, I. et al., *Biomed. Opt. Express* **12(3)**, 1609–1620 (2021).

Recognition of thymine microcrystals by CARS and SHG microscopy

Andrej Dementjev[1], Danielis Rutkauskas[1], Ivan Polovy[2], Mindaugas Macernis[3], Darius Abramavicius[3], Leonas Valkunas[1,3] Galina Dovbeshko[2]

[1] Center for Physical Sciences and Technology, Sauletekio ave. 3, Vilnius, LT-10257, Vilnius, Lithuania
[2]Institute of Physics, National Academy of Sciences of Ukraine, 46 Nauki Ave, Kyiv 03680, Ukraine
[3]Institute of Chemical Physics, Vilnius University, Sauletekio av. 9, LT-10222, Vilnius, Lithuania
andrej.dementjev@ftmc.lt

In the present work, we apply a combined approach of the *ab initio* calculations [1] with the microscopic imaging of the second harmonic generation (SHG) and the coherent anti-Stokes Raman scattering (CARS) to investigate polymorphism [2] of the thymine crystals. Compared to the regular bulk spectroscopic methods, the optical imaging allows for the detection of the possible structural heterogeneity on the length scale of the optical resolution. Then, the combination of a few different imaging modalities permits the spatial mapping of the sample areas with different characteristics that would otherwise be averaged out in a bulk measurement.

The presented experiment demonstrates perfect self-assembly of thymine molecules into two crystal configurations. Both configurations can be explained as formed by the ribbons of the dimerized molecular domains. In one crystal type the ribbons are oriented parallel, in the other - the ribbons are organized in anti-parallel configuration [3]. This could only be revealed by the combination of the CARS and SHG imaging.

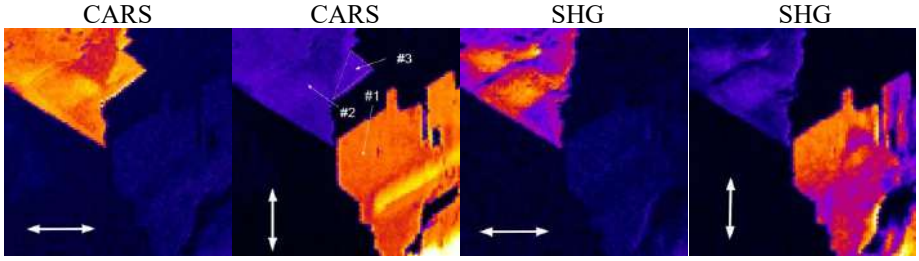

Fig. 3 The CARS and SHG images of thymine with two perpendicular linear polarizations of the incoming light indicated with white arrows. The areas #1 and #2 appear in the image at different polarization orientations of the incoming light. The region #3 is noteworthy for its lack of the SHG. The size of the images is 20x20 μm.

In the study, we performed the combined excitation polarization orientation-dependent CARS/SHG imaging of the glass-deposited thymine crystals. The quantitative dependences of the intensities of the non-linear signals on the orientation of the excitation polarization were related to the quantum chemical calculations. Experiments demonstrated several structural motifs even in the same crystalline droplets. Detailed analysis of self-assembly possibilities allowed to conclude that the most probable structural unit of the measured thymine crystals was the thymine-thymine inverse or thymine-thymine symmetric dimer.

Combined SHG and Raman microscopies have been used to reveal structures of thymine crystals and this constitutes a unique approach for molecular crystal characterization.

The Raman signal does not require macroscopic ordering, consequently, the generated signal from a crystalline sample will necessarily contain a background from noncrystalline phase. The situation is completely different in SHG where the signal generation requires macroscopic ordering. So the signal when applied to crystal studies is background free. This has been efficiently employed in mapping e. g. biological samples. By combining SHG and CARS modalities we get a high resolution information on local (microscopic) and global (macroscopic) picture of thymine ribbons. In this respect our approach is comparable to multiphoton multimodal generation microscopy, which has been used to map various structures of e. g. atomically thin tungsten diselenide .

This project has received funding from European Regional Development Fund under grant agreement No 01.2.2-LMT-K-718-03-0048 with the Research Council of Lithuania (LMTLT).

[1] Rashin, A. A., Young, L., Topol, I. A. & Burt, S. K. Molecular dipole moments calculated with density functional theory. Chem. Phys. Lett. 230, 182–188 (1994).
[2] Braun, D. E., Gelbrich, T., Wurst, K. & Griesser, U. J. Computational and Experimental Characterization of Five Crystal Forms of Thymine: Packing Polymorphism, Polytypism/Disorder, and Stoichiometric 0.8-Hydrate. Cryst. Growth Des. 16, 3480–3496 (2016).
[3] Braun, D. E., Gelbrich, T., Wurst, K. & Griesser, U. J. Computational and Experimental Characterization of Five Crystal Forms of Thymine: Packing Polymorphism, Polytypism/Disorder, and Stoichiometric 0.8-Hydrate. Cryst. Growth Des. 16, 3480–3496 (2016).

Custom-built magnetic tweezers microscope for single-molecule force measurements

Simona Šalčiūnaitė, Algirdas Toleikis

Vilnius University, Life Sciences Center, Saulėtekio al. 7, LT-10257 Vilnius, Lithuania

simona.salciunaite@gmc.stud.vu.lt

Traditional methods for studying the behavior of molecules in a given reaction are based on the assumption that all molecules of the same type are synchronous, but in fact, in most cases, they behave stochastically. Single-molecule research methods allow direct observation of target molecule action trajectories, including static and dynamic components of this process. From this data, intermediate reaction chains can be determined, which show the true heterogeneity of biomolecules [1]. Force manipulation-based single-molecule techniques, such as magnetic tweezers, are used to simulate and quantify force-dependent processes *in vitro*. Using this method, it is possible to precisely control the reaction conditions and reveal the mechanisms of action of macromolecules, such as myosin pulling against actin, kinesin walking along the microtubule, the folding of proteins, DNA and RNA, protein-protein and protein-DNA/RNA interactions [2].

In this work, we are developing a custom-built microscope, based on the Warwick Open Source Microscope (WOSM) project [3], with integrated magnetic tweezers for force-based single-molecule measurements. The microscope consists of an aluminium base with most other parts 3D-printed. The microscope stands out with its stability, compactness and simplicity of implementation. By using this microscope we hope to push the boundaries of the measurement limits of single-molecule magnetic tweezers experiments.

[1] A.N. Kapanidis, T. Strick, *Biology, one molecule at a time*, Cell Press, 2009

[2] H. Miller et al., *Single-molecule techniques in biophysics: a review of the progress in methods and applications*, Reports on Progress in Physics, 2018

[3] N. Carter, R. Cross, D. Martin, *WOSM website*, Centre for Mechanochemical Cell Biology, Open Source Hardware, WPH Charitable Trust, accessed 9 September 2022, < https://www.wosmic.org/>

The miEye: Bench-top super-resolution microscope with cost-effective equipment

Mohammad Nour Alsamsam[1,2], Aurimas Kopūstas[1,2], Meda Jurevičiūtė[2], Marijonas Tutkus[1,2]

[1]Department of Molecular Compound Physics, Center for Physical Sciences and Technology, Vilnius, Lithuania.
[2]Institute of Biotechnology, Life Sciences Center, Vilnius University, Vilnius, Lithuania.
nour.alsamsam@gmail.com

We present the miEye platform – a cost-effective microscope capable of high-resolution wide-field fluorescence imaging. Cutting-edge super-resolution (SR) imaging systems are commercially available under premium price tags. Affordable open-source microscopy systems often support single imaging modularity, do not live up to their high-cost siblings, or lack dedicated software. The miEye design revolves around an aluminum CNC milled modular microscope body that adapts with commercially available optomechanical elements, accompanied by the microEye open-source Python package for microscope control, data visualization, and analysis. The microEye integrates commonly used industrial- grade complementary metal oxide semiconductor (iCMOS) cameras, performs IR-based automatic focus stabilization, and allows for laser control via Arduino-based laser relay. The open-source project aims to facilitate the adaptation and contribution of the super-resolution community. The platform cost can sum up to roughly 50k €. It features two excitation regimes (SM-fiber and MM-fiber) that one can switch between and a flexible emission path. The miEye maintains less than 5 nm/min stability of lateral sample drift and achieves 10–30 nm lateral resolution for dSTORM and DNA PAINT single-molecule localization microscopy (SMLM) experiments after software drift correction. The platform is a cost-effective adaptable addition to the open-source microscopy community and potentially will allow high-quality SR imaging for limited-budget research groups.

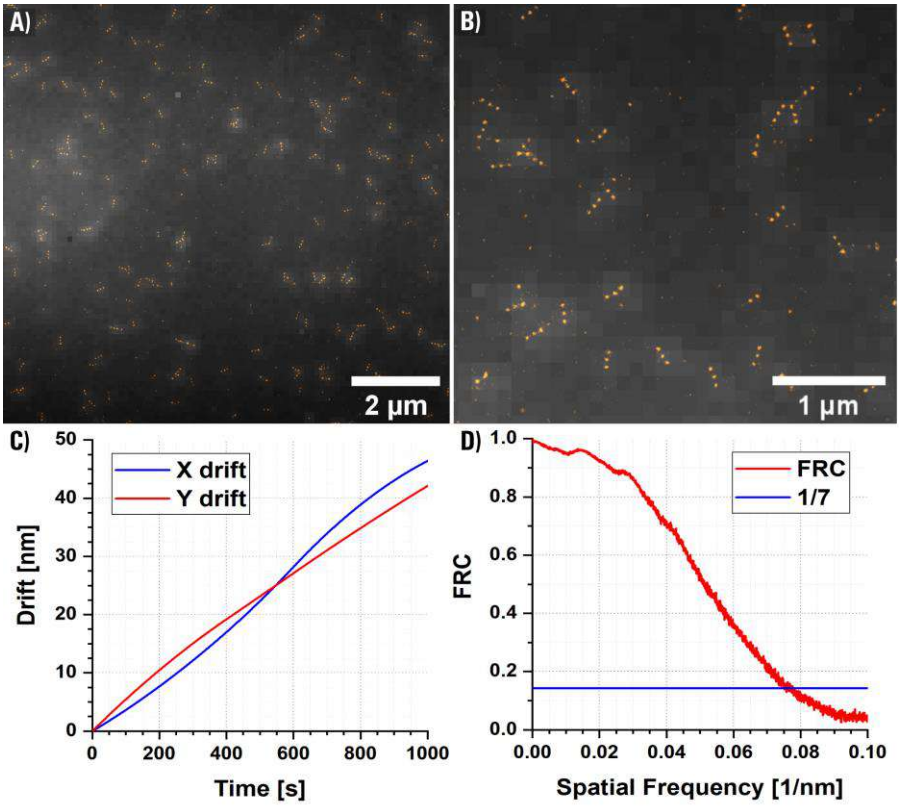

Figure 1. TIRF microscopy image of sparsely distributed DNA nano-rulers with 80-nm spacing. Three independent imaging experiments under the 638 nm wavelength excitation were done with a similar outcome. A) Larger field-of-view (FOV) conventional TIRF microscopy average stack overlaid with reconstructed super-resolution (SR) image. B) Zoomed image of the larger FOV presented in panel A. C) Graph showing curves of X and Y drift used for drift correction using cross-correlation. D) FRC curve, which showed a resolution value of 13.3 nm.

Mechanism of CRISPR-Cas3 helicase using magnetic tweezers

Miglė Šarpilo, Algirdas Toleikis

Vilnius University, Life Science Center, 7 Saulėtekio Ave, Vilnius, Lithuania

migle.sarpilo@gmc.stud.vu.lt

CRISPR-Cas provides RNA-guided adaptive immunity against invading genetic elements. CRISPR systems consist of multiple Cas proteins, which are responsible for CRISPR-dependent cell immunity mechanisms. The effector complex in CRISPR I-E consists of Cascade and Cas3. Cascade is responsible for foreign DNA targeting. Meanwhile, Cas3, which possesses helicase and nuclease activities, is a key protein of the system, necessary for crRNA-guided interference against virus proliferation.

Although single-component Class 2 CRISPR systems, such as type II Cas9 are widely used for genome-editing, the research on multi-component Class 1 proteins, including Cas3, of the same system has been less developed. Components of the I-E CRISPR system have already been used as a genome-editing tool to generate big deletions. However, the detailed mechanism by which Cas3 achieves its function is not well understood. The aim of this study is to elucidate the mechanism of Cas3 DNA unwinding and shredding. We are using single-molecule force microscopy, namely, magnetic tweezers, to probe the mechanical aspects of Cas3 unwinding activity. Greater knowledge of the Cas3 mechanism of action would improve the application of Cas3 as a tool for genome editing.

The Inactivation of Bacteria using Ultrasonic Techniques

Martynas Maciulevičius[1], Gabija Andreikė[1], Paulius Ruzgys[1], Simona Gelažunaitė[1], Saulius Šatkauskas[1]

[1] Biophysical Resaerch Group, Vytautas Magnus University, Kaunas 44248, Lithuania
martynas.maciulevicius@vdu.lt

The development of non-thermal technologies for the pasteurization of food is in demand, since they offer better food quality and longer shelf-life and, also, are more energy efficient than conventional processes [1].

The application of ultrasound (US) waves has been successfully applied for the delivery of biocompounds such as: anticancer drugs [2,3] and nucleic acids [2,4] to cells and tissues as well as for the reduction of the viability of mammalian cells [3,5] by irreversible sonoporation (SP).

In the current study we have applied mechanical waves of US to inactivate different species of bacteria. Two types of bacteria were used for the research: Gram-negative *Escherichia coli* and Gram-positive *Streptococcus thermophilus*. The effects of US alone and US in combination with US contrast agents, microbubbles (MBs), were investigated and compared with the efficiency of electroporation (EP).

US/ SP parameters: 1 MHz center frequency, 0 - 5 W/cm^2 intensity, 5 min exposure duration. EP parameters: 0 - 24 kV/cm electric field strength, 60 µs pulse duration, 99 pulses, 1 Hz pulse repetition frequency. Metabolic activity was evaluated using fluorescent dye AlamarBlue; cell viability - clonogenic assay.

EP was able to reduce the cell viability and metabolic activity of both bacteria Gram-positive *Streptococcus thermophilus* and Gram-negative *Escherichia coli*. However, the application of US alone in the range of explored US intensity (up to 5 W/cm^2, for 5 min.) was efficient for neither species.

The combined use of US and MBs (SP) was effective against *Escherichia coli* bacteria, reducing their viability and metabolic activity. However, SP was not effective against Gram-positive bacterium *Streptococcus thermophilus*.

Conclusions:

1. The use of US technologies (US intensity < 5 W/cm^2) for the inactivation of bacteria is only effective against Gram-negative *Escherichia coli*, but not against Gram-positive *Streptococcus thermophilus* bacteria.

2. The use of the contrast agents, MBs, in combination with US was more effective in reducing both the metabolic activity and cell viability of Gram-negative bacteria in comparison to the exposure to US alone.

Acknowledgment: this research was supported by the grant "Non-thermal inactivation of Gram-positive and Gram-negative bacteria using ultrasonic techniques (P-G-22-07)" from Vytautas Magnus University.

[1] F.M. Allai, Z.R.A.A. Azad, N.A. Mir, K. Gul, *Appl. Food Res.* **3**, 100258 (2023).
[2] Z. Fan, R.E. Kumon, C.X. Deng, *Ther Deliv*. **5**, 467-486 (2014).
[3] M. Maciulevičius, M. Tamošiūnas, M.S. Venslauskas, S. Šatkauskas, *Sci. Rep.* **10**, 7743 (2020).
[4] D.L. Miller, S.V. Pislaru, J.E. Greenleaf, *Cell Mol Genet.* **27**, 115-134 (2002).
[5] J. Rich, Z. Tian, T.J. Huang. *Adv Mater Technol.***7**, 2100885 (2022).

Index

Sponsors

CITY OF VILNIUS

NOVA

ŽEMAITIJOS PIENAS

LABORAMA
INTERLUX GROUP

TIME TO TASTE TIME TO APPRECIATE
DŽIUGAS
1924

NORDIC NUTRIS
CBD OILS

EX VII
expertus Vilnensis

Linea libera
SPARNAI ATRADIMAMS